FACULTY OF TECHNOLOGY

The komatiite-hosted Pahtavaara gold deposit, Central Lapland: geochemistry, hydrothermal alteration and statistical analyses of usability of the portable XRF data

Emmi-Kaisa Molkkari

MASTER'S PROGRAMME IN GEOSCIENCE

Master's thesis

2020

TIIVISTELMÄ
OPINNÄYTETYÖSTÄ Oulun yliopisto Teknillinen tiedekunta

Koulutusohjelma (kandidaatintyö, diplomityö) Geologian ja mineralogian koulutusohjelma		Pääaineopintojen ala (lisensiaatintyö)	
Tekijä Molkkari, Emmi-Kaisa Elina		Työn ohjaaja yliopistolla Ranta, J-P., filosofian tohtori	
Työn nimi Pahtavaaran komatiittinen kultaesiintymä Keski-Lapissa: geokemia, hydroterminen muuttuminen ja tilastollinen tutkimus käsikäyttöisen XRF-analysaattorin mittaustulosten käytettävyydestä			
Opintosuunta Geotieteet	Työn laji Pro gradu	Aika Toukokuu 2020	Sivumäärä 95 s., 10 liitettä

Tiivistelmä

Pahtavaaran kultaesiintymä sijaitsee Sodankylässä Keski-Lapin vyöhykkeellä ja se liittyy Sattasvaaran komatiittiseen muodostumaan. Kultaesiintymän alkuperä ei ole yksiselitteinen. Mahdolliseksi alkuperäksi on tyypillisesti ehdotettu orogeenista kultaesiintymää tai kultarikasta, merenpohjassa syntynyttä massiivista sulfidiesiintymää (VMS). Molemmat esiintymätyypit ovat syntyneet hydrotermisten prosessien vaikutuksesta. Näin ollen hydrotermisten prosessien, kuten hydrotermisen muuttumisen tunteminen on ensisijaisen tärkeää, kun halutaan ymmärtää hydrotermisten kultaesiintymien muodostumista. Pahtavaaran kultaesiintymästä on kattavasti kairasydämiä, mutta geokemiallisista analyyseista puuttuu osittain monialkuaineanalyysit. Käsikäyttöisen XRF-analysaattorin käyttö geotieteellisissä tutkimuksissa on kasvanut viime vuosina. Sen lisäksi, että se on nopea ja kustannustehokas analysointimenetelmä, myös laitteiden määritysrajat ja mittaustarkkuus ovat kehittyneet. Nämä ominaisuudet huomioiden on perusteltavaa tutkia, kuinka käsikäyttöinen XRF-analysaattori soveltuu jauhettujen laboratorionäytteiden analysointiin.

Tutkimus koostuu kahdesta osasta: 1) tilastollinen tutkimus käsikäyttöisen XRF-analysaattorin mittaustulosten käytettävyydestä ja 2) Pahtavaaran kultaesiintymän komatiittisen isäntäkiven ja hydrotermisen muuttumisen geokemiallinen tutkimus hyödyntäen jo olemassa olevia monialkuaineanalyyseja ja aikaisemmin julkaistuja tutkimuksia muista Keski-Lapin komatiittisista esiintymistä.

Tilastollinen tutkimus käsikäyttöisen XRF-analysaattorin käytettävyydestä osoitti, että alkuaineiden Ca, Fe, Ni, Sr, Zn, Mn, Al ja Mg mittaustulosten tarkkuus ja toistettavuus olivat erinomaisia tai hyviä. Alkuaineet Cr, Cu, S ja Y osoittivat tyydyttävää mittaustarkkuutta, kun taas alkuaineiden Ti, V ja Zr mittaustulokset korreloivat huonosti laboratorioanalyysien kanssa. Huolimatta hyvistä tilastollisen tutkimuksen tuloksista, käsikäyttöisen XRF-analysaattorin käyttäminen on suositeltavaa vain suuntaa antavana analysointimenetelmänä, eikä sillä voi korvata laboratoriossa suoritettuja monialkuaineanalyyseja.

Pahtavaaran, Peuramaan, Lomalammen ja Jeesiörovan komatiittisten kivien geokemiassa ei ollut havaittavissa merkittävää samankaltaisuutta. Protoliitin löytäminen Pahtavaaran kiville osoittautui hankalaksi. Liikkumattomien alkuaineiden vaihteleviin pitoisuuksiin perustuen, Pahtavaaran eri litologisilla yksiköillä voi olla eri protoliitit. Massatasapainolaskut osoittivat, että tutkimusalueen kaikki litologiset yksiköt, talkki-kloriitti- ja amfiboliittiliuske sekä aktinoliitti-tremoliittikivi, olivat rikastuneet MgO-, CaO-, TiO_2- ja MnO-yhdisteistä sekä bariumista ja strontiumista, ja köyhtyneet Fe_2O_3-, Na_2O- ja K_2O-yhdisteistä. Massatasapainolaskuihin ja hydrotermista muuttumista mallintaviin kuvaajiin perustuen aktinoliitti-tremoliittikivet ovat karbonaattiutuneet. Talkki-kloriitti- ja amfiboliittiliuskeet osoittivat merkkejä kloriittimineraalien syntymisestä hydrotermisen muuttumisen seurauksena, mikä todennäköisemmin liittyy tremoliittirikkaiden kivien karbonaattiutumiseen eikä kloriittiutumiseen. Näin ollen aktinoliitti-tremoliittikivi saattaa olla lähempänä Pahtavaaran kivien todellista protoliittia kuin aikaisemmissa tutkimuksissa ehdotettu talkki-kloriittiliuske.

Muita tietoja

Asiasanat: hydroterminen muuttuminen, kultaesiintymät, geokemia, käsikäyttöinen XRF-analysaattori, tilastollinen tutkimus

ABSTRACT
FOR THESIS

University of Oulu Faculty of Technology

Degree Programme (Bachelor's Thesis, Master's Thesis) Degree Programme in Geology and Mineralogy	Major Subject (Licentiate Thesis)
Author Molkkari, Emmi-Kaisa Elina	Thesis Supervisor Ranta, J-P., PhD

Title of Thesis
The komatiite-hosted Pahtavaara gold deposit, Central Lapland: geochemistry, hydrothermal alteration and statistical analyses of usability of the portable XRF data

Major Subject	Type of Thesis	Submission Date	Number of Pages
Geosciences	Master's Thesis	May 2020	95 p., 10 App.

Abstract

Pahtavaara gold-only deposit in Sodankylä, Central Lapland, is hosted by komatiites of the Sattasvaara formation. The genesis of the deposit remains unsolved. Orogenic gold or Au-rich volcanogenic massive sulphide deposits have been typically proposed as the genesis of the deposit. Both types of deposit have formed by hydrothermal processes and thus, the study of hydrothermal processes such as hydrothermal alteration, is crucial for understanding the formation of the deposit. The Pahtavaara gold deposit is comprehensively drilled but the laboratory analyses lack partially of multi-elemental analyses. The use of portable XRF analyser in geoscience has increased in the previous years due to its time- and cost efficiency features and, development of detection limits and accuracy. As such, it is reasonable to the test the usability of pXRF measurements of laboratory-returned pulp samples.

The study consists of two parts: 1) statistical analyses of the pXRF data and its usability and, 2) geochemical studies comprising the komatiitic host rock and hydrothermal alteration by utilising the pre-existing, laboratory analysed multi-elemental data and previously published studies of the other komatiitic deposits in the Central Lapland.

Based on the statistical analyses, the pXRF measurement of Ca, Fe, Ni, Sr, Zn, Mn, Al, and Mg showed excellent or good accuracy and repeatability. The results were satisfactory for Cr, Cu, S and Y and bad for Ti, V and Zr. Despite of the good results of statistical analyses, the use of pXRF analyser is recommended only as an indicative method in geochemical studies and it cannot replace the laboratory multi-elemental analyses.

The Pahtavaara komatiites did not show a significant correlation with Peuramaa, Lomalampi and Jeesiörova komatiitic rocks. The precursor of the Pahtavaara rocks proved to be complex. Based on the varying contents of immobile elements, the precursor may not be the same for all the lithological units. The mass balance calculations of the lithological units of the study area—talc-chlorite and amphibolite schists and, actinolite-tremolite rock—showed enrichment of MgO, CaO, TiO_2, MnO, Ba and Sr and, depletion of Fe_2O_3, Na_2O, and K_2O. On the grounds of mass balance calculation and the graphs of hydrothermal alteration, the actinolite-tremolite rocks are trending towards carbonatisation. The talc-chlorite and amphibolite schists were characterised by a formation of chlorite minerals which in fact, is more likely related to carbonate alteration of tremolite-rich rocks instead of chloritisation. Due to this, the actinolite-tremolite precursor is more probable than the talc-chlorite schist suggested in the literature.

Additional Information

Keywords: hydrothermal alteration, gold deposits, geochemistry, portable XRF analyser, statistical analysis

TABLE OF CONTENTS

APPENDICES:

Appendix 1. The drill holes and number of samples included in the project.

Appendix 2. Geochemistry of the outliers.

Appendix 3. Scatter plots and line diagrams for the determination of distribution and comparison of accuracy of the pXRF and laboratory ME-MS61 analyses.

Appendix 4. Numerical results of the mass balance calculation of the talc-chlorite schist.

Appendix 5. Numerical results of the mass balance calculation of the amphibolite schist.

Appendix 6. Numerical results of the mass balance calculation of the actinolite-tremolite rock.

Appendix 7. Combined data for the downhole plot of drill hole 116227.

Appendix 8. Combined data for the downhole plot of drill hole 116231.

Appendix 9. Combined data for the downhole plot of drill hole 117310.

Appendix 10. Combined data for the downhole plot of drill hole 117312.

1 INTRODUCTION

The use of portable XRF (pXRF) analysers has become more popular in geosciences during the previous years. The pXRF analysers provide a fast and cost-efficient method for analysing various types of sample material. Sarala et al. (2014) and Hatakka et al. (2016) have studied the reliability of pXRF measurements of till and soil samples, and Hokka and Soukka (2016), in turn, applied the method for grinded drill core samples and noted that the grinded samples give better results compared to the measurements which were conducted directly from a solid drill core.

Orogenic gold deposit is the most common type of gold deposit in the metamorphosed terrains due to the preservation potential compared to the deposits formed in more shallow crustal settings (e.g. Goldfarb et al., 2005). Thus, it is the most typical gold deposit type in Finland (Eilu, 2015). Other identified gold deposits in Finland include Au-rich volcanogenic massive sulphides, intrusion related gold deposits, epithermal Au, iron-oxide-copper-gold and, placer and palaeoplacer gold deposits (Eilu, 2015). The formation of gold deposits is linked to hydrothermal or magmatic-hydrothermal processes (Mathieu, 2018) and thus, understanding of these processes is crucial in planning and conducting exploration activities as well as in modelling the results. Hydrothermal alteration, produced by the interaction between the hydrothermal fluid and country rocks, has usually a larger extend than the mineralisation itself (Eilu et al., 1999). Due to that, the study of hydrothermal alteration comprising the recognition, classification and quantification of the alteration style provides a significant knowledge of the formation of hydrothermal gold deposits (Mathieu, 2018).

Pahtavaara gold deposit is located 25 km north of Sodankylä, Central Lapland. Geologically, it is hosted by Palaeoproterozoic volcano-sedimentary sequence, Central Lapland belt (Figure 1). Similar supracrustal belts are found elsewhere in the Karelian craton and are referred as Karelian supergroup (e.g. Luukas et al., 2017) with a great number of gold occurrences in northern Finland (Figure 1). These belts have been found to be potential for orogenic type gold-only deposits (e.g. the largest gold mine in Europe, Suurikuusikko; Figure 1), but also for gold deposits with anomalous metal assemblages (Au-Co-Cu-U) (Eilu, 2015).

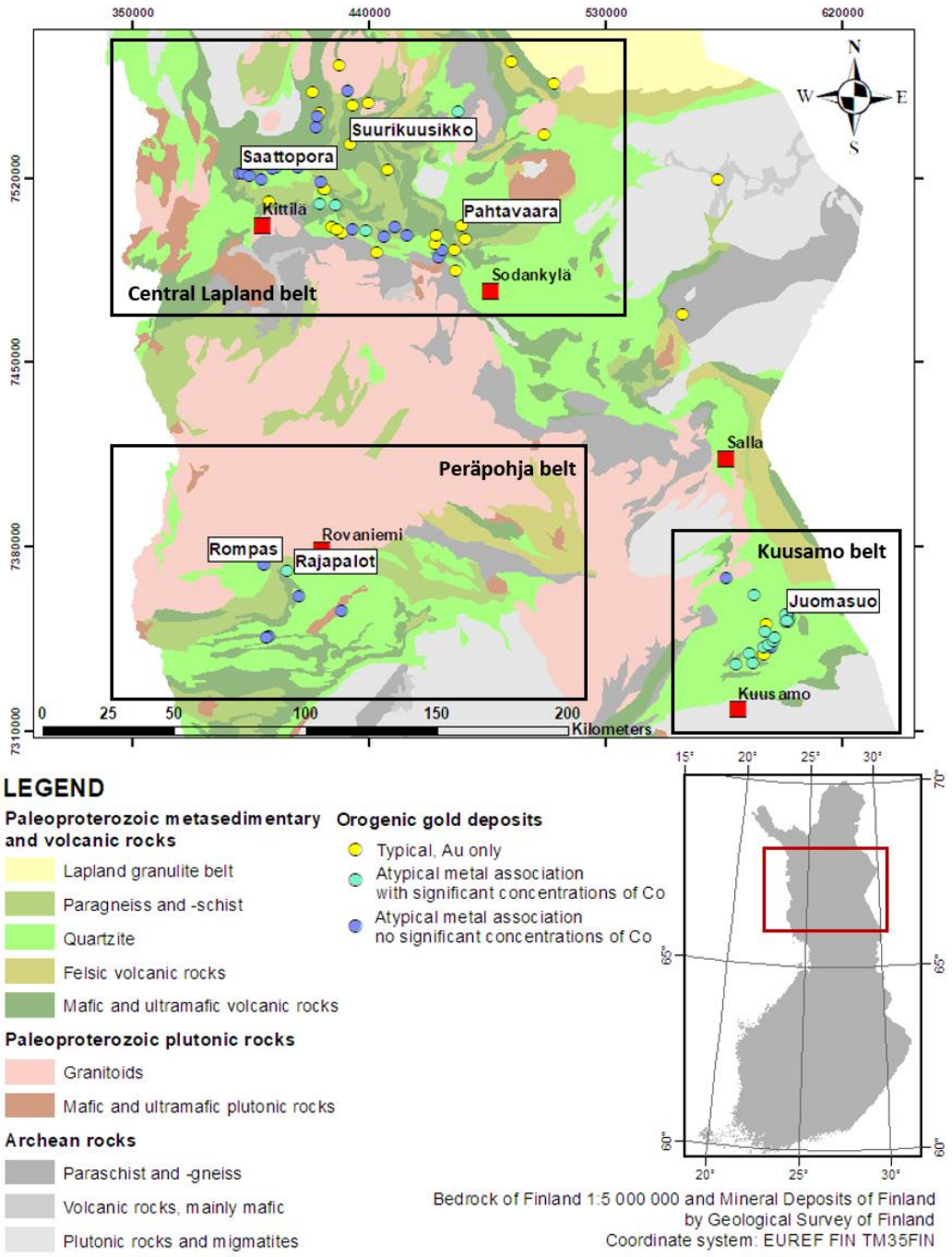

Figure 1. Gold deposits classified as orogenic gold in the northern Finland. Modified after Eilu et al. (2007), Molnár (2019) and the DigiKP version 2.0 of Bedrock of Finland and version 1.0 of Mineral Deposit of Finland.

The Pahtavaara gold deposit was discovered in 1985 by the Geological Survey of Finland. Gold is hosted in komatiitic volcanic rocks (e.g. Korkiakoski, 1992). Despite the over 30 years since the discovery, the genesis of the Pahtavaara deposit is still not understood completely. The proposed classifications have varied from orogenic type (e.g. Korkiakoski, 1992) to volcanogenic massive sulphide type deposit (e.g. Hulkki, 1990; Eilu, 2015). Approximately 10 t of gold has been mined from the Pahtavaara deposit

during its mining history between 1996-2014 and the current inferred mineral resources cover 14.7 t of Au (Rupert Resources, 2018).

Although the deposit is extensively drilled, the laboratory analyses partially lack multi-elemental data since many drill cores have been analysed for gold only. In this study, 692 samples from 13 drill cores were analysed using a portable XRF analyser in order to increase the geochemical data for samples which only had gold analysed in laboratory. Furthermore, samples with pre-existing multi-elemental analytical data were used as a reference for the quality and reliability of the pXRF measurements. Previously analysed multi-elemental data (617 analyses) was also used to map the hydrothermal alteration and to determine the protolith of the hydrothermally altered gold-enriched host rocks.

2 HYDROTHERMAL ORE DEPOSITS

2.1 Sources of fluid

Hydrothermal ore deposits consist of a wide range of deposit types which have formed by complex processes in which a circulation of hot aqueous solutions in the Earth's crust acts as a mineralising agent when dissolving, transporting and precipitating metals. The sources of hydrothermal fluids can be variable: 1) water released from magmas as they crystallise, 2) meteoric water, 3) sea water, 4) connate water from uncompact sediments released during lithification and 5) metamorphic water released in dehydration (Pirajno, 200) or decarbonation reactions (Robb, 2005) during prograde metamorphism. Additionally, a mix of these fluid sources are common (Skinner, 1997). There is a division between magmatic-hydrothermal and hydrothermal ore deposits, where the fluid source of the former is mainly magmatic origin, and the latter, mainly from other sources than magmatic. However, in many times fluids from magmatic source have mixed with fluids from the other origins (e.g. meteoric) and hence, a term magmatic-hydrothermal deposit is commonly used (Robb. 2005).

The hydrothermal fluid can occur in various physical stages such as liquid, vapour and supercritical fluid depending on the temperature, pressure, and density of the fluid. Composition of hydrothermal fluid is controlled by the source of the fluids and elemental compounds dissolved into the fluid composition from country rocks during the fluid's path in the crust (Robb, 2005). Due to the comprehensive interaction between fluids and the crustal rocks, and possible mixing with other fluids, the composition of fluid is changing and evolving continuously on its path (Reed, 1997). The fluid flow is highly controlled by a stage of deformation of country rocks (Sibson et al., 1975, according to Robb, 2005) and on account of that, the formation of hydrothermal ore deposits is clearly linked to tectonic processes that has caused the crustal deformation (Eilu, 2015).

2.2 Metal transportation

The hydrothermal fluids are multicomponent aqueous electrolyte solutions in which the major salt component is typically NaCl (Seward et al., 2014). In addition to NaCl, the other important solute components in hydrothermal fluids are CO_2, H_2S and NH_3. The former is present especially in metamorphic terrains (Seward et al., 2014) where it is

related to metamorphic source of the fluid and more specially, by the breakdown reactions of minerals during a medium grade metamorphism (Robb, 2005).

Wood and Samson (1998) have defined the term solubility as *"an upper limit to the amount of dissolved metal that a hydrothermal fluid can transport"*. The solubility of metals is depending on temperature and pressure conditions, composition of the fluid by solute components and, acidity and redox potential (Robb, 2005). High temperature and pressure with association of salt component are fundamental in processes of complexing and transporting metals and, thus, in formation of hydrothermal ore deposits (Pirajno, 2009). Ligands are elements or elemental compounds which combine with metal ions and allow the transportation of the metals as a metal-ligand complexes in the hydrothermal fluid solutions (Skinner, 1997). There are a wide range of ligands which can form metal complexes (Robb, 2005) but the most important ligand in the hydrothermal systems is chlorite ion Cl^-. In addition to Cl^-, other important ligands in hydrothermal systems are HS^- and OH^- with respect of their availability and concentration in the hydrothermal fluids (Seward et al., 2014).

A molecule or atom which can accept a lone pair of valence electrons is called a Lewis acid whereas a molecule or atom which can donate an electron pair, in turn, is called a Lewis base. The Lewis acids and bases are a concept used for understanding how the metals go into solutions of hydrothermal fluids and form the metal-ligand complexations. The Lewis acids can be divided into three groups (Table 1) based on their electronegativity. "Hard" Lewis acids are strongly electropositive metals (e.g. K^+, Na^+, Ca^{2+}, Mg^{2+}) which tend to bond with strongly electronegative elements (e.g. O^{2-}) whereas "soft" Lewis acids (e.g. Au^+, Cu^+, Ag^+), in turn, bond with elements of low electronegativity (e.g. S^{2-}). Hard metals, electron acceptors, tend to bond with hard ligands, electron donors, and soft metals with soft ligands in a competitive situation according to *Pearson's Principle* (Pearson, 1963). Metals such as Cl^-, which are able to bond with both hard and soft ligands, are grouped in a borderline category. (see Robb, 2005)

The Pearson's principle is totally valid only as a theoretical consideration due to a fact that in natural situations metals tend to bond with the most suitable ligands available and as such the metal-ligand complexes may be different than those on the theoretical grounds (Robb, 2005). For example at 500 ºC and 500 bar, a gold iodide complex AuI_2^- is more stable than a gold chloride complex $AuCl_2^-$, but in spite of that, the gold ion tends to bond

more likely with the chloride ion if chloride ions occur with higher concentrations in hydrothermal fluid (Seward et al., 2014).

Table 1. Hard, borderline and soft ligands and metals according to Pearson (1963) (see Robb, 2005).

Hard ligands	**Borderline ligand**	**Soft ligands**
NH^3 OH^-, F^-, NO_3^-, HCO_3^-, CH_3COO^- CO_3^{2-}, SO_4^{2-} PO_4^{3-}	Cl^-, Br^-	HS^-, I^-, CN^-, H_2S, $S_2O_3^{2-}$
Hard metals	**Borderline metals**	**Soft metals**
Li^+, Na^+, K^+, Rb^+, Cs^+ Ba^{2+}, Sr^{2+}, Be^{2+}, Fe^{3+}, Ce^{4+}, Sn^{4+}, Mo^{4+}, W^{4+}, V^{4+}, Mn^{4+} As^{5+}, Sb^{5+}, U^{6+}	Divalent transition metals such as Zn^{2+}, Pb^{2+}, Fe^{2+}	Au^+, Ag^+, Cu^+ Pd^{2+}, Pt^{2+}, Sn^{2+}, Cd^{2+}, Hg^{2+} Au^{3+}, Tl^{3+}

The chloride ion Cl^- is the most abundant ion acting as a ligand in hydrothermal fluids. It forms stable complexes with multiple elements, both hard and soft metals in condition of high temperature and pressure. These elements include e.g. Au, Cu, Co, Ti, Mn, Fe, Ni, Zn, Cd, Sn, Sb, Pb, and REEs (Seward et al., 2014). Gold-chloride complexes $Au(Cl)_2^-$ and $Au(Cl)_4^-$ are stable in saline, oxidising and acidic conditions (Robb, 2005) and the complexes occur typically at the deeper and hotter regions of magmatic and hydrothermal systems with a temperature higher than 250 ºC (Pirajno, 2009). Other halite ligands such as iodide I^-, bromide Br^- and fluoride F^- have been detected forming metal complexes in the hydrothermal solutions, especially the latter has a significant role in transportation of Ti, Sn, REEs, Zr and U (Seward et al., 2014).

The hydrosulphide ion HS^- can be considered as one of the most fundamental ligands in transportation of metals especially with Au^+ which transportation is dominated by AuHS and $Au(HS)_2^-$ complexes. The former is typical at low pH conditions whereas the latter dominates under weakly acidic to basic condition and is stable over a wide temperature range (Robb, 2005). According to Pirajno (2009), $Au(HS)_2^-$ are found to be stable up to 300 ºC and 1500 bar with pH of 3-10. Other soft metals such as Cu and Ag are also in many cases forming stable complexes with hydrosulphide ion (Seward et al., 2014). However, whether the dominant metal transport occurs as Cl^- or HS^- complexes is depending especially on concentration (e.g. availability) of the ligands in addition to temperature-pressure and pH conditions (e.g. Stefansson and Seward, 2003b, according to Seward et al., 2014).

The hydroxide ion OH^- is another common ligand in hydrothermal solutions due to its availability in aqueous solution ($H_2O = H^+ + OH^-$) and a fact that metal ions tends to

hydrolyse in aqueous solution at higher temperatures (Seward et al., 2014). The solubility of metal oxides in aqueous solution is highly depending on pH (Wesolowski et al., 2004, according to Seward et al., 2014). The hydroxide ion is acting as a ligand for many hard metals such as W, Mo, As and Sb, with which the OH^- forms stable in the certain T-P and oxidation conditions (Robb, 2015). Also, the gold-hydroxide complexes have been detected in the certain conditions among Cl^- and HS^- complexes (Seward et al., 2014). Other oxygen electron donors such as carbonate CO_3^{2-} and bicarbonate HCO^{3-} may act as ligands for the hard and borderline metals when forming stable complexes with Pb, U and some REEs although these complexes are also very sensitive to pH changes (Seward et al., 2014).

2.3 Hydrothermal alteration

When hot aqueous solution is passing through crustal rocks, there is always interaction between rocks and the fluid. *Hydrothermal alteration* is defined as an open system process that results changes in rock's mineralogical and chemical properties. Such a definition is also used for *metamorphism*, but these two processes are distinguished by an intensity of changes of chemical composition: the changes of chemical composition in metamorphic rocks is usually less intense (Mathieu, 2018) and metamorphism results changes in mineralogical properties of rock when involving a transformation of minerals to another with better stability in prevailing conditions at higher temperature and pressure while the chemical composition of rock remains rather unchanged (Robb, 2005). A distinction between hydrothermal alteration and metamorphism is needed especially when studying deposits where both processes have been present, such as orogenic gold deposits (Phillips and Powell, 2010). Hydrothermal fluids may origin from devolatilisation during metamorphic processes and these fluids are the ones resulting further hydrothermal alteration. A term *metasomatism* is used beside of hydrothermal alteration as it also reflects to chemical and mineralogical changes of rocks due to the circulation of hydrothermal fluids (Mathieu, 2018).

According to Reed (1997), five main variables can be seen as the main factors affecting to the hydrothermal alteration: temperature, pressure, composition of fluid and host rock, and a fluid/rock ratio. The products of hydrothermal alteration provide significant information about hydrothermal systems and due to this fact, they also reveal crucial knowledge of formation of hydrothermal ore deposits. Hydrothermal alteration produces

typically alteration zones or alteration halos which have much wider extension than the mineralisation itself and thus, the study of alteration is an effective tool also in ore exploration (Eilu et al., 1999).

A fluid with aqueous composition, containing nothing but dissolved components H^+ and OH^- in water solution, can cause isochemical hydrothermal alteration producing muscovite by a reaction between K-Feldspar and H^+ (Pirajno, 2009). The hydrolysis or, so called *H^+ ion metasomatism* is hydrothermal alteration at its simplest form. When including other dissolved constituents in addition to hydrogen ions, processes and reactions of hydrothermal alteration become more complex. The concentration of cations in evolving aqueous fluid solution affects to the nature of downstream alteration when the cations themselves may react wall-rocks causing i.e. *cation metasomatism*. (Robb, 2005)

Common hydrothermal alteration styles, their characteristics and typically associated deposits are listed on Table 2. However, in many cases, the terms used in the discussion of alteration styles reflect directly to the mineral assemblages produced in alteration such as biotitisation which signify formation of biotite for example during potassic alteration.

Alteration of gold deposits is commonly characterised by carbonatisation, sulphidation and muscovite/biotite alteration which are shown as major enrichments of K, Rb, S and CO_2. Minor enrichment of elements Ag, As, Sb, B, Se, Te, Hg, Bi, Mo and/or W may occur besides Au in gold-related alteration (Phillips and Powell, 2010). Typical alteration styles of gold occurrences in Palaeoproterozoic greenstone belts in the northern Lapland include most commonly albitisation, carbonatisation and sericitisation, and in some cases biotitisation and scapolitisation (Eilu et al., 2007). Pre-mineralisation alteration, especially albite alteration may act as a ground preparation for later mineralisation and make country rock more competent and that way more favourable for precipitation of metals from hydrothermal solutions during deformation (Eilu, 2015).

Table 2. Common alteration styles and their characteristics according to Mathieu (2018), Robb (2005), Eilu et al. (2007) and Pirajno (2009) and references therein.

Alteration style	**Gains/losses**	**Mineral assemblages**	**Example of ore system**	**Other characteristics**
Albite (sodium) alteration	+Na, -K	Alkali feldspar → Albite + hornblende ± biotite-quartz	Epigenetic gold occurrences in Palaeoproterozoic greenstone belt in northern Lapland, porphyry systems	Acting as a ground preparation in many deposits
Agrillic alteration	+H	Plagioclase feldspar → kaolinite + smectite group minerals	Porphyry systems	<250°C
Advanced argillic alteration	+H	Alkali elements → Kaolinite + pyrophyllite + dickite + alunite (+ quartz, topaz, tourmaline)	Porphyry systems, epithermal precious metal deposits	Very acidic conditions, high fluid/rock ratio
Carbonatisation	+C, (+Ca)	→ Carbonate minerals ± quartz-muscovite-chlorite (VMS) → Talc + chlorite +carbonate (Komatiites in orogenic gold system)	Epigenetic gold occurrences in Palaeoproterozoiz greenstone belt in northern Lapland, VMS	High partial pressures of carbon dioxide, neutral to alkaline pH
Chloritisation	+Fe, +Mg, +H, -Na, -Ca, -K	→ Chlorite + pyrite + muscovite ± quartz	VMS	Alteration zonation: Mg-chlorite more distal than Fe-chlorite
Greisenisation	+H, (+Li, +F, +B)	→ Quartz + muscovite + topaz (+ tourmaline, fluorite)	Porphyry systems	Starts with albitisation (H^+ gain), may accompany by silification
Potassic (K-silicate) alteration	+H, +K, -Na	→ K-feldspar ± biotite + quartz (+sericite, chlorite, magnetite, hematite, anhydrite)	Porphyry systems	450-600°C

Table 2. (continued)

Alteration style	Gains/losses	Mineral assemblages	Example of ore system	Other characteristics
Phyllic (sericitic) alteration	+K or -K +H, -Na, -Ca	K-feldspar → sericite (+quartz, pyrite, chlorite)	Epigenetic gold occurrences in Palaeoproterozoic greenstone belt in northern Lapland, porphyry-Cu, VMS in felsic rocks, mesothermal precious metal deposits	Very common alteration style, wide temperature range
Propylitic alteration	+H, +C	→ Epidote + chlorite (+ albite + carbonate) (Same assemblages as regional greenschist facies metamorphism)	Porphyry systems, epithermal precious metal ores	Mild form and the most widespread alteration style, 200-350°C, low fluid/rock ratio
Silication	+cation meta-somatism	Carbonate → silicate mineral	Polymetallic skarns	Interaction between enriched, acidic magmatic fluid and carbonate rocks, extended temperature range, high fluid/rock ratio
Silicification	+Si	→ New quartz or amorphous silica minerals	Many different ore deposits, epithermal precious metal deposits	Si as by-product of hydrolysis reactions or Si leached from country rocks
Sulphidation	+S, +metals	→ Any minerals + sulphides		Lithological control

2.4 Precipitation mechanisms

There are a large variety of precipitation mechanisms involving physico-chemical changes in the hydrothermal systems which can make a hydrothermal fluid destabilised and causing reduction of the metal solubility (Robb, 2005). The most important precipitation mechanisms include decreasing temperature, pressure changes and boiling, mixing of fluids and chemical reactions between a fluid and crustal rocks (Pirajno, 2009). At shallow crustal levels, for example at the seafloor, the precipitation occurs mainly as a result of decreasing temperature when a hot hydrothermal fluid mix with sea water and, as a result precipitates a volcanogenic massive sulphide deposit (Robb, 2005). Mixing of fluids can cause the precipitation of metal solution by destabilising of metal-ligand complexes and changing the properties of fluid in addition to cooling the hotter metal-carrying fluid (Skinner, 1997). At the deeper crustal levels, however, where the porosity of the rocks is low and the temperature gradients remain minimal, the deposition is usually provided by changing properties or composition of the hydrothermal fluid (Robb, 2005).

Decreasing pressure itself rarely affects to the precipitation but in fact, it increases the metal solubility of fluid (Robb, 2005). However, pressure is controlling an important isothermal effect, *boiling*, which many times plays a fundamental role in the precipitation of metals such as Au and Ag (Skinner, 1997; Pirajno, 2009). Boiling has two effects: it increases the solution concentration and more importantly, leads to a removal of volatiles from the hydrothermal fluid which leads to a situation in which the composition of the remaining fluid solution is dramatically changed in the way it is less capable of keeping the metals constituents in the solution (Skinner, 1997).

When the pressure drops episodically for example due to crack-seal process, it makes it possible a low-salinity H_2O-CO_2 fluid to precipitate the ore components of mesothermal lode-gold deposit as a result of boiling (Robb, 2005). That is, because of suddenly decreasing of pressure will increase temperature of the fluid (Brown, 1998, according to Robb, 2015) and make the initially homogenous liquid solution to form two different phases segregating H_2O and, CO_2 and other volatiles such as H_2S (Pirajno, 2009). The removal of H_2S from fluid solution affects dramatically for the solubility of metals (e.g. Au) which were transported as metal-hydrosulphide complexes in the original fluid solution i.e. the metals precipitate as the complexing ligand is removed into the volatile phase (Robb, 2005).

According to Skinner (1997), the chemical reactions between a hydrothermal fluid and wall rocks are the main reason for the metal precipitation. The reactions between the fluid and wall rocks may promote the precipitation of fluid-carrying metal-complexes due to changing properties such as acidity and redox states of the prevailing fluid. The oxidation of an initially reduced, neutral fluid with $Au(HS)^{-}_{2}$ complex will dramatically decrease the solubility of the complex and cause the precipitation of gold from the fluid. On the other hand, decreasing of acidity of the fluid from 7 to 3 pH may lead to reduction gold solubility (Robb, 2005). According to Phillips and Powell (2010) the most significant role in the depositional systems of gold is played by the reactions between the fluid and wall rocks whereas the other precipitation mechanisms such as fluid mixing, temperature and pressure changes have had a minor locally effect in the gold precipitation.

3 GOLD DEPOSITS

Before the 1980s, the classification models for genetic types of gold deposits were based on the depth of formations, mineralogy of ores, alteration assemblages, sources and composition of gold-carrying fluids, types of host rocks, age and location of deposits and involved hydrothermal processes, for instance. Since the price of gold started to increase from the 1980s, the interest of gold exploration activities increased significantly. New researches were conducted, and they provided much more information about the genesis of various types of gold deposits (Goldfarb et al., 2005). Böhlke (1982) was one of the first introducers of the term orogenic gold deposit regarding to structurally controlled, epigenetic lode gold deposits hosted in metamorphic rocks (see Goldfarb et al., 2005). Sillitoe (1991), in turn, introduced a group of gold deposits with evidences of intrusion-related origin. The intrusion related gold deposits differ from the orogenic ones by the timing of formations since the orogenic gold deposits are clearly related to the later stages of ongoing regional deformation whereas the intrusion-related Au-deposits were formed obviously more commonly during a post-regional deformation (Goldfarb et al., 2005).

Mainly all epigenetic gold deposits found in metamorphic belts around the world formed episodically during the pre-Neoproterozoic 2.80-2.55 Ga, 2.10-1.80 Ga and younger Cordilleran-style 600-50 Ma orogenies (Goldfarb et al., 2005). The Finnish bedrock has formed mainly during Archean and Palaeoproterozoic eons and have been affected by multiple deformation stages with metamorphic grades from greenschist to granulite facies. Due to the age and multi-deformation history of Finnish bedrock, the most common gold deposit type in Finland is orogenic gold (e.g. Goldfarb et al., 2005). The gold deposit types formed at shallow levels of the crust (e.g. epithermal Au-deposits) are not well preserved in Finland due to a low preservation potential of such deposits (e.g. erosion). In Finland, ages of gold deposits and occurrences are correlating to global tectonic activity and thermal events (Eilu, 2015). Although different deposit types are linked to the major tectonic settings, metamorphic grades and regional deformation, Goldfarb et al. (2001) suggested the formation of the gold deposit may not be totally connected to the plate tectonics because any thermal event with a suitable fluid composition and country rock may form the same type of gold deposit.

In this thesis, the focus is on orogenic gold deposits, orogenic gold deposits with atypical metal associations and volcanogenic massive sulphides which are possibly related to the genesis of the Pahtavaara gold deposit. Other types of gold deposits are listed in Table 3.

3.1 Orogenic gold deposits

In Finland, the deformation and related gold mineralisation in the Archean greenstone belts took place during the global Neoarchean orogenic activity and peak of crustal growth between 2.72 and 2.64 Ga (Sorjonen-Ward, 1993; Rasilainen, 1996). Hölttä et al. (2012), in turn, suggested that the formation of gold mineralisation occurred most probably between 2.68-2.64 Ga (see Eilu, 2015). The formation of second group of orogenic gold deposits, within the Palaeoproterozoic belts, is connected to the Svecofennian orogenic events between 1.91 and 1.77 Ga (Groves et al., 2005, according to Eilu, 2015). Although the Palaeoproterozoic deformation events have locally overprinted the Archean greenstone belts, there is no evidence that it has caused a deposition of gold mineralisation in the Archean rocks (Eilu, 2015). The deposition and related alteration events of orogenic gold deposits took place under post-peak metamorphic conditions, most commonly with the metamorphic grades from greenschist to mid-amphibole facies (Goldfard et al., 2005) but a small number of Palaeoproterozoic orogenic gold occurrences in Finland have went through upper-amphibolite or even granulite facies conditions. This kind of higher-grade metamorphism may be a post-mineralisation metamorphism and, it may result remobilisation of gold locally. Orogenic gold mineralisation can be hosted by any competent or reactive supracrustal rocks within the metamorphic belt (Eilu, 2015).

3.1.1 Composition of the ore forming fluid

Gold deposits with orogenic origin have formed by syn- to late-orogenic fluids in orogenic belts, including accretionary and collisional tectonic settings (Eilu, 2015) at deep mid-crustal regimes with moderately low-grade metamorphic conditions from greenschist to mid-amphibole facies (Goldfard et al., 2005). The fluids forming the orogenic gold deposit are typically low-salinity carbonic bearing aqueous fluids which typically contain 5-20 mol-% CO_2 and 3-7 w-% NaCl with a near-neutral pH 5.5 (Goldfarb and Groves, 2015). The composition of fluids in the formation of orogenic gold deposit tends to be produced by metamorphic devolatilisation (Phillips and Powell, 2010) in mid-crustal levels having a temperature between 180-700 °C (Groves et al., 1995) but most likely 300-350 °C (Ridley and Diamond, 2000), without any significant mixing with fluids from the other sources (Eilu, 2015). The low-salinity, H_2O-CO_2 fluids contain CH_4,

N_2 and H_2S as minor amounts, and the gold is dominantly carried as bisulphide AuHS complexes. In the case of orogenic gold deposits, there is no detectable or substantial inputs from local rocks into the fluid composition (Eilu, 2015).

3.1.2 Precipitation

Orogenic gold deposits are typically structurally controlled (e.g. Eilu, 2015). The deposition of orogenic gold deposits has taken place at the deeper crustal levels where porosity in rocks is at minimum and the temperature gradients remain minimal and thus, the deposition is usually provided by changing properties or composition of hydrothermal fluid (Robb, 2005). Groves et al. (2018) suggested that the deposits occur more likely in second- or third-order faults and shear zones whereas the major fist-order structures have provided the conduits for auriferous fluids. They also suggested that the structural control in orogenic gold deposits is resulted by a failure of more competent rock units and reactivation and dilation of pre-existing structures which leads to enhanced fluid migration and focussing into sites of favourable for gold precipitation such as structural (e.g. the hinge zones and back limbs of the anticlines; Groves et al., 2018) and geochemical traps (e.g. competent and reactive lithological units; Eilu, 2015). Typically, orogenic gold deposits are flat, lense-shaped and lineated as result of the latest regional deformation, and they usually consist of several gold lodes along the structure. The length of the ore bodies may vary from tens of meters to over a kilometre with a width of 0.5-10 meters (Eilu, 2015).

3.1.3 Hydrothermal alteration

The hydrothermal alteration in orogenic gold systems are characterised typically by sericitisation and carbonatisation at lower-greenschist to mid-greenschist facies conditions, biotitisation and carbonatisation at upper-greenschist to lower-amphibolite facies conditions and biotitisation and formation of calc-silicate and K-feldspar in higher metamorphic conditions (Eilu, 2015). Typical elements enriched in the ore and alteration halos in case of orogenic gold deposits are Ag, As, Au, Bi, CO_2, K, Rb, S, Sb, Se, Te, and/or W (Nurmi et al., 1991). Mass balance calculation have shown that elements Al, Cr, Ni, P, Ti and Zr were immobile in the alteration halos whereas Ba, Bi, CO_2, Cu, K, Rb, S, Sb, Te and W were enriched and, Na, Li and Sr depleted (Eilu, 2015).

3.1.4 Ore minerals

Ore in the orogenic gold systems contain typically 1-5 vol-% of sulphides: pyrite and arsenopyrite in greenschist-facies rocks, and pyrrhotite, löllingite and arsenopyrite in rocks of higher metamorphic grade (Eilu and Pankka, 2009 according to Eilu, 2015). Other ore minerals such as chalcopyrite, sphalerite and galena may occur as minor constituent in orogenic ore deposits. Gold is usually the sole economic commodity in the orogenic gold deposits, and it occurs most commonly in its native form in fractures within and between sulphides and gangue minerals (Eilu, 2015).

3.1.5 Type example

Several Archean and approximately 30 Palaeoproterozoic rock hosted orogenic gold deposits in Finland have been detected with varying sizes from 0.04 to 64 Mt and grades 1-15g/t Au. The largest orogenic gold deposit is Suurikuusikko in Kittilä, in the south-western Lapland with ca. 138 t remaining ore reserves and 410 t total gold production (at the end of the 2018; Agnico Eagle, 2019), being the largest gold deposit in Europe. Most of the orogenic deposits of Finland have resources less than 1 t Au (Eilu, 2015).

3.2 Orogenic gold deposits with atypical metal associations

Several gold deposits in Finland that have characteristics of typical orogenic gold deposits, also show anomalous concentration of other elements such as Ag, Cu, Co, Ni, Sb and U. These kind of gold deposits and occurrences are called “Orogenic gold with atypical metal association” (Eilu, 2015). Whereas orogenic gold deposit has pyrite, pyrrhotite and arsenopyrite associated with the mineralisation, an orogenic gold deposit with atypical base metal associations may contain substantial amounts of cobaltite, chalcopyrite, pentlandite, gersdorffite and stibnite (e.g. Eilu et al., 2007). In Finland, these atypical deposits seem to be concentrated within the Palaeoproterzoic supracrustal belts, including Central Lapland, Kuusamo and Peräpohja belts (Molnár, 2019).

3.2.1 Composition of the ore forming fluid

The origin of enriched base metals in orogenic gold deposits have been explained mainly by a different composition of ore forming fluids. According to Goldfarb et al. (2001), the base metal enriched fluids have turned into anomalously saline as a result of deformation of an older intracratonic basin during Palaeoproterozoic tectonism. Yardley and Graham (2002) in turn, suggested that an orogeny mobilised initially base metal enriched basinal fluids, formed for example by seafloor hydrothermal or diagenetic process, under moderate to high-grade metamorphic facies. There are still many questions on how the possibly initially metal-bearing occurrences, their pre-orogenic deformation and finally the re-deformation and mobilisation during orogenic processes have affect to the deposition of base metal enriched gold deposits (Eilu, 2015).

3.2.2 Type examples

In the Central Lapland, there are several metal-rich gold occurrences which can be classified as orogenic gold deposit with atypical metal association. All the gold occurrences with base metal enrichment have copper as a potential commodity, like in the case of Saattopora deposit where copper was mined along with gold (Eilu et al., 2007). Komatiite-hosted or near komatiites occurring deposits may have significant and profitable volumes of Ni and Co sulphides, and therefore it has been suggested that the base metals have a local origin. Gold deposits with atypical metal associations in the CLB are characterised by carbonatisation and albitisation prior to mineralisation and fluid salinities of 10-25 wt-% NaCl (Eilu, 2015). In addition to high salinity fluids, low-salinity CO_2-H_2O fluids have been detected in the orogenic gold deposits with atypical metal association which reflects variable sources of hydrothermal fluid (Molnár, 2019). Mineralisation of these deposits took place during the late regional metamorphism based on the structural relationships (Eilu, 2015).

Gold occurrences with atypical metal associations have been detected in the Kuusamo and Peräpohja belts, locations shown in Figure 1. In the Kuusamo belt (KB), several gold occurrences are characterised by Au-Co ± Cu ± U ± LREE mineralisation (e.g. the Juomasuo Au-Co deposit; Vasilopoulos et al., 2019). Historically, the gold occurrences in the KB have classified into various types of deposits such as orogenic gold with atypical metal associations, iron-oxide-copper-gold (IOCG), syngenetic or Blackbird-

type deposits (Eilu, 2015). Eilu (2015) classified them as the “Kuusamo-type” deposits relating to their unique features of having many similarities with orogenic and Blackbird type gold deposits, but also atypical features including the fineness of gold, which does not fit into any of those deposit models.

In the Peräpohja belt (PB) there are two types of gold occurrences detected: Au-Cu in quartz veins and Au-U mineralisation in multiply veined and altered supracrustal rocks (Eilu, 2015). Both types are clearly epigenetic and usually classified as orogenic gold deposits with anomalous metal associations, but the genetic types of these deposits are uncertain (Eilu, 2015). Ranta (2018) suggested the characterisation of the Rompas-Rajapalot Au-U mineralisation in the PSB fit neither orogenic gold nor intrusion-related gold origin and recommended to use a term “Rompas-Rajapalot type Au”.

3.3 Volcanogenic massive sulphides (VMS)

The VMS deposits have a markable high polymetallic content with major enrichments of Cu, Zn, Pb, Ag and Au and, substantial amounts of Co, Cn, Se, Mn, Cd, In, Bi, Te, Ga, Ge, As, Sb and Hg (Galley et al., 2007). There are different classifications of the VMS deposits based on base metal content, gold content and host-rock lithology. According to Poulsen and Hannington (1995) the classification includes two groups: normal VMS and Au-rich VMS where the latter is defined based on the numerically greater abundance of Au in ppm comparing to combined abundance of base metals Zn±Cu±Pb in wt-% (see Galley et al., 2007).

3.3.1 Composition of the ore forming fluid

In case of the VMS deposit, fluid originating from seawater is the dominant mineralising agent and its circulation in the VMS system is driven by magmatic heat (Shanks, 2012). According to Ridley (2012), the salinity of ore forming fluid in the VMS system is typically close to that of seawater (3-6 wt-% NaCl) but enhanced salinities have also been detected in the fluids modified from seawater. He also noted that in some cases, very high salinities and low-salinity vapor phases have been detected in fluid inclusion studies and they are usually interpreted as results of boiling fluids and related phase separation.

According to an excellent summary provided by Shanks (2012), the most abundant complexing ligand in the VMS systems is chloride Cl^- followed by sulphate SO_4^{2-}, bicarbonate HCO_3^-, bromide Br^- and borate $H_3BO_4^-$, based on the availability and concentrations. He also suggested that magmatic water and related volatiles play a minor role in formation of the VMS deposits. Magmatic gases consist mainly of water (~90 mol-%) but also CO_2 (5-10 mol-%), SO_2 (1-2 mol-%) and lesser amounts of HCl, H_2 and HF and thus, the addition of magmatic fluid in the mainly hydrothermal VMS system may increase carbon and sulphur contents and, some fluid inclusion studies have indicated that the magmatic source of fluid may be significant in providing metals in the VMS systems.

3.3.2 Precipitation

Volcanogenic massive sulphide deposits are formed in extensional settings related to oceanic seafloor spreading and arc environments near or at the seafloor, and in association with submarine volcanism (Galley et al., 2007). The dominating factor controlling the precipitation in the VMS systems in the decreasing temperature as a result of mixing a hot rising hydrothermal fluid with a cold sea water (Pirajno, 2009). The VMS deposits consist of typically strata-bound massive or semi-massive sulphide lenses which are commonly underlain by a sulphide-silicate stockwork. However, the deposits may vary greatly in size, morphology, and composition. These factors are controlled by syn-volcanic faulting, lithology of footwall and host rock, depth of water, temperature gradients and, intensity of hydrothermal processes (Galley et al., 2007).

3.3.3 Hydrothermal alteration

Hydrothermal alteration associated with the VMS vary in a district- and even deposits-scale (Shanks, 2012). The stockwork system of the VMS deposits is typically characterised by a wide extensive alteration halo which has formed as a result of an interaction between the rising hydrothermal fluids, circulating seawater and surrounding rocks. The extension of the stockwork system and associated hydrothermal alteration may reach several hundred meters (Galley et al., 2007). Alteration styles in VMS deposits includes argillic, advanced argillic, sericitic, chloritic and carbonate propylitic alteration styles, and the alteration is typically characterised by zonation (Shanks, 2012). The proximal alteration zone, associated with the core of the stockwork, is characterised by a

zone of Fe-chlorite-quartz-sulphide±sericite±talc minerals followed by a wider zone of Fe-Mg-chlorite-sericite, and an outermost zone of sericite-phengite-Mg-chlorite±carbonate±barite±albite (Galley et al., 2007). In some cases, distal low-temperature alteration assemblages are not able to be distinguished from the mineral assemblages produced by regional greenschist facies metamorphism (op.cit.).

3.3.4 Type examples

Although the VMS deposits provide a significant source of base metals worldwide, some of the VMS deposits can be considered also a world-class gold deposit including for example the Au-rich VMS deposits Horne and LaRonde in Canada with resources of 330t and 258Mt gold (Galley et al., 2007). In Finland, there are several Au-rich VMS deposits and prospects with gold as a major commodity (e.g. The Iijärvi Au-Ag-Cu-Zn-Pb deposits in Uusimaa area and Haveri Au-Cu deposit in Tampere; Eilu, 2015). However, there are also deposits with characteristics of syngenetic VMS and possibly SEDEX deposits which seem to be overprinted by a later orogenic gold event (e.g. at Riikonkoski in the CLB; Eilu, 2015). However, due to a lack of radiometric dating, it is hard to solve the genetic issues of these overprinted, almost completely deformed metamorphic rocks. In many cases, these genetically complicated deposits have been classified to have been produced by two different mineralisation events (Eilu, 2015).

Table 3. Other gold deposit types with typical metal associations, formation environment, key features and type examples.

Deposit type	Metal association	Formation environment	Key features	Example	Literature (and references therein)
Carlin type	Au-As-Sb-Tl-Hg-Ag	Extensional settings following earlier subduction-related processes, in depth of 0.3-5 km	Similar features with orogenic gold deposit. Reduced, low-salinity H_2O-CO_2 fluid with moderate temperature 150-250°C, metamorphic fluid possibly mixed with meteoric water. Typically associated with carbonate-rich sedimentary rocks	Nevada districts, USA	Hofstra and Cline (2000), Cline et al. (2005), Robb (2005)
Porphyry Au	Au(-Cu-Mo)	Above active subduction zone at convergent plate margins, in depth of 1-5 km	Oxidised, I-type or "calc-alkaline" magmas. Weak preservation potential regarding the shallow formation depth.	Grasberg, Indonesia	Sillitoe (2010), Eilu (2015)
Reduced intrusion related gold system	Au-Bi-Te-W	After an active orogeny and peak metamorphism behind an accretionary orogenic system, in depth of 4-6 km	Associated with ilmenite-series granitoids with moderately low oxidation state. Multiple mineralisation styles such as veins, skarns, disseminations, stockworks, replacements and breccias.	Fort Knox, Alaska Dublin Gulch, Canada	Lang and Baker (2001), Hart (2007), Hart and Goldfarb (2005)
Epithermal Au	Au-Ag (Cu, Pb, Zn)	Extensional settings, active volcanism in island- and continental arc setting and volcanic centres, in depth of ≤ 1.5 km	Low-, intermediate- and high-sulphidation subtypes: each subtype has own characteristics of alteration, textures, occurrences, and associated metal contents. Weak preservation potential regarding the shallow formation depth	Blackdome and Toodoggone River camp, British Columbia Kutemajärvi, Tampere, Finland	Taylor (2007), Eilu (2015)

Table 3. (continued)

Deposit type	Metal association	Formation environment	Key features	Example	Literature (and references therein)
Placer and palaeoplacer gold	Au(-U-PGE)	Eluvial, alluvial, beach and aerolian environments	Sedimentary gold deposit, formation driven by hydrodynamic mechanism.	Witwaterstrand, South Africa Kumpu conglomerates, Sodankylä, Finland	Boyle (1979) Robb (2005)
Iron Oxide Copper Gold (IOCG)	Fe-Cu-Au	Anorogenic tectonic settings with magmatism and associated hydrothermal activity, plumes and/or mantle underplating as driving forces, in depth of >10 km	Copper with or without gold as economic commodities, strong structural control and style of hydrothermal ore. Abundant magnetite and/or hematite. Temporal, not spatial association with igneous intrusions	Olympic Dam, south Australia Kolari district, Finland	Williams et al., (2005) Groves et al., (2010) Eilu (2015)

4 REGIONAL GEOLOGICAL SETTINGS

4.1 Central Lapland belt

Central Lapland belt (CLB, previously called Central Lapland Greenstone belt) is one of the three greenstone belts in the northern Finland. The CLB continues to northern Norway, Sweden and Russian Karelia. It covers approximately an 100x200 km area (Hanski and Huhma, 2005), and it is the largest Palaeoproterozoic greenstone terrain in Finland (Hölttä et al., 2007). The CLB consists of multiply sequences of Palaeoproterozoic metavolcanic and metasedimentary rocks overlaying the Archean basement. The CLB has formed during a complex tectonic history of several hundreds of million years between ca. 2.45 Ga and 1.88 Ga (Hanski and Huhma, 2005).

According to Lehtonen et al. (1998), the Palaeoproterozoic lithostratigraphic units in the CLB include Salla, Onkamo, Sodankylä, Savukoski, Kittilä, Lainio and Kumpu group. However, the Onkamo group has been recently re-named as Kuusamo group and Kittilä group as Kittilä suite (Luukas et al., 2017). The Lainio and Kumpu groups were united as Kumpu group by Hanski and Huhma (2005). In addition to the Archean basement and supracrustal rocks of the CLB, three stages of magmatism at 2.44 Ga, 2.22 Ga and 2.05 Ga are identified from the area and are represented as sills and mafic-ultramafic layered intrusions with economic potential (Hanski and Huhma, 2005). The lithostratigraphic units and their distribution in the CLB are presented in Figure 2.

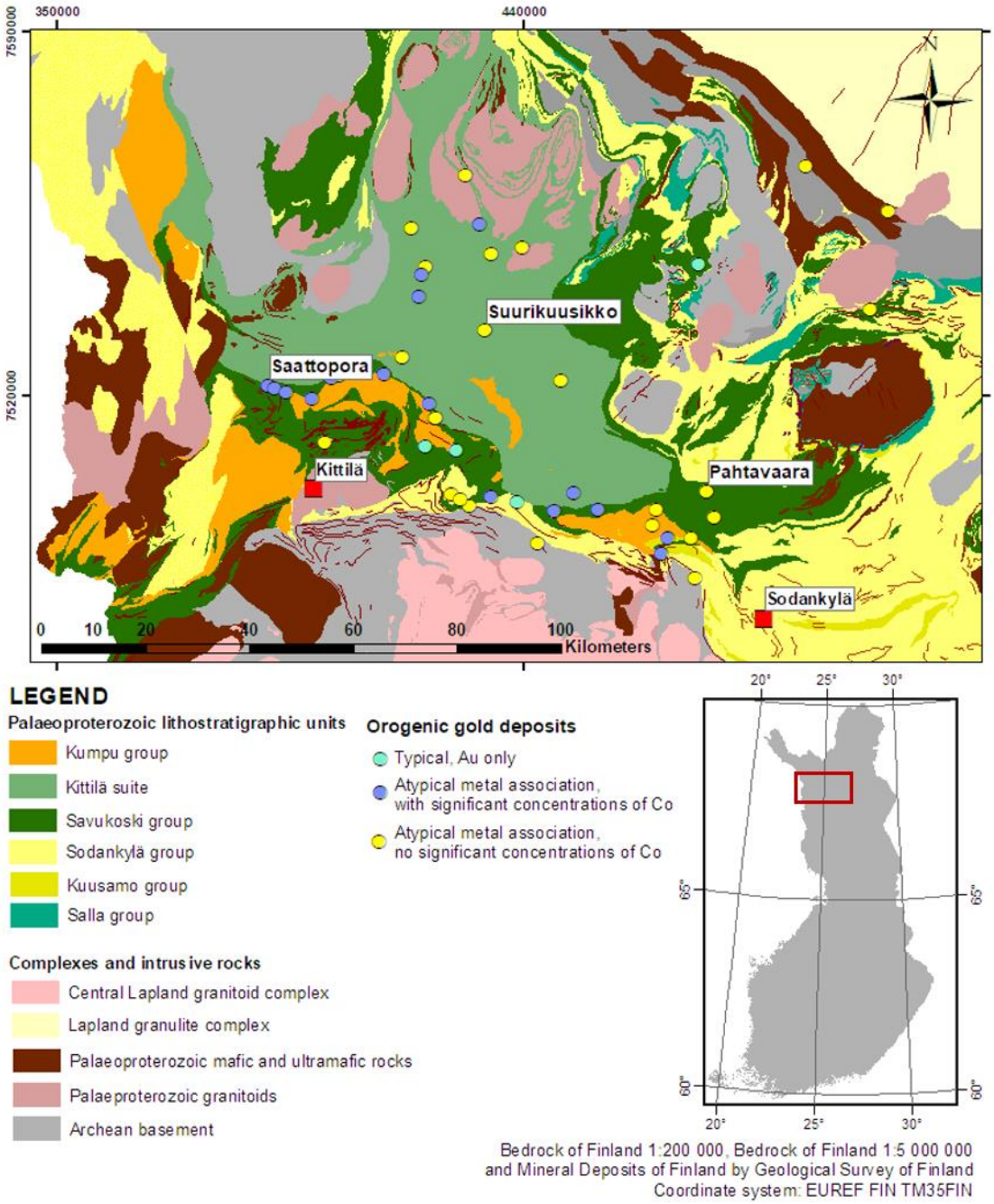

Figure 2. Distribution of lithostratigraphic units and orogenic gold deposits in the Central Lapland belt. Modified after the DigiKP version 2.0 of Bedrock of Finland 1:5 000 000, version 2.1 of Bedrock of Finland 1:200 000 and version 1.0 of Mineral Deposit of Finland.

4.1.1 Development of the Central Lapland belt

Evolution of the Central Lapland belt started at ca. 2.45 Ga, lasting approximately 600 Ma and culminating in orogenic deformation at ca. 1.90 Ga (Hanski and Huhma, 2005). Formation of the Palaeoproterozoic units began with a rifting of the older Archean craton producing andesite lava flow and intermediate and felsic tuffs forming Salla group

subaerially erupted volcanic rocks. The Salla group is disturbed by Koitelainen layered intrusion (ca. 2.44 Ga; Mutanen and Huhma, 2001) which gives a minimum age for the Salla group rocks. The composition of magma became more basic after the formation of Salla group rocks and Kuusamo group crustal contaminated komatiites, mafic volcanic rock and siliceous high-Mg basalt were formed. The rifting-related magmatism slowed down, and the environment was suitable for sedimentary rocks to deposit (Hölttä et al., 2007). Sodankylä group rocks consist typically of mica schist, arkosic-quartzites and carbonate rocks which are ca. 2.20 Ga at their minimum age based on age determinations of mafic-ultramafic sills of the gabbro-wehrlite association (Hanski, 1986, according to Hölttä et al., 2007) intruding the Sodankylä group sediments (Hölttä et al., 2007). The depositional basins became deeper which allowed fine-grained sediments such as black schist and phyllites of the Matarakoski formation to settle down. These pelitic metasedimentary rock are overlain by mafic and ultramafic volcanic rock of Sattasvaara formation. The Matarakoski and Sattasvaara formations are included to the Savukoski group with a minimum age of 2.05 Ga based on the age constrain of Kevitsa layered intrusion that is penetrating the rocks of Savukoski group (Hölttä et al., 2007).

The above-mentioned groups have a tectonic contact at the west with the Kittilä suite rocks which include different types of volcanic rocks formed in an oceanic environment and, chemical sediments (e.g. cherts, manganiferous carbonate rocks; Hanski, 1997). The Kittilä suite is also considered be an ensialic autochtonous unit instead of allotchtonous according to Sorjonen-Ward et al. (1997) (see Patison, 2007). At ca. 1.97 Ga, the rifting culminated to large scale volcanism and formation of oceanic crust (Eilu et al., 2007). Lainio and Kumpu group sedimentary rocks overlay all the older rocks but with unconformities. According to Hanski et al., (2000), ages of the latter groups are less than 1.88 Ga based on the age determinations of the molasses-types sediments (see Hölttä et al., 2007).

Several granitic intrusions have been found in the CLB. The oldest Proterozoic intrusion found in the Central Lapland is the Niilipää granite intrusion with an age of ca. 2.10 Ga (Huhma, 1986), located in the north of Central Lapland granitoid complex. Granodiorites, monzonites and deformed tonalities of the Haaparanta suite (1.89-1.85 Ga; Lehtonen et al., 1998), in the western side of Central Lapland and from the Sodankylä area (Räsänen and Huhma, 2001). These intrusions are considered to represent the same Svecofennian accretional tectonic event (Hölttä et al., 2007). Ca. 1.80 Ga Hetta granites are situated in the northern part of Kittilä (Huhma, 1986). The youngest granitic intrusions of

Palaeoproterozoic eon are Nattanen-type post-orogenic granites with an age of 1.77 Ga (op.cit.).

According to Lahtinen et al. (2003), the evolution of the region after 1.92 Ga includes 1) microcontinent accretion during 1.92-1.80 Ga, 2) continental extension during 1.88-1.85 Ga, 3) continent-continent collision during 1.85-1.79 Ga and 4) collapse of orogeny and stabilisation during 1.80-1.70 Ga (see Eilu et al., 2007). All these epochs have potential for orogenic gold mineralisation in northern Finland (e.g. Eilu et al., 2007). Sorjonen-Ward et al. (2003), in turn, suggested that two major orogenic epochs in the CLB are 1) collision and compression of crustal plates at 1.91-1.86 Ga and 2) deformation and regional metamorphism at 1.84-1.80 Ga. The latter is most significantly related to the orogenic mineralisation (see Eilu et al., 2007).

4.1.2 Stratigraphic units

The Salla group represents the lowermost lithostratigraphic unit of the Central Lapland belt, overlying the Archean basement. It occurs mostly in the south-eastern part of the CLB and extending over the Russian border (Hanski and Huhma, 2005). The succession began with a basal volcanoclastic conglomerate containing clasts of rounded Archean rocks (Peltonen et al., 1988, according to Hanski and Huhma, 2005). The composition of the Salla volcanic rocks vary from intermediate to felsic and the primary minerals indicate of upper-greenschist facies regional metamorphism. The Salla group metavolcanics rocks are found in layered intrusions of Akanvaara and Koitelainen whereas they are missing in the western parts of the CLB (Hanski and Huhma, 2005). U-Pb analyses on zircons at Koitelainen and Akanvaara yielded a minimum age of ca. 2.44 Ga (Mutanen and Huhma, 2001) of the Salla group rocks.

The Kuusamo group is comprised of intermediate to ultramafic volcanic rocks with a more primitive composition compared to Salla group volcanic rocks. Although the Kuusamo group rocks are widely distributed in the CLB, they are discontinuous. In the Salla area, the Salla group volcanics are underlain by Kuusamo group volcanics whereas at Möykkelmä, in Sodankylä, the Kuusamo group rocks are situated directly on the top of Archean basement (Räsänen et al., 1989). Based on the geochemical composition and geological position of the Kuusamo group rocks, there is a correlation between them and the Vetreny belt komatiites and dacite in Russian Karelian with ages of 2449 ± 35 Ma, 2410 ± 34 Ma and 2437 ± 3 Ma (Puchtel et al., 1997). Due to the small difference in ages

of the Salla and Kuusamo group volcanics, it seems that both have formed during the same magmatic event (Hanski and Huhma, 2005).

The magmatism which produced the Salla and Kuusamo group metavolcanics rocks was followed by a tranquil period during which the Sodankylä group sedimentary rocks formed (Hanski and Huhma, 2005). The Sodankylä group rocks located in the eastern and southern side of the Kittilä greenstone area. The rocks consist mainly of quartzites, carbonate rocks, and mica schists which are deposited on the top of the previous volcanic rocks or directly on the top of the Archean basement (Hölttä et al., 2007). The Sodankylä group quartzites have typically a greenish tint due to the abundance Cr-bearing fuchsite. The group includes also carbonate rocks such as dolomites with stromatolitic structures, and metavolcanic lava units with mainly mafic composition and a thickness of some tens of meters. The age determination of differentiated mafic sills (e.g. 2222+6 Ma Harjunoja formation; Mutanen and Huhma, 2001) which penetrate the base of Sodankylä group sedimentary rocks gave a minimum age of the group (Hanski and Huhma 2005).

After the formation of clastic Sodankylä group metasedimentary rocks, the deposition of fine-grained Savukoski group metasediments took place. Based on the lack of sharp hiatus between these two groups of metasedimentary rocks, it seems that the deepening of the depositional basin occurred gradually. The Savukoski group metasedimentary rocks include mafic tuffites, phyllites and black schists, but also lava beds within the pelitic metasediments. The komatiitic rocks are present at the Sattasvaara formation in Sodankylä, Kummitsova in Savukoski and Jeesiörova in Kittilä whereas the picritic rock can be found in Sotkaselkä area. The Sattasvaara komatiites are characterised by highly altered mineralogy but they are still presenting the primary structures like pillow and massive lavas and, volcaniclastic rocks (Hanski and Huhma, 2005). Saverikko (1985) classified Sattasvaara komatiites into komatiitic basalts, (basaltic) komatiites and komatiites based on the MgO contents. According to Lehtonen and Rastas (1988), and Räsänen et al. (1989), ultramafic Sattasvaara komatiites are depleted in Al, LREE and HREE. Near the Sirkka shear zone the komatiitic rocks show an intense carbonatisation producing deep-green Cr-bearing marbles (Hanski and Huhma, 2005). The minimum age of ca. 2.06 Ga for the Savukoski group is determined from the cutting Kevitsa layered intrusion (Mutanen and Huhma, 2001).

The Kittilä suite consists of a large volume of mafic volcanic rocks, serpentinites, felsic intrusions and minor sedimentary rocks. The Kittilä suite mafic metavolcanics rocks cover an area of 2600 km^2 in Kittilä which is called as the Kittilä greenstone complex

(Hanski and Huhma, 2005). The Kittilä suite metavolcanics rocks can be divided into two genetically unrelated formations by their mode of occurrence and geochemistry: Vesmajärvi and Kautoselkä formations (Hanski and Huhma, 2005). The former consists of different types of submarine metavolcanics rocks with a composition of tholeiitic basalt whereas the latter has a composition of more evolved, Fe-rich tholeiitic basalt and andesite (Lehtonen et al., 1998). The whole-rock and pyroxene analyses of the Vesmajärvi tholeiitic lavas have yielded an age of 1987 ± 36 Ma (Hanski and Huhma, 2005). The felsic porphyries occurring as subvolcanic dikes, lavas and crystal tuffs, are associated with mafic rock units in the western part of Kittilä greenstone area. By their volume, the felsic rocks are minor but geotectonically significant based on the field relations, which suggested that the basaltic and acidic magmatism producing the mafic and felsic rocks were coeval (Lehtonen et al., 1998). The metasedimentary rocks of the Kittilä suite include phyllites, metagraywackes, graphite- and sulphide-bearing schist and carbonate rocks. Additionally, banded iron formations are associated with the Kittilä suite metasedimentary rocks in Porkonen formation (Hanski and Huhma, 2005).

The Lainio group metasedimentary rocks overlay the above-mentioned stratigraphic groups forming fells and hills Aakestunturi and Ylläs. Kumputunturi and Levi in Kittilä, Kaasestunturi in Sodankylä and Pyhätunturi in Pelkosenniemi, in turn, are included to the Kumpu group. Together both groups form 200-2000 m thick unit comprising quartzites, conglomerates, graywackes, meta-arkoses and siltstones. The Lainio group has considered to be older than the Kumpu group because of the latter does not show evidences of the earliest deformation phases of Svecofennian orogeny (Lehtonen et al., 1998). However, Hanski and Huhma (2005) suggested that it is evident that the deposition of the both groups took place at post-1.88 stage of the development of the CLB and therefore, they started to treat the groups as one, the Kumpu group.

The litostratigraphic units of the Central Lapland belt (Figure 3) are penetrated several times by mafic intrusions and sills with ages of ca. 2.44, 2.22 and 2.05 Ga (Hanski and Huhma, 2005). Two layered intrusions, Akanvaara and Koitelainen with substantial reserves of chromite, are related to mafic intrusions formed at ca. 2.44 Ga and approximately the same U-Pb zircon ages indicate that their formation was coeval (Mutanen and Huhma, 2001). At the time of ca. 2.2 Ga, mafic differentiated sills were intruded into the Sodankylä Group quartzites. Piispanen (1972) classified theses sills as albite diabases but Hanski (1986, 1987), in turn, suggested the sills to be most likely a gabbro-wehrlite association (see Hanski and Huhma, 2005). Sills with the same age have

been detected in Jatulian quartzites and their Archean basement in the eastern Finland and the Peräpohja belt (e.g. Hanski, 1987; Perttunen and Vaasjoki, 2001). However, the sills with that age are missing elsewhere in the Fennoscandian Shield and, therefore, the magmatic stage forming the sills was short-lived and it did not form intrusions with economic potential (Hanski and Huhma, 2005). Mafic intrusion with an age of ca. 2.05 Ga are found in many locations in northern Finland, especially associated with the Savukoski group rocks (Rastas et al., 2001). The differentiated mafic-ultramafic Kevitsa Ni-Cu deposit with a significant size and economic commodities is included the mafic intrusions of this age (Mutanen and Huhma, 2001).

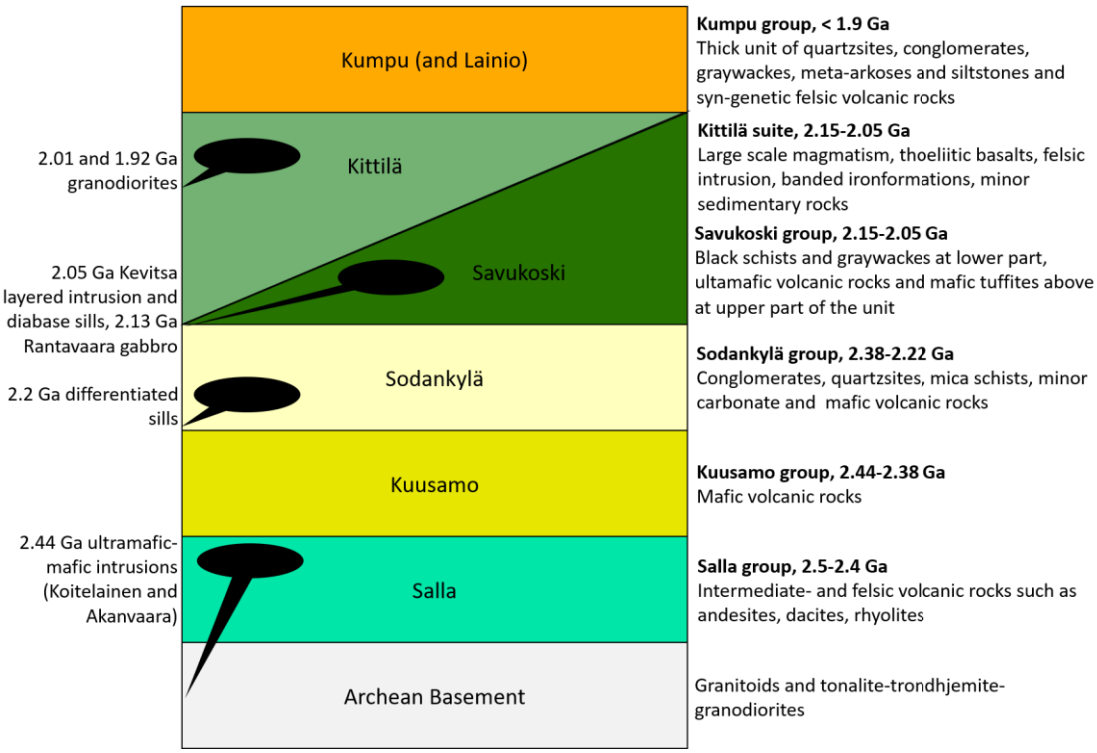

Figure 3. Lithostratigraphic units of Central Lapland belt after Köykkä and Luukas (2019) and references therein.

4.1.3 Gold occurrences

During 1985-2004, over 60 gold occurrences with a grade > 1 g/t have been reported in the Palaeoproterozoic belts in northern Finland. Most of the occurrences are classified as orogenic gold with or without atypical metal association, IOCG and palaeoplacer gold deposits. Regionally, the structural control is strong but locally, the type of host rock has a significant role. (Eilu et al., 2007)

In many cases, gold deposits and occurrences in the CLB are spatially connected with the Sirkka Shear Zone (SSZ), usually within 0.2-2.0 km distance (Eilu, et al., 2007). The SSZ

is a long-lived, crustal-scale shear zone with several parallel faults (e.g. Patison, 2007). Some drilling-indicated gold occurrences are associated directly within the SSZ which has, in fact, gold anomalies along its whole length, but major gold deposits are located in higher-order shear or fault zones originating from the SSZ with a distance of 3 km (Eilu, 1999, according to Patison, 2007) from the main structure. A typical feature of the SSZ and related gold mineralisation is the intense alteration such as albitisation, sericitisation and carbonatisation (Eilu et al. 2007).

Saattopora gold deposit is located at the western trending section of the SSZ. It is hosted by metasedimentary and metavolcanic rocks of the Savukoski group and Kittilä suite and, has been under mining during 1988-1995 producing a total of 6278 kg of gold and 5177 t of copper (Korvuo, 1997). Other Au-Cu mineralisation within the SSZ are Sirkka kaivos and Sirkka W. (Eilu et al. 2007).

Most of the significant gold occurrences in the CLB are related to the SSZ by strike-slip faults or re-oriented pre-existing thrusts (e.g. Patison 2007). The NNE-trending Kiistala shear zone is hosting the largest gold deposits of Europe, the Suurikuusikko gold deposit with approximately 410 t total gold production and 138 t remaining ore reserves (at the end of the 2018; Agnico Eagle, 2019) hosted by the Kittilä suite mafic metavolcanic rocks. The Kiistala shear zone is extending approximately 30 km in which 15 km is anomalous in gold (e.g. Härkönen, 1992, 1997; Eilu et al., 2007). Other gold occurrences, not within the SSZ but in minor shear zones connected with it, are found at Kaaresselkä in Sodankylä hosted by the Savukoski group volcano-sedimentary rocks, and at Kuotko within Kuotko shear zone in the north of the Suurikuusikko, hosted by the Kittilä suite metavolcanic rocks (Eilu et al. 2007).

4.2 Pahtavaara gold deposit

4.2.1 Discovery and mining history

Pahtavaara gold deposit was discovered in 1985 by the Geological Survey of Finland. The gold anomalies were detected in a detailed till survey after the previous discoveries of significant Ni-Cu-Co-Pb anomalies in the regional till survey. The subsequent drilling of weathered bedrock, lithogeochemical studies of exposures and exploration trenches resulted the discovery of a wide, hydrothermally altered Pahtavaara alteration zone with

increased gold concentration with approximately 100x600m in extent. (Korkiakoski et al., 1987, according to Korkiakoski, 1992)

During the Pahtavaara mining history 1996-2000 and 2003-2014 approximately 10 t of gold was mined from three open pits and underground (2006-2014) by three mining operators: Terra Mining Oy 1996-2000, Scan Mining Oy 2000-2008 and Lapland Goldminers Oy 2008-2014 (Rupert Resources, 2018). After a bankruptcy of the latest mining operator, the ownership of Pahtavaara mine has been held by Rupert Resources Oy which has focused on the regional exploration in addition to geological study of the mine site.

4.2.2 Geological settings

The Pahtavaara gold deposit is in the eastern part of the Central Lapland belt (Figure 1). It is hosted by variable altered pyroclastic komatiites of the Sattasvaara formation, in the Savukoski group (Korkiakoski, 1992). The formation of the Sattasvaara komatiite complex is interpreted to have occurred in an E-striking rift-system (Räsänen, 1999, according to Patison, 2007). An inherent crustal weakness of the host rock provided by extension-related structures of the Sattasvaara komatiites, has probably played a significant role in the later deformation stages (Patison, 2007). As mentioned earlier, some of the gold occurrences in the CLB are associated immediately adjacent to or within 3 km from the Sirkka shear zone (Eilu, 1999, according to Patison, 2007). However, the Pahtavaara gold deposit is situated in a structurally more complicated location. The location of the Pahtavaara gold deposit is also connected to a shear zone with interpreted strike-slip movements but it is not known if the shear zone is generated or reactivated during the D_3 deformation stage of the CLB (Patison, 2007). Sorjonen-Ward et al. (1992) suggested that the hosting shear zone was evolved during a reorientation of a regional strike-slip foliation D_3, but on the other hand, due to the nature the host shear zone and the timing of the mineralisation, ~1.85-1.82 Ga (Mänttäri, 1995), the formation of the Pahtavaara gold mineralisation may be related to a late event of the D_3 stage (see Patison, 2007). Nonetheless, Korkiakoski (1992) noted that the earlier timing for the gold mineralisation, even related to a sea floor alteration during the pre-orogenic volcanism stage, cannot be dismissed when considering the origin and age of the Pahtavaara gold mineralisation.

4.2.3 Lithological units

The Sattasvaara komatiites have been classified into three rock types: 1) amphibole-chlorite schists 2) biotite schists and 3) coarse-grained and non-schistose amphibole rocks and associated quartz-barite veins, lenses and irregular pods. The former type represents the least altered komatiites with amphibole-chlorite alteration assemblages as a result of regional greenschist facies metamorphism and it is the dominant rock type outside the Pahtavaara alteration zone. They occur rarely in the Pahtavaara alteration zone and if so, commonly as talc and carbonate-rich varieties. The latter two rock types represent the intensively altered lithological groups. All the rocks types in the Pahtavaara area are characterised by mineralogical and geochemical gradations. (Korkiakoski, 1992)

The vein types of the area are divided into two main groups: 1) talc-carbonate ± pyrite veins and 2) quartz-veins and pods. The veins of the first group occur within all three rocks types but are most abundant in the biotite schists. The latter group is commonly the one associated with the native gold. Locally, amphiboles may occur also as veins in addition to forming the main lithological units for example when replacing the talc-carbonate precursors. Light-coloured and coarse-grained amphiboles may be also be present in quartz-barite veins. A notable feature of the vein mineralogy in Pahtavaara is that the quartz veins are relatively rare although they characterise many hydrothermal gold deposits. (Korkiakoski, 1992)

The amphibole-chlorite rocks are relatively homogeneous in their composition. They are characterised by high MgO (ca. 24-26%) and low CO_2, K_2O, N_2O and Ba contents. Based on the definition of komatiite composition after Arndt and Nisbet (1982), high Cr and Ni contents and, low TiO_2 and alkali contents are consistent for the komatiitic composition of the Sattasvaara volcanic rocks. Nesbitt et al. (1979) in turn, classified the komatiites into Al-depleted and Al-undepleted types: the former type is characterised by low Al_2O_3/TiO_2 ratio and high CaO/Al_2O_3 whereas the latter has high Al_2O_3/TiO_2 ratio and CaO/Al_2O_3 ratio close to unity. The low Al_2O_3/TiO_2 ratios of both the Pahtavaara and Sattasvaara komatiites indicate of the Al-depleted type of komatiites (e.g. Räsänen et al, 1989). Additionally, the low LREE and HREE contents of Pahtavaara rocks are suitable for the Al-depleted type komatiites (Korkiakoski, 1992). However, the CaO/Al_2O_3 ratio of the Pahtavaara komatiites is close to unity and which indicates of the Al-undepleted type komatiites. On the other hand, the Al_2O_3/TiO_2 ratio of the Pahtavaara komatiites may be low due to higher TiO_2 content instead of the depletion of Al and taking this into

account, the Pahtavaara komatiites may originally be Ti-enriched Al-undepleted komatiites (Korkiakoski, 1992).

The biotite schists are fine-grained and heterogeneous consisting of variable amounts of dark mica and chlorite. The formation of biotite is typically linked to the regional metamorphism although the effect of sea floor alteration cannot be totally excluded. The distribution of biotite is related to the distribution of chlorite which indicates that the former has replaced the latter during the hydrothermal alteration. The alteration of chlorite to biotite is its greatest adjacent to talc-carbonate ± pyrite veins. In addition to talc-carbonate veins, these minerals can be found as evenly distributed disseminations in the biotite and chlorite dominating units. The amount of magnetite is commonly higher in biotite schists than in the amphibole-chlorite schists and may comprise up to 10 % of the rock. This suggests that at least some of the magnetite was produced by hydrothermal alteration. The biotite schists have relatively higher Fe, K, and Ba and, lower Mg, Si and Ca contents in comparison with the least altered amphibole-chlorite schists. (Korkiakoski, 1992)

The coarse-grained and non-schistose amphibole rock is mineralogically more homogeneous than the other rock types in the area. It consists mainly of amphibole with talc, carbonate, albite and locally abundant quartz and barite as accessory minerals. Pyrite and minor chalcopyrite are commonly associated with quartz-barite veins. Albite-rich veins occur locally. Based on the lack of regional NE-trending schistosity and cross-cutting nature in relation to the other rock types in the area, the amphibole growth postdates the formation of biotite schist and talc-carbonate veining and, took place late in the hydrothermal and metamorphic history. Despite of the homogeneous mineralogical content of the amphibole rock, they are compositionally heterogeneous and can be further divided into 1) high-alumina dark amphibole rocks and 2) low-alumina light amphibole rocks. Generally, the amphibole rock differs from the amphibole-chlorite schist in higher contents of CaO and SiO_2 and lower MgO. (Korkiakoski, 1992)

4.2.4 Hydrothermal alteration

Alteration zone at Pahtavaara can be distinguished from the surrounding komatiites by higher abundances of K, Ba and Sr lower contents of Mg, Co and Zn. (Koskiakoski et al., 1987). Korkiakoski (1992) suggested that all the altered rock types of Pahtavaara have a komatiitic protolith and the mineralogical assemblage presented at Pahtavaara is resulted

by combination of both metamorphic and hydrothermal processes. Comparing to the regional greenschist facies metamorphism of the surrounding rocks, the metamorphic grade of the Pahtavaara gold deposit may locally have reached a higher, amphibolite facies metamorphic grade (Korkiakoski, 1992).

Korkiakoski (1992) divided the hydrothermal processes associated with the Pahtavaara komatiites into two individual stages: 1) biotitisation (potassic alteration) with the coeval formation of talc-carbonate ± pyrite veins and 2) later amphibole overgrowth (calc-silicate alteration) and related quartz ± barite veins and pods. The enrichments, depletions, and related mineral assemblages of the two alteration stages are listed in Table 4. He also suggested that the biotitisation occurred during the regional metamorphism instead of a sea-floor alteration, but the latter option cannot be completely dismissed. The decarbonation and calc-silicate alteration resulting the amphibole overgrowth postdates the biotitisation and associated carbonatisation, and it is considered to have taken place during the later stage of metamorphism and deformation.

Table 4. Enrichments, depletions, and related mineral assemblages of the biotitisation and amphibole overgrowth alteration stages at Pahtavaara after Korkiakoski (1992).

	Biotitisation	**Amphibole overgrowth**
Changes in volume	Decreasing 10-30%	Increasing
Enrichment	Massive introduction of H_2O-CO_2, K and Fe. Minor enrichments of S, Ba, Au, Mn, W, Sr and Te.	Si, Ca, Na, Ba, Au, Te, S, W, P and Sr.
Depletion	Mg, Ca, Na, Zn, Co and minor Si	CO_2, Co, Mg, Fe and Zn.
Mineral assemblages	Biotite-chlorite-magnetite ± carbonate ± amphibole ± albite ± Bi-Te-Se minerals	Amphibole ± chlorite ± talc ± carbonate ± biotite ± albite ± pyrite

Eilu et al. (2007) divided the hydrothermal alteration of Pahtavaara rocks into two stages: 1) partial albitisation and carbonatisation preceding the gold mineralisation and preparing the ground by making the host rocks more competent and structurally more favourable for the gold-bearing fluids to precipitate and, 2) biotitisation, formation of tremolite in breccia zones, and additional carbonation together with the formation of abundant quartz veins and associated gold mineralisation. Mineral assemblage of the latter stage includes biotite-talc-dolomite/ankerite-tremolite/actinolite-quartz-barite-rutile ± barite, albite, richterite, magnetite and tourmaline in the host rock.

4.2.5 Mineralisation

The most common ore minerals in the Pahtavaara deposit are magnetite and pyrite. The former is heterogeneously distributed throughout the deposit but is most abundant in the biotite schists where it can comprise up to 10 % of the rock (Korkiakoski, 1992). Other oxides present in the deposit include chromite, ilmenite, hematite and rutile (Kojonen and Johanson, 1989) but they occur only in small concentrations. Pyrite also show heterogeneous distribution and is the dominant sulphide everywhere in the deposit. However, its proportion is relatively low, commonly less than 1 % of the rock in both amphibole rocks and biotite schists (Koskiakoski, 1992). Other sulphides include pyrrhotite, chalcopyrite, pentlandite and violarite, and they commonly occur as inclusions in pyrite. Rarer ore minerals such as clausthalite, merenskyite and other Bi-Se-Te minerals have been detected in the deposit (Kojonen and Johanson, 1989).

Korkiakoski (1992) suggested that the gold mineralisation took place during the two geochemically distinct alteration stages which are introduced above. The formation of the two alteration and mineralisation types are probably resulted by the evolution of ore forming fluids and the development of shear zones. At the first stage of hydrothermal alteration, biotitisation, the mineralisation is controlled by combination of 1) higher permeability the komatiitic tuffs comparing to the associated pillow lavas and 2) development of the regional schistosity which together provided the channel ways for the gold bearing hydrothermal fluids during the metamorphism. The gold in biotite schist is commonly fine-grained and associated with magnetite and talc-carbonate veins together with pyrite. The gold mineralisation at the biotitisation stage took place during or directly after the peak of metamorphism under greenschist or amphibolite facies metamorphic grade under ductile deformation. (Korkiakoski, 1992)

The second stage of alteration and gold mineralisation event occurred during the amphibole overgrowth postdating the former biotitisation stage. The gold is typically coarse-grained and occurs in its native form. Some gold may be associated with pyrite. The formation of the second gold mineralisation was related to retrograde stage of metamorphism, structurally controlled permeability as a result of late stage shearing under brittle-ductile deformation, and fluid flow. The correlation matrix for gold samples with higher grade than 20 ppb showed a high positive correlation with Au and Ba, and weak correlations with S and SiO_2. The gold had weak negative correlations with CO_2 and MgO. (Korkiakoski, 1992)

Patison (2007) classified two types of mineralisation phases related to the structures in the Pahtavaara deposits occurring in the area of most intensive shearing. The oldest structure hosts the higher-grade mineralisation, occurring within a series of alteration zones dipping 70º to 80º N with an E-strike (Korkiakoski and Kilpelä, 1997). The higher-grade mineralisation is associated with irregularly oriented barite-carbonate-quartz veins and infill breccias. The overprinting structure hosting the lower-grade gold mineralisation is associated within the same alteration zone by a series of NNW-striking and less abundant E-striking quartz-dominated veins. However, it is not clear are these two mineralisation phases related to the same fluid event or not (Patison, 2007).

4.2.6 Genetic model

Different authors have proposed various genetic models for the formation of the Pahtavaara gold deposit. Hulkki (1990) stated in her master thesis that the styles of alteration and mineralisation are results of syn-volcanic fumarolic processes in submarine environment. In papers by Korkiakoski et al. (1989), Ward et. al (1989) and Korkiakoski (1992) proposed that the formation of the gold deposit was probably connected to a wider cratonisation processes related to Svecokarelian orogeny and emplacement of extensive granitoid intrusives at 1.9-1.8 Ga at the late stage of development of the Central Lapland belt. However, Korkiakoski (1992) also pointed out that an earlier timing for the mineralisation, possibly during the sea floor alteration cannot be totally excluded. Eilu et al., (2012) and Eilu (2015), proposed that the genesis of Pahtavaara gold mineralisation may be linked to a VMS-type, metamorphosed seafloor alteration system in which the gold may have been introduced later. However, Eilu (2015) also noted that the features of gold such as grain size, high fineness, free and native form, and occurrences mainly with silicates instead of sulphides indicate of a pre-peak metamorphic timing, which is not typical for orogenic gold deposits.

5 GEOCHEMICAL DATA

5.1 Nature of the geochemical data

Many classical statistical analysis methods require that the data shows a normal distribution. However, geochemical data, or any environmental data, are rarely normally distributed. Reasons for this are that the geochemical data are strongly dependent on other measured values, and the characteristics to be investigated may originate from different processes. (Reimann and Filzmoser, 1999)

Geochemical data are compositional i.e. analytical results of each element are depending on the other measured variables (Reimann et al., 2017). Measurements may be imprecise due to multiple sources of error involved in sampling, sample preparation and analysing process. Analyses below detection limits, typical for example for trace elements, may cause false values. Additionally, the precision may vary due to changes of element concentrations: values may be less precise at very high and low concentrations. The geochemical data are commonly characterised by *data outliers* i.e. strongly skewed samples with unusually high concentration which may originate even from a different population than the main body of data (Reimann and Filzmoser, 1999).

Ahrens (e.g. 1954, see Reimann and Filzmoser, 1999) proposed that a lognormal distribution can be assumed in the case of geochemical data. However, Reimann and Filzmoser (1999) suggested that the lognormal distribution of the data is a rare expectation in geochemistry and using a normal or lognormal distribution as an assumption in statistical treatment of data can lead to significant misconstruction. Non-parametric and robust methods are recommended in statistical analyses of geochemical data in addition to a visual examination of the distribution and outliers before any further statistical analyses (Reimann and Filzmoser, 1999).

5.2 Data visualisation

According to Reimann and Filzmoser (1999), the graphical examination of the distribution and relationship of measured variables is the first thing to do before starting to analyse any datasets. It can be conducted by using a variable graphics such as scatter

plots. If graphical presentation of data shows regularity in distribution, the intense of relationship of the variables can be further studied using correlation factors.

A complete picture of relationships between the variables makes scatter plots an effective tool in the statistical data analyses. They provide significant information about the relationship such as strength, direction and shape presented on biaxial X-Y -diagram. The visual presentation of data provides a sight of outliers and distribution of data and tells if the correlation of the variable is positive or negative. (Hartwig and Dearling, 1979)

5.3 Correlation coefficients

Pearson, Spearman and Kendall correlation methods, named after the first introducers, are used to calculate correlation coefficients between two variables. All these methods give a number between -1 and +1 in which the extreme values indicate of clear correlation whereas number 0 indicates that no systematic relationship exists between the variables. Value of ± 0.5 can be considered to indicate of correlation if the number of samples is high enough. (Reimann et al., 2017)

The Pearson correlation coefficient is the most used correlation method. The method estimates the correlation of true analytical values of the two variables. However, the Pearson correlation coefficient is parametric and expects the results to be linear and normally distributed that the geochemical data rarely represents and therefore, the Pearson method is not recommended for statistical analyses of geochemical data. (Reimann et al., 2017)

The Spearman rank method in turn, is based on non-parametric correlation measurements of two variables which makes it distribution free and more usable for the statistical analyses of geochemical data. Instead of measuring a linear relation between the variables, it estimates if the relationships between the variables is monotonically increasing or decreasing by ranking the values. After ranking, the correlation coefficient is calculated as the Pearson's. Due to the fact that the calculation is conducted with the ranks of the sorted values and not the actual data values, the possible data outliers are not affecting to the results that much and thus, the Spearman method is relatively robust against the data outliers. Another significant advantage of this method is that the results do not have to be log-transformed because it would not change the order of data-value ranking. (Reimann et al., 2017)

Kendall-tau method has many similarities with the non-parametric Spearman method, but it uses different calculation method based on a sign of the slope which are connecting each existing pair of points. Like the latter, it does not dependent of the true measured values which makes is quite robust against the outliers. However, the results of Kendall-tau method are not easily visualised as a graph. (Reimann et al., 2017)

5.4 Previous studies by using the pXRF analyser

Portable X-ray fluorescence analysers have been used in recycling, environmental and mine site research for quite some time but lately, the use has been increased for exploration purposes as well. Sarala et al. (2014) compared the pXRF measurements of moist till samples, measured with Innov-X Systems'n Olympus Delta 6000 Premium, to the traditional laboratory provided geochemical analyses. They noted that the pXRF measurements are correlating well with the laboratory ones and regardless of how the samples was processed, it was possible to detect the trends of anomalies form the results. They also noted that the pXRF analyser worked well with base metals Co, Cr, Cu, Fe, Mn, Ni, V and Zn, and major elements Al, Ca and K. The results of Bi, Pb, Rb, Sb, Sr an Ti in turn, were reasonably good. However, the pXRF measurements of major element Mg and P did not show sufficient accuracy and the results of Ag, As, Cd, Hg, Mo, S, Se, Sn, W, Th and U were not either detected in the research or the given results were questionable.

Similar study has been done by Hatakka et al. (2016) with an aim to examine the suitability of the pXRF, Innov-X Systems'n Olympus Delta 6000 Premium, for geochemical background studies in terms of how different samples processing methods affect to the results. They noted that the water content affects to the results decreasingly and, therefore, the dry samples may give better results. Fineness of the sample material improves the precision of the results in term of better repeatability due to the homogeneity of sample material. However, the grinding affected to the detection of different elements in the soil samples: elements associated within the structures of minerals were emphasised in the detection after grinding whereas the elements associated with surfaces of the minerals were better detected without grinding.

Hokka and Soukka (2016) in turn, studied the accuracy of pXRF measurements of self-grinded drill core sample compared to the measurements straight from the solid drill core

using Innov-X Delta pXRF analyser. The measurement straight from the solid drill core depends on mineral distribution of the rock: if the rock shows heterogenic and coarse-grained texture, the pXRF measurement from the core rarely represents the whole-rock chemistry of the measured sample. They concluded that the results of grinded drill core samples showed a clear improvement in the pXRF measurements. They suggested that the pXRF is a usable tool in classification of volcanic rocks and determining an intense of alteration zones. However, they also noted that the pXRF measurements are rather indicative than exact and therefore, the pXRF measurements cannot replace the laboratory provided whole-rock geochemical analyses.

6 MATERIALS AND METHODS

6.1 Study area

Figure 4 shows ore zones in the Pahtavaara deposit. The classification of the zones is based on the distribution of distinct ore bodies. Variation in alteration and ore mineralogy has been detected between the distinct ore bodies but however, no systematic study has been done (Rupert Resources, unpublished report). The samples chosen to the study were located between "Länsi" and "Harpoon" zones.

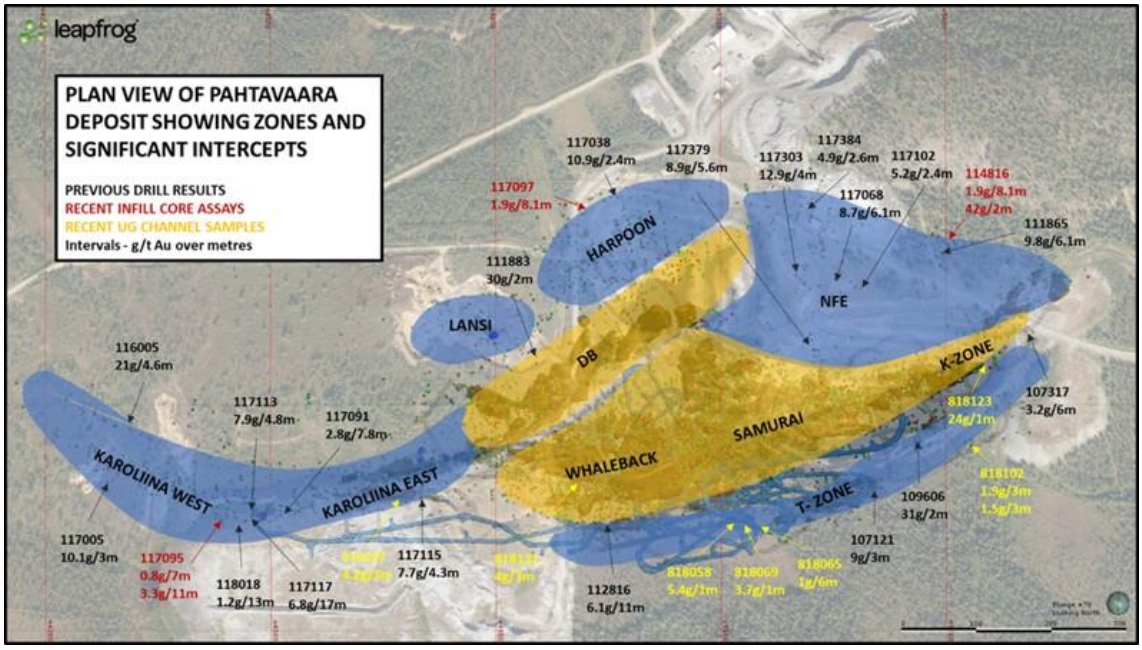

Figure 4. Zones of Pahtavaara deposit (Rupert Resources, 2020).

6.2 Portable XRF

Pulp samples returned from the laboratory analyses were used as sample material in the pXRF measurements. In total 692 pulp samples from 13 drill cores (Appendix 1) were measured during the summer 2019. All the samples were previously analysed for gold but only 58 samples had pre-existing multi-elemental analyses from the ALS laboratories.

Portable XRF measurements were conducted with Olympus Vanta C analyser by using GeoChem mode and 3 x 30s measurement times. The devise is capable to detect following elements: Ag, Al, As, Bi, Ca, Cd, Co, Cr, Cu, Fe, Hg, K, LE (light earth elements) Mg, Mn, Mo, Nd, Ni, P, Pb, Rb, S, Si, Sb, Se, Sn, Sr, Th, Ti, U, V, W, Y, Zn and Zr.

6.2.1 Sample preparation and measurement process

Sample preparation tools included 15 ml measuring spoons, small plastic bags, rubber bands, syringe presser and Prolene® thin films (Figure 5). The measuring spoon was covered with a rubber band sealed plastic bag and placed inside of a pulp bag. The sample was pressed into the measuring spoon with the syringe presser from outside of the sample bag. Before measuring, the tightly packed sample was covered with Prolene® thin film (Figure 6). Each sample was measured three times with 30s timing and after that, the average of the three measurements was given. The plastic bag and Prolene® thin film were changed for each sample. Gloves and breathing mask were used all the time when handling and preparing samples.

Figure 5. Sample preparation tools: 15 ml measuring spoons, rubber bands, candy bags, a syringe presser and Prolene® thin films.

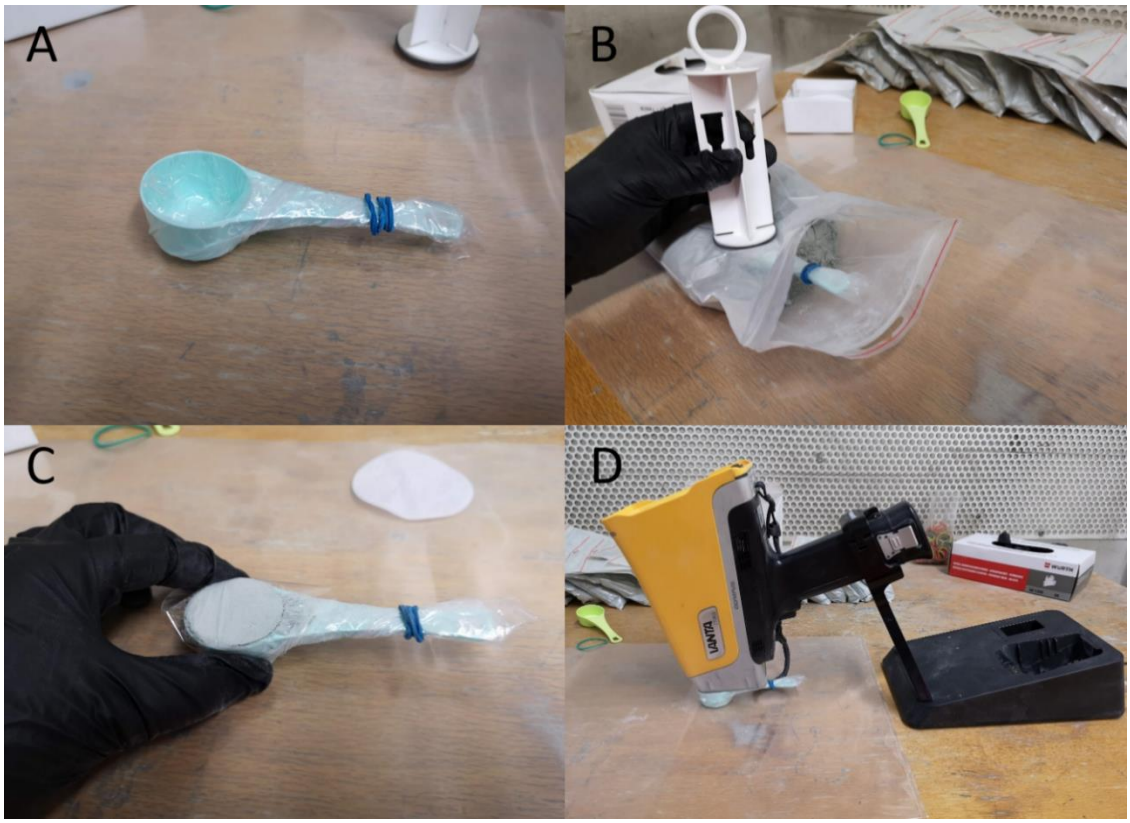

Figure 6. Sample preparation steps. A) Covered and sealed measuring spoon, B) sample pressing, C) sample covered with a thin film and D) measurement in progress.

6.2.2 Quality control

Every set of 20 samples included a blank, standard and duplicate. Grinded quartz sand was used as a blank whereas the samples with pre-existing multi-elemental analyses were used as standards. Small changes in the QC-program occurred during the project. Some standards were changing at the beginning and one more standard with higher K concentration was added later in the project. At first non-grinded quartz sand was used as a blank but it was changed to grinded one after the first drill hole measured. Excluding those changes, otherwise the QC-program was used systematically.

6.3 ICP-MS, fire assay and gold cyanidation

All the pulp samples were analysed for gold and the analyses were conducted with either gold cyanidation (Au_AA15) or fire assay (Au_AA26) methods (ALS, 2020) in the ALS laboratories. The partly existing multi-elemental analyses of were gained with four acid digestion with ICP-MS finish (ME-MS61) for following elements: Ag, Al, As, Ba, Be, Bi, Ca, Cd, Ce, Co, Cr, Cs, Cu, Fe, Ga, Ge, Hf, In, K, La, Li, Mg, Mn, Mo, Na, Nb, Ni,

P, Pb, Rb, Re, S, Sb, Sc, Se, Sn, Sr, Ta, Te, Th, Ti, Tl, U, V, W, Y, Zn and Zr. The multi-elemental analyses were also conducted in the ALS laboratories.

In total 617 laboratory analysed samples were included to the project (Appendix 1) in which 58 samples were also analysed with pXRF and these samples are used in the comparison of pXRF and laboratory analyses. The laboratory analyses were also used in geochemical studies of Pahtavaara komatiites and hydrothermal alteration. Laboratory-analysed exploration drill hole 117300 was included to the project due to its least-altered features compared to the rocks from the other drill cores.

6.4 Previously published data

Previously published data from Lomalampi (Törmänen et al., 2016), Peuramaa and Jeesiörova (Hanski et al., 2001) and Sattasvaara (Saverikko, 1985; Hanski, 1992) were used in comparison with Pahtavaara komatiites.

The data of the Lomalampi PGE-(Cu-Ni) deposit, part of the Sattavaara formation, with a chromite unsaturated, Al-undepleted high-Mg basalt or low-Mg komatiite host rock, included 10 selected whole-rock analyses. The analyses were conducted with X-ray fluorescence method (XRF) on pressed powder pellets in the geochemical laboratory of GTK and Labtium Oy.

The Peuramaa and Jeesiörova deposits are located in the most southwestern part of the Kittilä greenstone belt. The former exhibits a komatiitic composition whereas the volcanic rocks of the latter are mainly basaltic. The whole-rock data of major and minor elements of deposits were conducted with the XRF method in facilities of GTK and University of Tasmania. For the analyses of REE and other trace elements were used the ICP-MS method in the same facilities or alternatively, the pre-existing data from the study of Lehtonen et al. (1998) was utilised. The dataset of Peuramaa included 11 samples and Jeesiörova 15 samples.

The geochemical data of Sattavaara pyroclastic amphibole-chlorite rocks in the paper of Saverikko (1985) was analysed by Väino Hoffrén from GTK using the XRF method. The dataset consists of whole-rock analyses from 15 samples with major elements. Two samples from Sattasvaara with whole-rock chemistry and trace element concentrations in the study of Hanski were analysed by using multiple methods such as XRF, instrumental neutron activation analysis (INAA), graphite furnace atomic absorption spectrometry

(GFAAS), inductively coupled plasma-atomic emission spectrometry (ICP-AES), fire assay and radiochemical neutron activation analysis (RNAA). For more detailed information about the laboratory facilities see Hanski (1992).

6.5 Modelling the results

For statistical analyses of geochemical data measured with the pXRF, Excel and XLSTAT add-on software were used. Scatter plots and line diagrams are used for visualising the data and determining the distribution of data and outliers. Pearson, Spearman and Kendall-tau correlation coefficients are calculated for both original and outlier-removed datasets.

Hatakka et al. (2016) used R%-charts in the study of reference samples. It shows the deviation of the measured values from solid line presenting the median. Other lines represent the deviation of ± 10%, ± 20% and ± 30% from the median value (Figure 7). R%-charts are used in this study for the deviation of measurements of blank and standards samples. However, a little modification was done in the latter: instead of using the median of the measured values, values from laboratory analyses were used as the solid line in the R%-charts of each element.

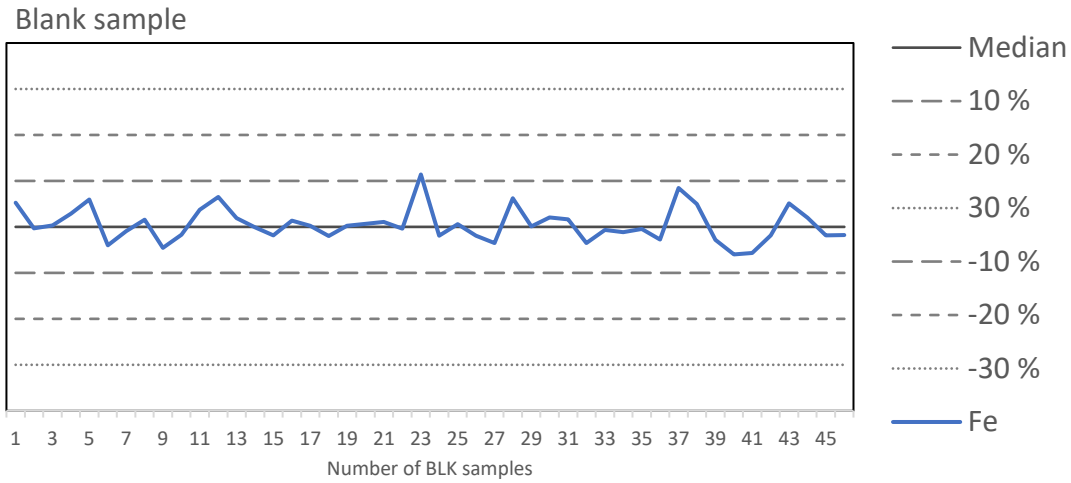

Figure 7. Example of R%-chart. Solid line presents the median whereas the dotter lines the percentage deviation from that.

Geochemical modelling of the results was conducted with the ioGAS software. EASYGRESGRANT Microsoft Excel spreadsheet created by López Moro (2012) were used for mass balance calculations and creating ISOCON plots.

7 RESULTS

7.1 Statistical analyses of the pXRF data

7.1.1 pXRF vs laboratory analyses

The statistical comparison of pXRF and laboratory analyses was possible to conduct for 15 regularly detected elements in the pXRF measurements: Al, Ca, Cr, Cu, Fe, Mg, Mn, Ni, S, Sr, Ti, V, Y, Zn and Zr. Elements Ag, As, Bi, Cd, Co, K, Mo, P, Pb, Rb, Sb, Se, Sn, Th, U and W were usually below the limits of detection or occurred randomly. Hg, Nd, Si, in turn, did not have comparable laboratory analyses.

Two distinct outliers were detected from the dataset of 58 comparable samples. They both show a significant concentration spike of thorium in the pXRF measurements although in laboratory analyses the Th concentrations were under the detection limit. The outliers show substantial contents 34.7 and 40.9 ppm of uranium in laboratory analyses comparing to other samples with uranium concentrations lower than 5.5 ppm. The samples with thorium spikes are skewed in relation to other elements as well. For example, Mn and Sr which are otherwise detected very precisely in ppm scale show extreme values with the presence of outlies. The outliers are present also in Cr, Mg, S, Ti, V and Zr measurements whereas they have only a small effect in Al, Ca, Cu, Fe, Ni, Y and Zn values. Some elements such as As, Mo and W which were commonly absent in pXRF measurements with the same laboratory determined values, were detected from these outliers. Geochemistry of the outliers are presented in Appendix 2.

Following figures illustrate the distribution and accuracy (i.e. how exact the measurements are) of the pXRF measurements compared to the laboratory analyses of the regularly detected elements. Due to the number of presentable figures, only the key points are presented here. All the figures are listed in Appendix 3.

Figure 8 shows that Ca, Fe, Ni and Cu have a positive and linear correlation between the pXRF and laboratory analyses, and the outliers do not significant effect to the distribution of measured values. The line diagrams illustrate that also the accuracy of the pXRF measurements of these elements is good.

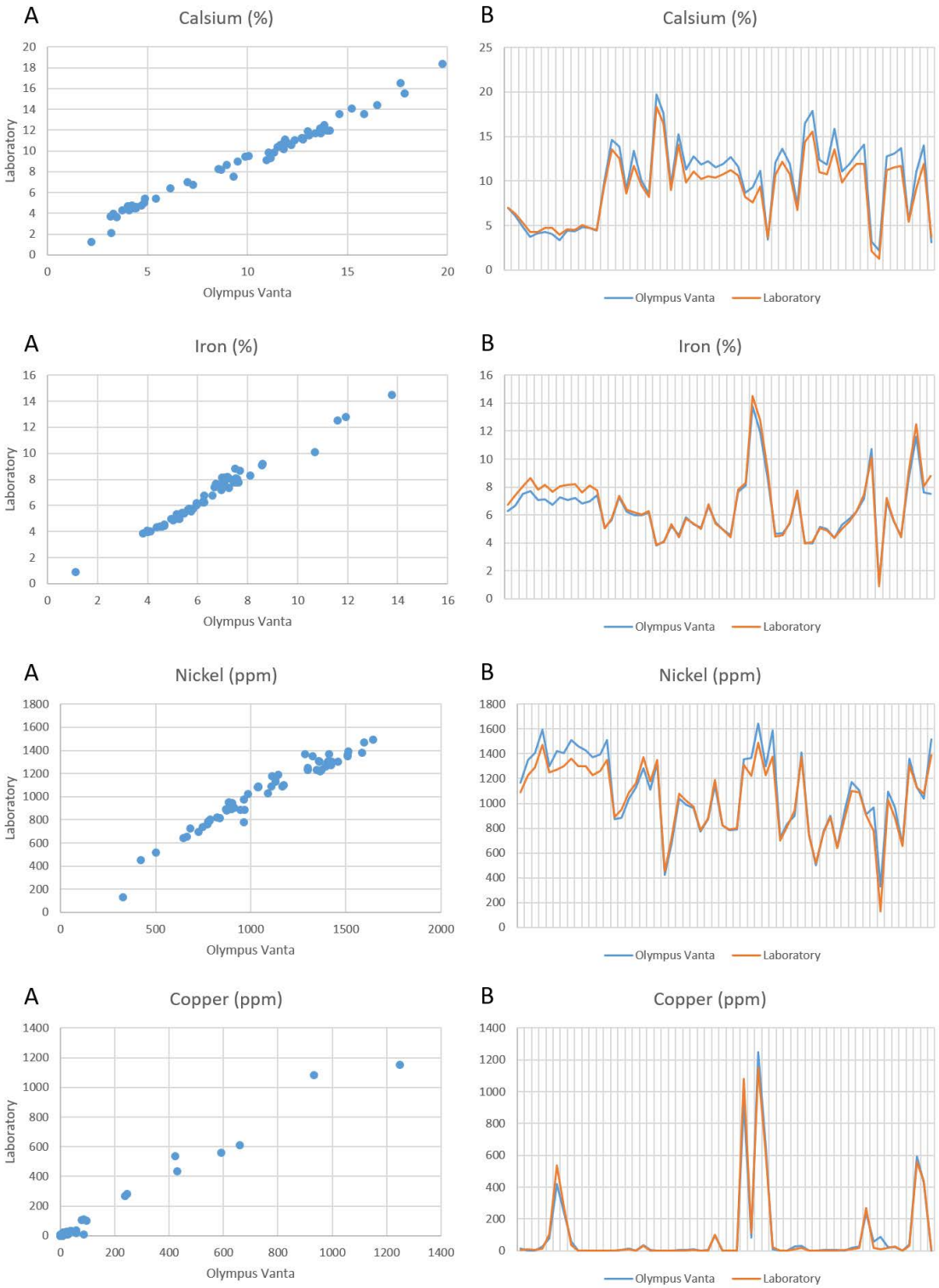

Figure 8. A) pXRF vs laboratory measurements showing the distribution of Ca, Fe, Ni and Cu, and B) line diagram of pXRF and laboratory measurements showing the accuracy.

Figures 9-11 show the distribution and accuracy of S, Mn and Sr. All of them have been significantly affected by the outliers but after removing them, the correlation between the pXRF and laboratory analyses is well improved. Without the outliers, the correlation in cases of Mn and Sr in clearly positive and linear with excellent accuracy. Although the distribution of S is clearly improved without the outliers, it is not as narrow as the others. However, the measurements of S are relatively accurate.

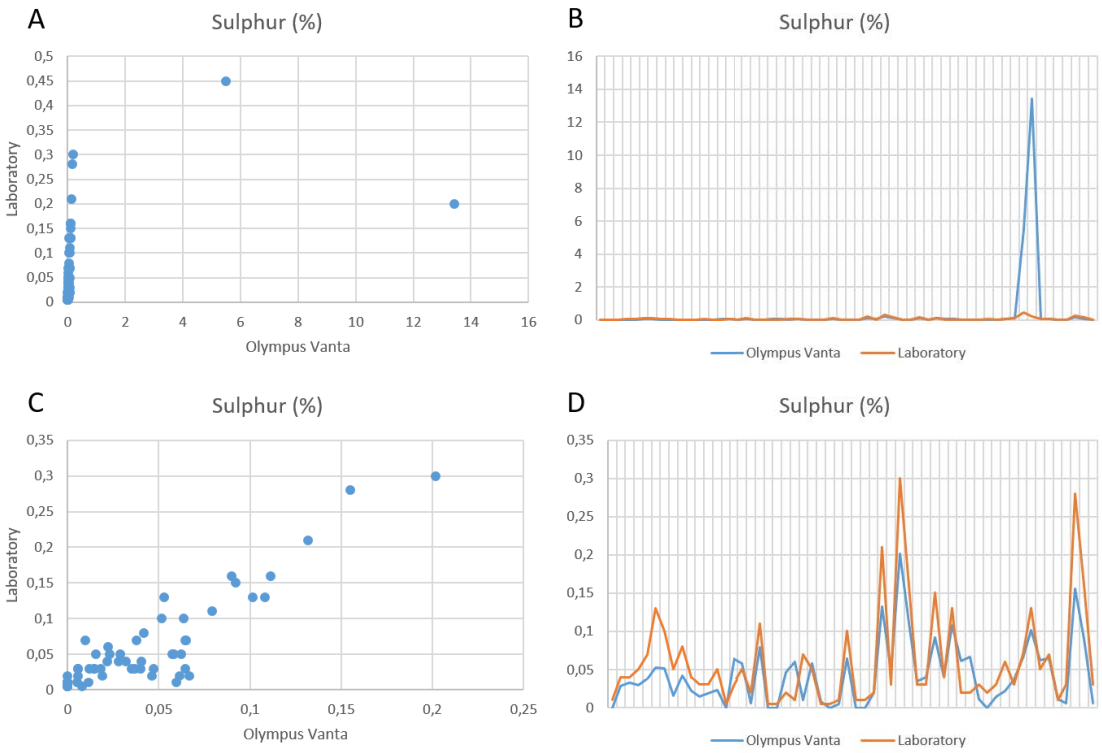

Figure 9. A) pXRF vs laboratory measurements showing the distribution of S with the outliers, B) line diagram of pXRF and laboratory measurements showing the accuracy with the outliers, C) distribution of S without the outliers and D) accuracy without the outliers.

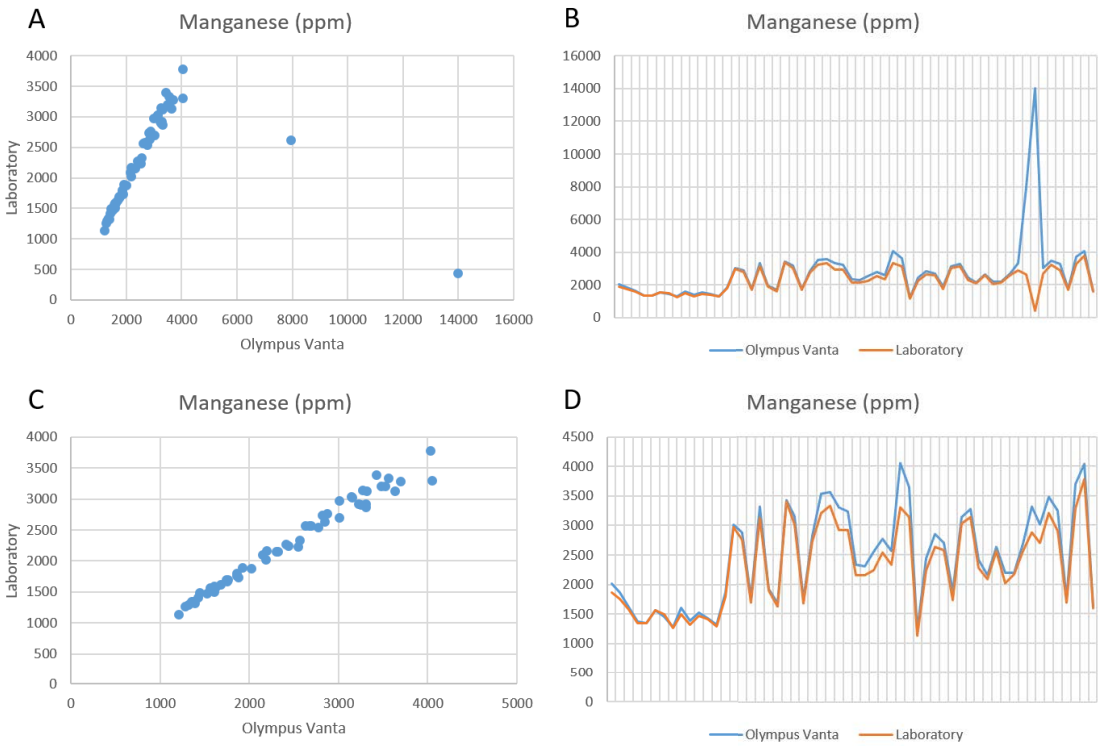

Figure 10. A) pXRF vs laboratory measurements showing the distribution of Mn with the outliers, B) line diagram of pXRF and laboratory measurements showing the accuracy with the outliers, C) distribution of Mn without the outliers and D) accuracy without the outliers.

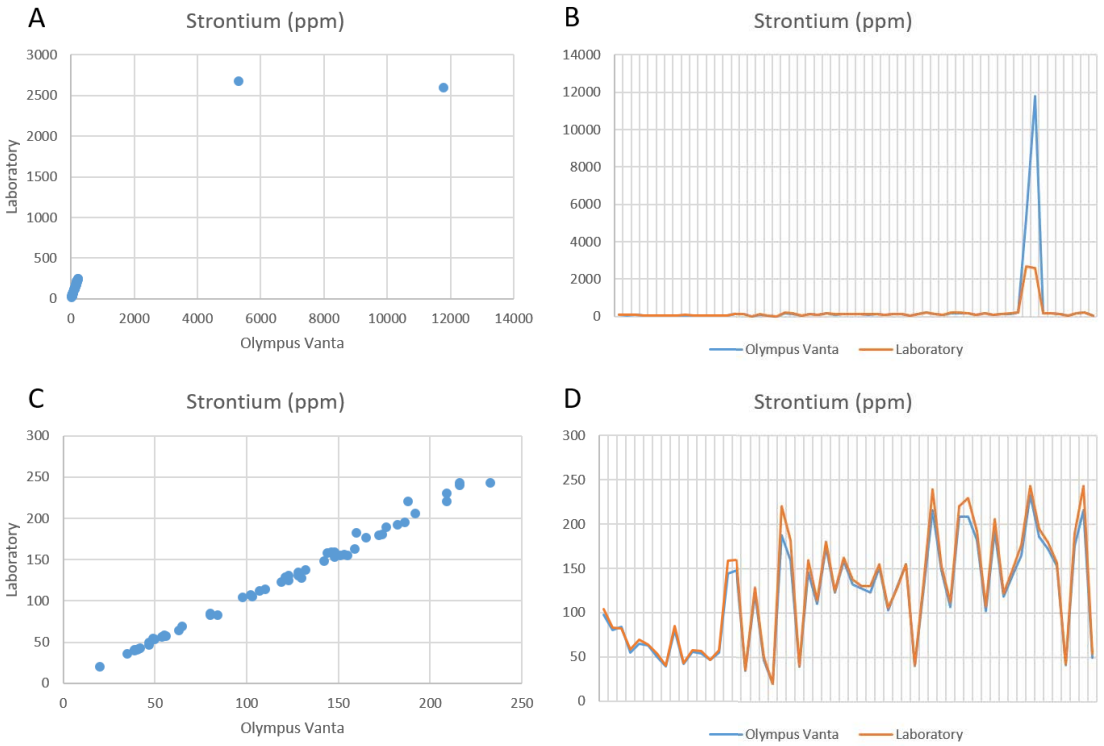

Figure 11. A) pXRF vs laboratory measurements showing the distribution of Sr with the outliers, B) line diagram of pXRF and laboratory measurements showing the accuracy with the outliers, C) distribution of S without the outliers and D) accuracy without the outliers.

Elements Al, Cr, Mg, Y and Zn are slightly affected by the outliers (see Appendix 3). The show a positive correlation between the pXRF and laboratory analyses but the distribution of some of these elements seems to be a little wider. The accuracy of Al, Cr, Mg, Y and Zn is good.

Figures 12-14 show the distribution and accuracy of the elements Ti, V and Zr. All of them are clearly affected by the outliers but, however, even after removing them from the dataset, the correlation between the pXRF and laboratory analyses is non-linear. The distribution is wide, and the line diagrams show that the accuracy of these elements in the pXRF measurements is weak.

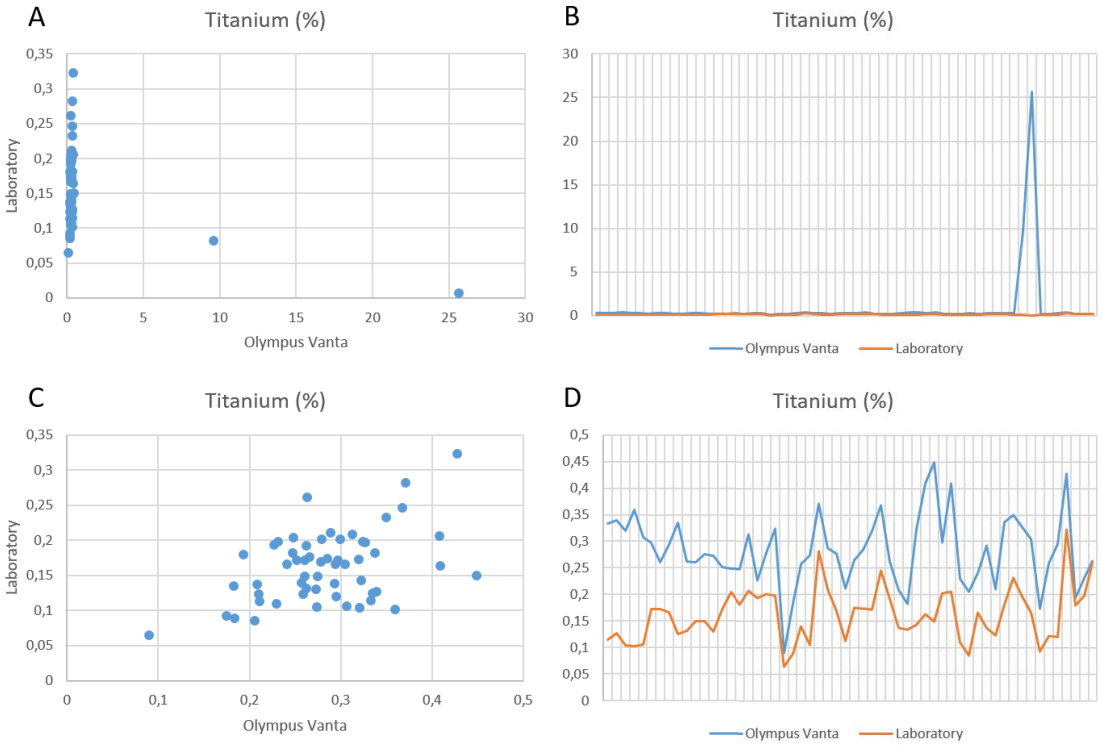

Figure 12. A) pXRF vs laboratory measurements showing the distribution of Ti with the outliers, B) line diagram of pXRF and laboratory measurements showing the accuracy with the outliers, C) distribution of Ti without the outliers and D) accuracy without the outliers.

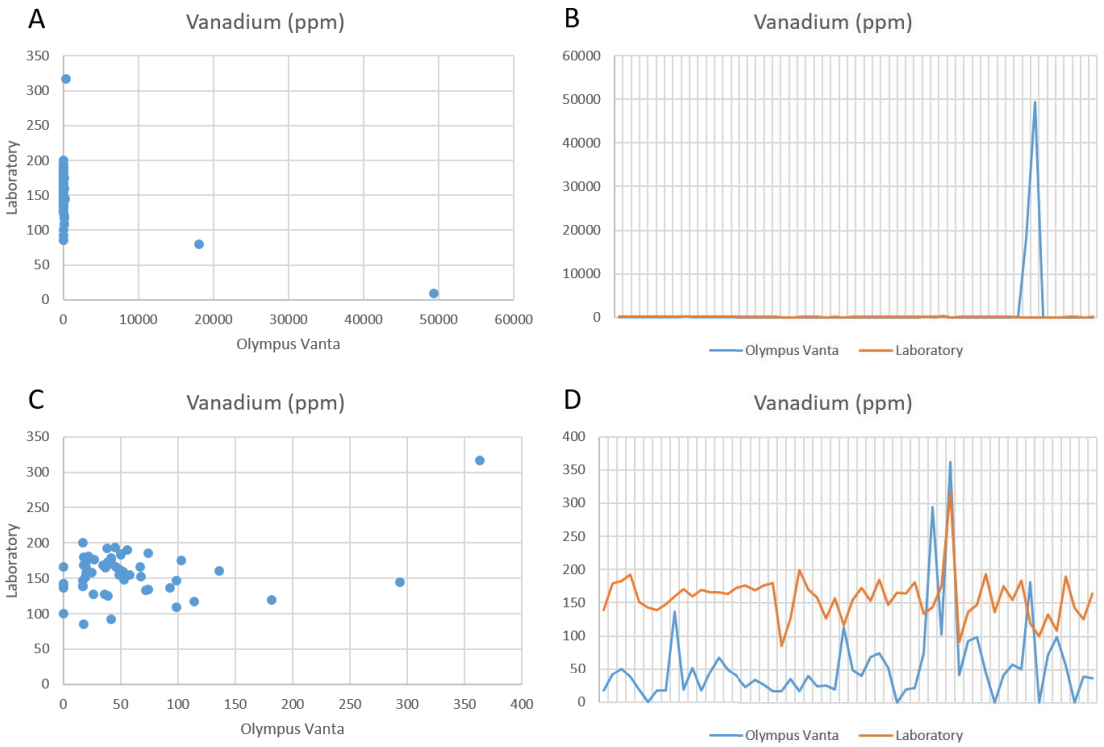

Figure 13. A) pXRF vs laboratory measurements showing the distribution of V with the outliers, B) line diagram of pXRF and laboratory measurements showing the accuracy with the outliers, C) distribution of V without the outliers and D) accuracy without the outliers.

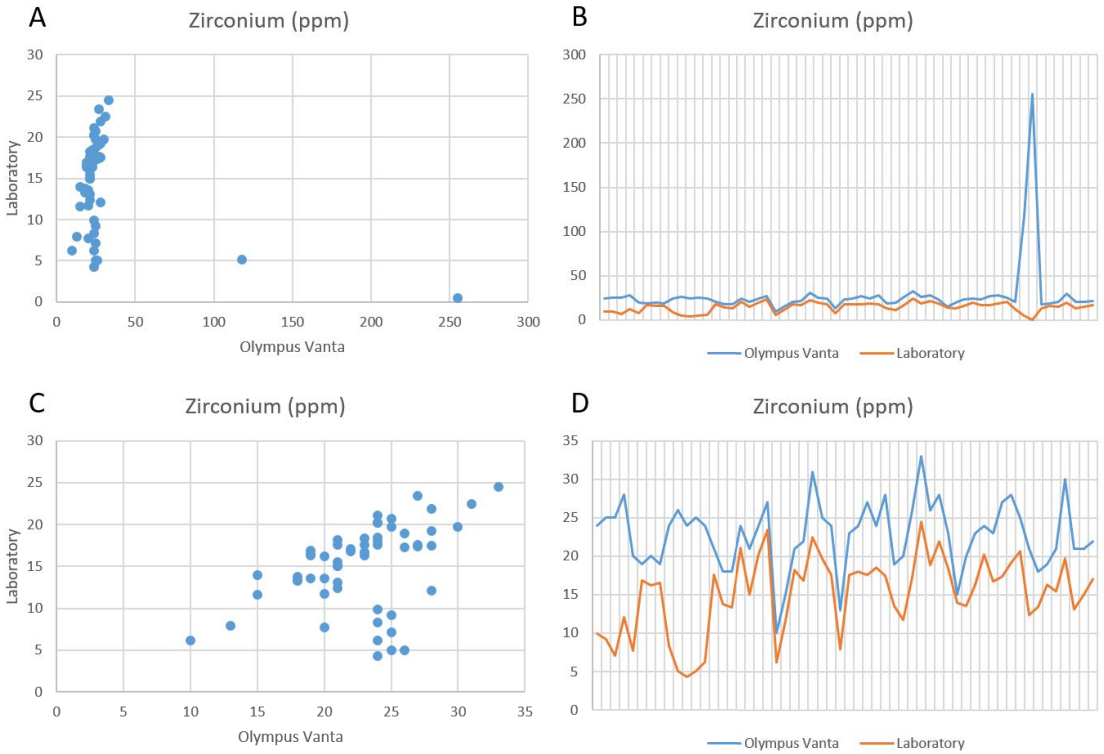

Figure 14. A) pXRF vs laboratory measurements showing the distribution of Zr with the outliers, B) line diagram of pXRF and laboratory measurements showing the accuracy with the outliers, C) distribution of Zr without the outliers and D) accuracy without the outliers.

7.1.2 Correlation coefficients

The calculation of correlation coefficients was conducted for the same 58 sample dataset, which included both pXRF and laboratory analyses. The correlation coefficients were calculated for the 15 regularly in pXRF measurements detected elements for both original and outlier-removed dataset (Table 5). All the correlation coefficients in the case of the original data set show a significant positive correlation between the pXRF and laboratory analyses mainly for elements Al, Ca, Cr, Cu, Fe, Mg, Ni, Sr, Y and Zn whereas the Pearson correlation coefficient shows only a low correlation for Mn, S, Ti, V and Zr measurements. However, the more outlier robust correlation coefficient Spearman and Kendall show much better correlation for Mn and S. Although the Pearson's method shows a slight negative correlation for V, the other coefficients indicate almost no correlation at all. All the coefficients indicate that there is no significant correlation between the pXRF and laboratory analyses for the elements Ti and Zr.

Considering the correlation coefficients in the dataset without the outliers, the notable improvement can be seen in the Pearson's correlation method for the elements Mn and S. The elements which showed positive correlation coefficients with the outliers remain pretty much the same. However, the removal of the outliers affects for Ti, V and Zr only slightly and no significant correlation is still not present.

Table 5. Pearson, Spearman and Kendall correlation coefficients for the the 15 regularly in pXRF measurements detected elements. Bolded ones have a value greater than ±0.5.

Original dataset (58 samples)				**Dataset without outliers (56 samples)**			
	Pearson	Spearman	Kendall		Pearson	Spearman	Kendall
Al	**0.820**	**0.786**	**0.609**	Al	**0.806**	**0.764**	**0.588**
Ca	**0.992**	**0.992**	**0.938**	Ca	**0.993**	**0.991**	**0.935**
Cr	**0.959**	**0.960**	**0.836**	Cr	**0.964**	**0.955**	**0.827**
Cu	**0.991**	**0.855**	**0.725**	Cu	**0.992**	**0.852**	**0.734**
Fe	**0.987**	**0.977**	**0.907**	Fe	**0.989**	**0.975**	**0.900**
Mg	**0.801**	**0.877**	**0.703**	Mg	**0.927**	**0.885**	**0.712**
Mn	0.154	**0.875**	**0.837**	Mn	**0.990**	**0.990**	**0.926**
Ni	**0.972**	**0.966**	**0.870**	Ni	**0.979**	**0.969**	**0.877**
S	0.442	**0.788**	**0.647**	S	**0.890**	**0.765**	**0.625**
Sr	**0.921**	**0.996**	**0.963**	Sr	**0.997**	**0.995**	**0.962**
Ti	-0.406	0.212	0.155	Ti	0.465	0.343	0.238
V	**-0.545**	-0.070	-0.051	V	0.346	0.033	0.019
Y	**0.836**	**0.664**	**0.543**	Y	**0.754**	**0.626**	**0.506**
Zn	**0.968**	**0.943**	**0.842**	Zn	**0.984**	**0.975**	**0.882**
Zr	-0.363	0.311	0.267	Zr	0.430	0.454	0.360

7.1.3 Blanks

Grinded quartz sand was used as the blank sample material and it was measured 46 times during the project. The results of blank measurements can be used for an examination of precision (i.e. how repeatable the measurements are) as well as to study the contamination level of the project because the all the blank measurements were conducted with the same sample.

Figure 15 shows deviations of the values of each regularly detected element from the blank sample: Al, Fe, K, Mg, Mn, Rb, Si, Sr, Ti, V and Zr. Elements Al, Fe, K, Rb, Si and Sr showed the smallest deviation. Except for few measurements, these elements have the deviation under 10 %. Elements Mg, Mn, Ti, V and Zr in turn, had wider deviation, commonly more than 30 %. However, the results do not show remarkable changes from the first measurements to the last ones which indicates that no significant contamination has been affecting to the results.

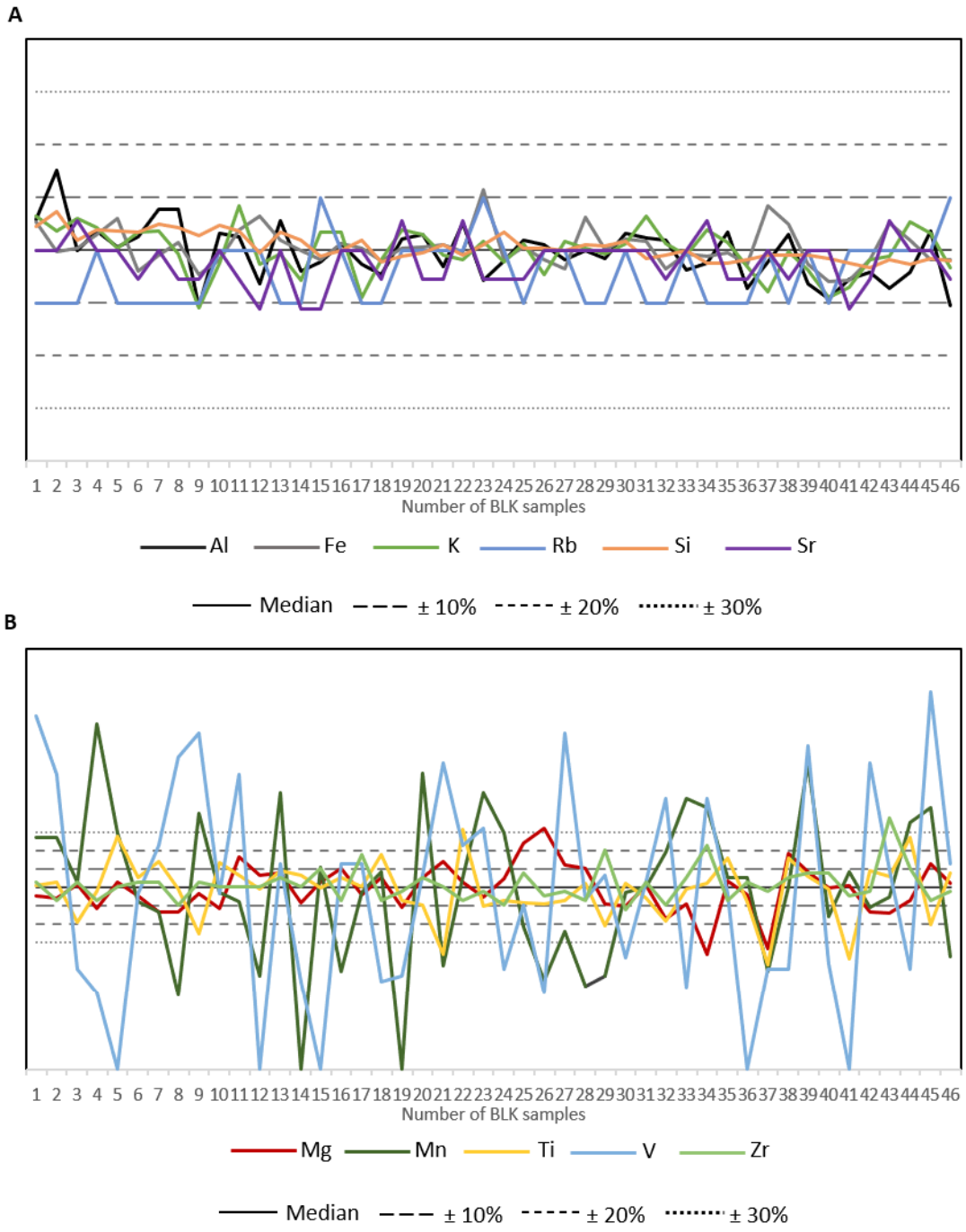

Figure 15. R%-charts of the deviation of element detected from the blank sample. A) Elements with the smallest deviation and B) elements with the largest deviation.

7.1.4 Standards

Pulp samples with pre-existing multi-elemental data were used as standards and the four most measured standards, with 39 measurements in total, were included to the study of precision of the measurements. The results are presented as R% -charts, where the middle line shows the result of laboratory analyses and the other lines the deviation from that as percentages ±10 %, ±20 % and ±30 %.

In the following Figures 16 and 17 are presented the R% -charts for the each regularly detected elements in the four standards samples. Potassium was detected only from one standard. The figures show that the deviation from the laboratory analysis is relatively low, under 10 % only in the case of Sr. Elements Al, Ca, Fe, K, Mn, Ni and Zn show a deviation under 20 %, and Mg under 30 %. Also, in the case of Y, most of the measurement are under the 30 % deviation. The measurements of two of the four standards in the case of V seem to fit in 30 % deviation but the rest two are a way under the -30 % deviation. Cr, Ti and Zr show deviations much higher than 30 % and, the deviation of Cu and S are largely varying.

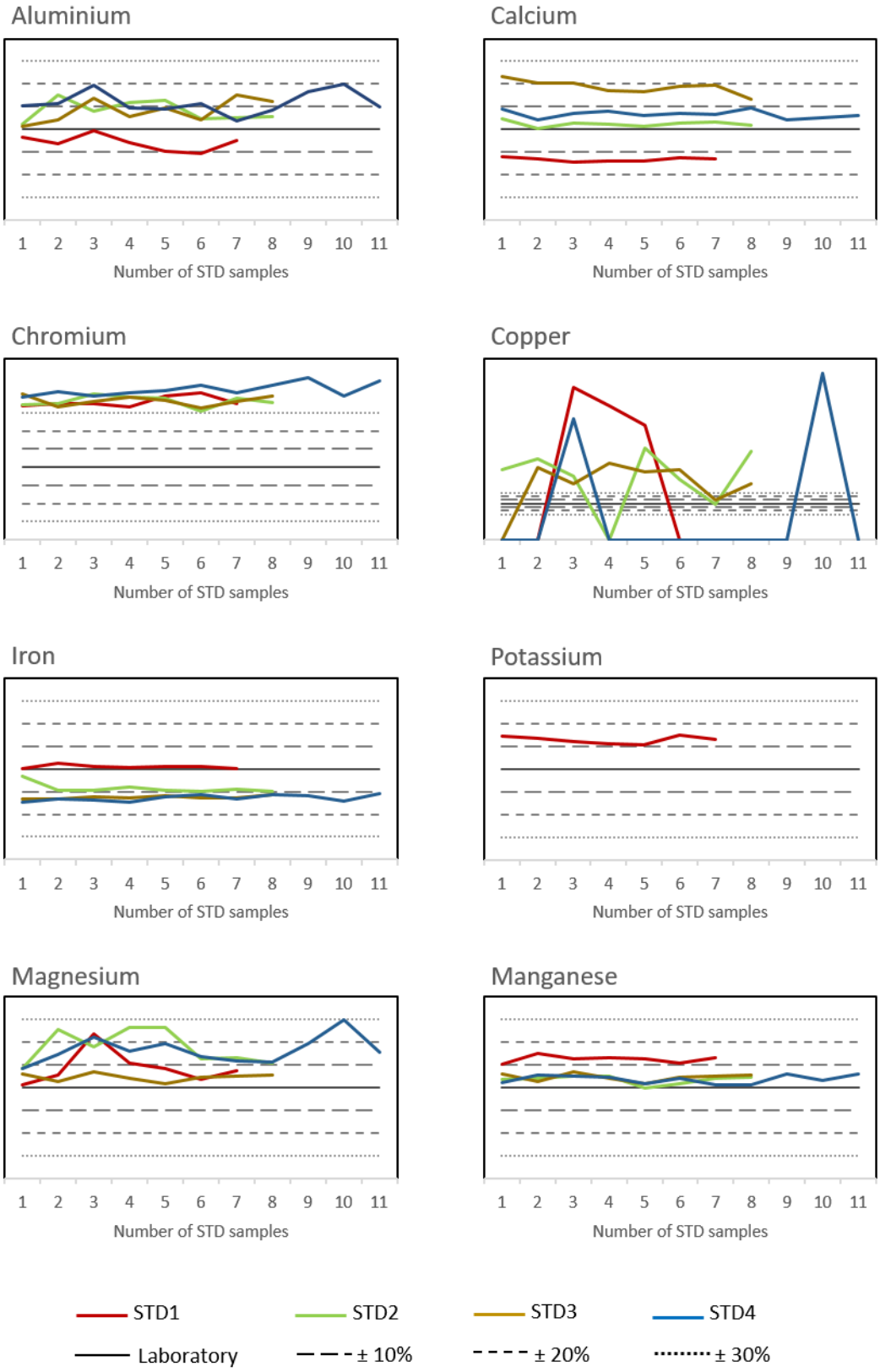

Figure 16. R %-charts for the elements Al, Ca, Cr, Cu, Fe, K, Mg and Mn. The solid line refers to the laboratory analysis, the dotted lines show deviations with different percentages.

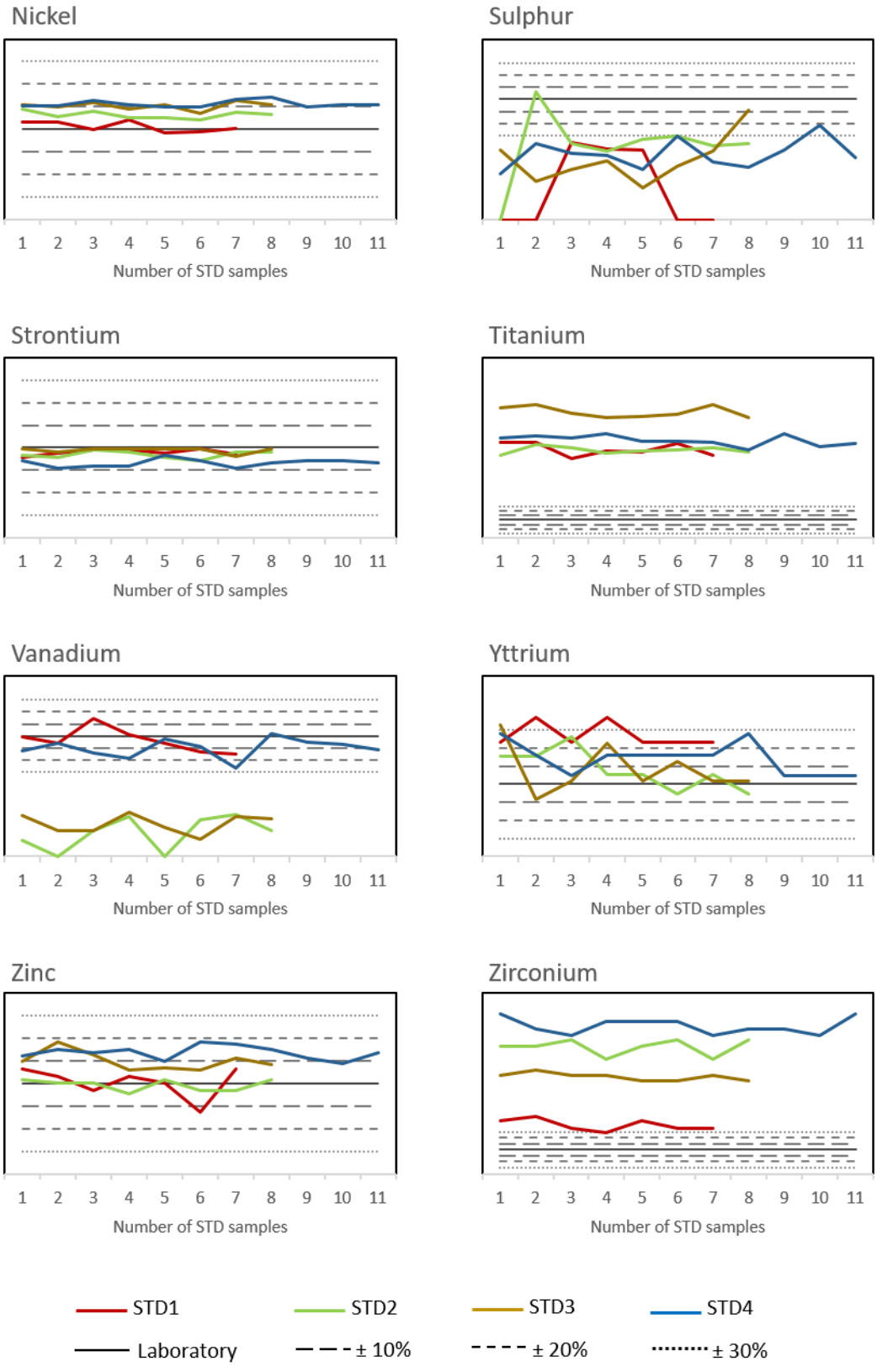

Figure 17. R %-charts for the elements Ni, S, Sr, Ti, V, Y, Zn and Zr. The solid line refers to the laboratory analysis, the dotted lines show deviations with different percentages.

7.1.5 Duplicates

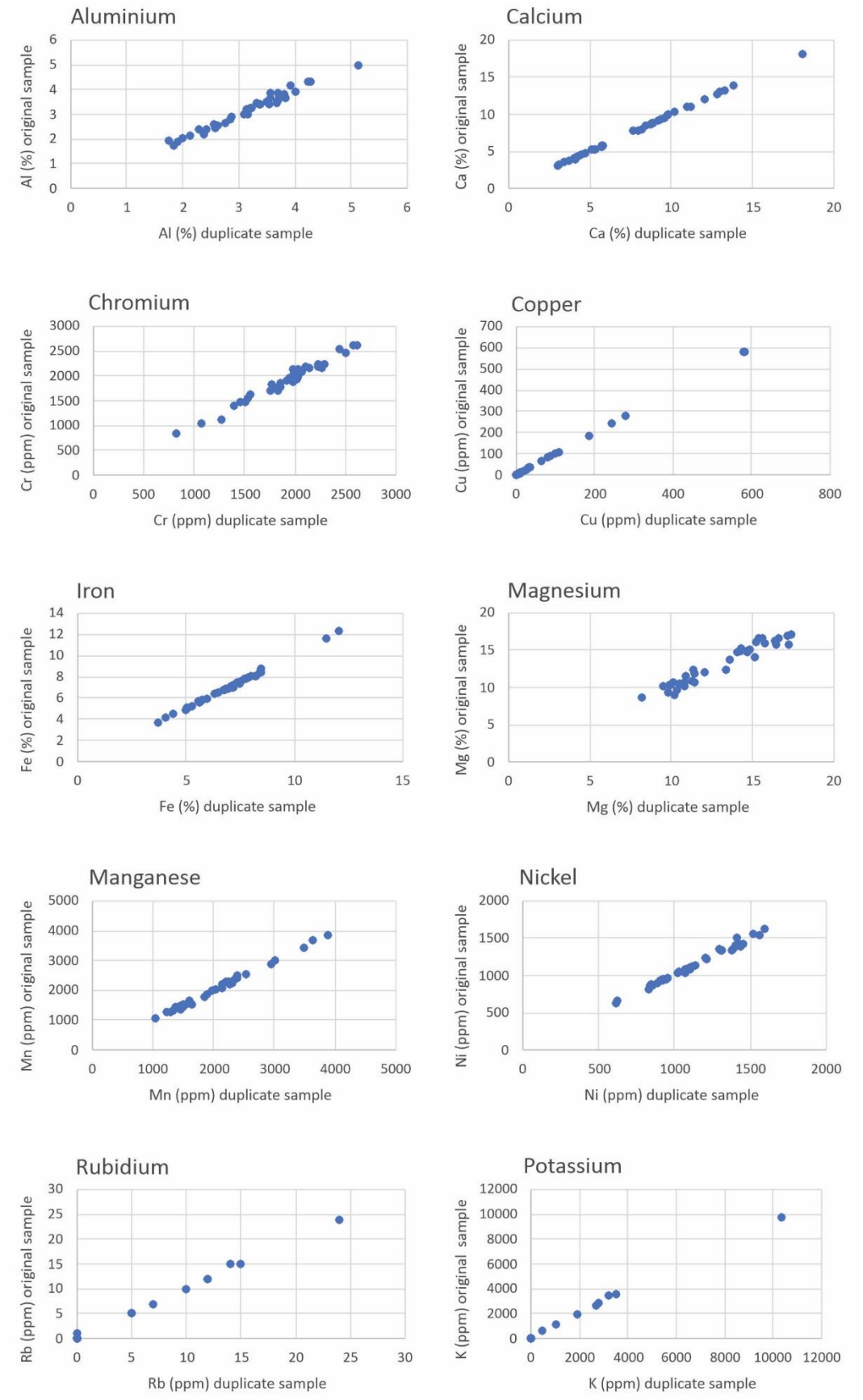

Figure 18. Duplicate sample vs original samples scatter plot illustrating the precision of duplicate sample measurements of the elements Al, Ca, Cr, Cu, Fe, Mg, Mn, Ni, Rb and K.

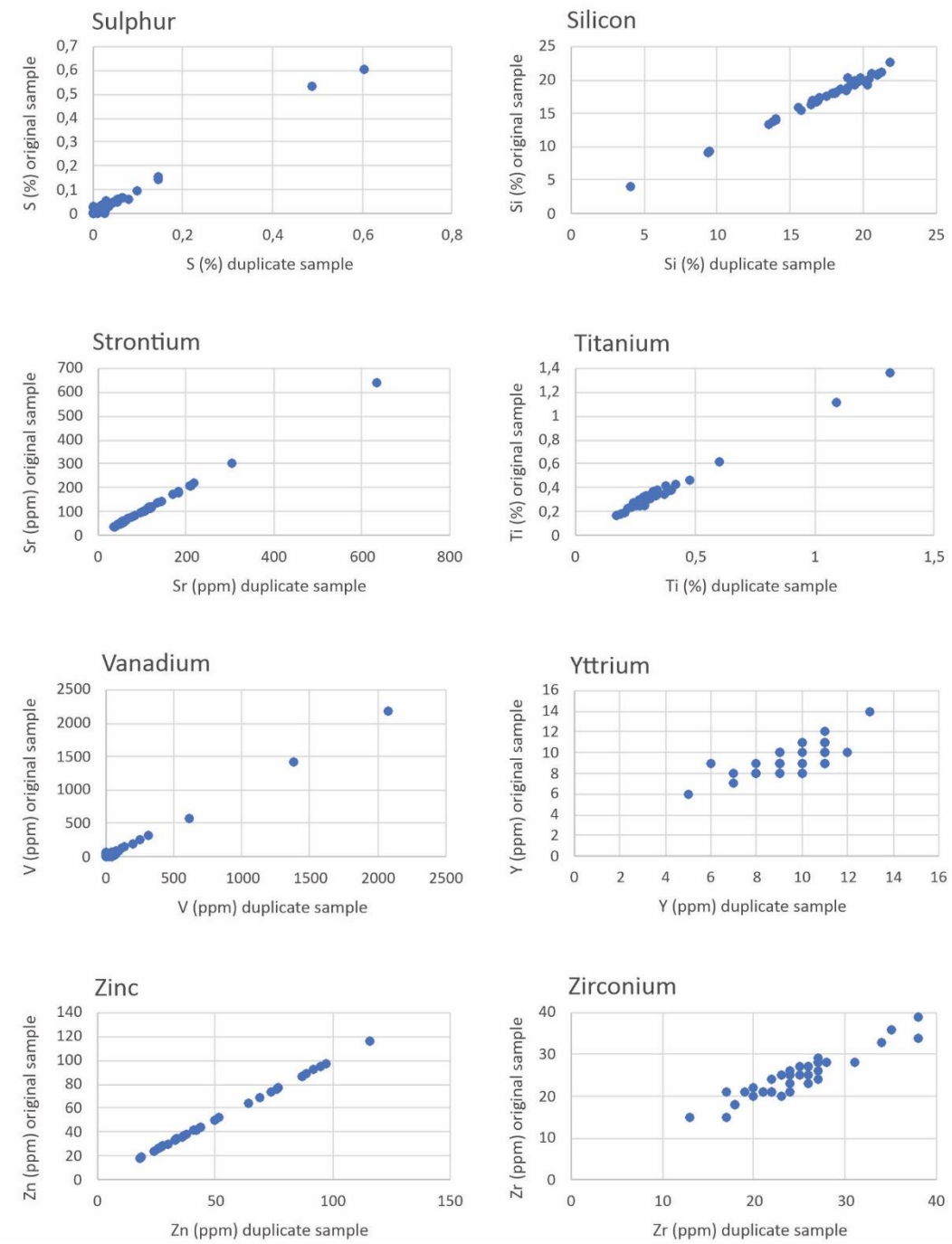

Figure 19. Duplicate sample vs original samples scatter plot illustrating the precision of duplicate sample measurements of the elements S, Si, Sr, Ti, V, Y, Zn and Zr.

Scatter plots of the duplicate sample vs. the original sample (Figures 18 and 19) illustrate the precision of the measurements. The precision is excellent for most of the elements. However, the distribution of Mg, Y and Zr is wider than the others. As a note, Rb and P were not detected from all samples.

7.2 Geochemistry of komatiites

7.2.1 Comparison of the Pahtavaara komatiites

For the comparison of the Pahtavaara komatiites with the other komatiitic deposits in Central Lapland, Lomalampi, Jeesiörova and Peuramaa, the previously published data from the studies of Törmänen et al. (2016) and Hanski et al. (2001) have been used in addition to the laboratory analyses from the study area of Pahtavaara. Figure 20a-c shows three diagrams, in which have been utilised the relatively immobile elements Zr and Ti, plotted in the binary diagram, and Zr, Sc and Y, plotted in the ternary diagram. Also, a chondrite normalised spider diagram (McDonough and Sun, 1995) with certain trace elements is plotted. However, in the chondrite normalised diagram, it is needed to note that some elements are missing in the analyses of different deposits.

Based on the immobile element plots in Figure 20, it is possible to see that Pahtavaara komatiites differ significantly from the Peuramaa komatiites. The values of Lomalampi and Jeesiörova komatiites are distributed closer the ones of Pahtavaara. The chondrite normalized diagram shows that all the deposits have depleted in P and enriched in Ba, Sr, Ce, U, Hf, Zr, Ti and Y. However, the values of Peuramaa, are notable higher than the others. Notable differences compared to the Pahtavaara deposits can be seen in concentrations of Th, Nb, Zr and Hf which are a way below the concentrations of the other deposits.

7.2.2 Pahtavaara komatiites

Figure 21 shows the distribution of different lithological units of the Pahtavaara in the Zr vs. Ti binary diagram. The distribution of the lithological units differs from each other. The talc-chlorite schists are characterised by low Zr and low or slightly increased Ti concentrations. The amphibolite schists in turn, have variable concentration of Zr whereas the concentration of Ti remains relatively low. The number of actinolite-tremolite samples were low compared to the other units, but they seem to be located in the area of relatively high Zr concentration.

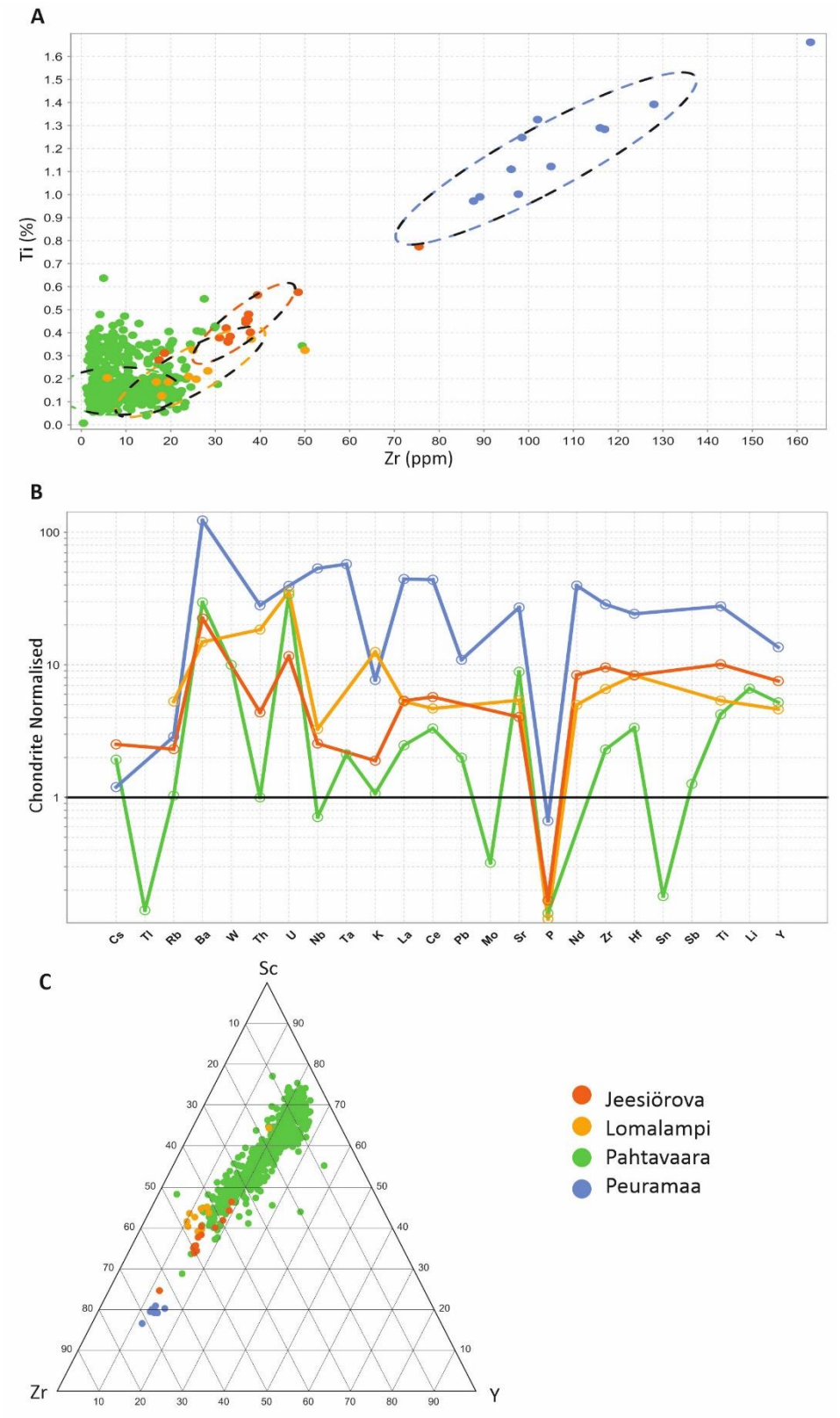

Figure 20. Diagrams for the comparison of Pahtavaara komatiites with the other komatiitic deposits in the Central Lapland. A) Binary Zr vs. Ti diagram, B) chondrite normalised (normalisation values after McDonough and Sun, 1995) spider diagram and C) Zr-Sc-Ti ternary diagram.

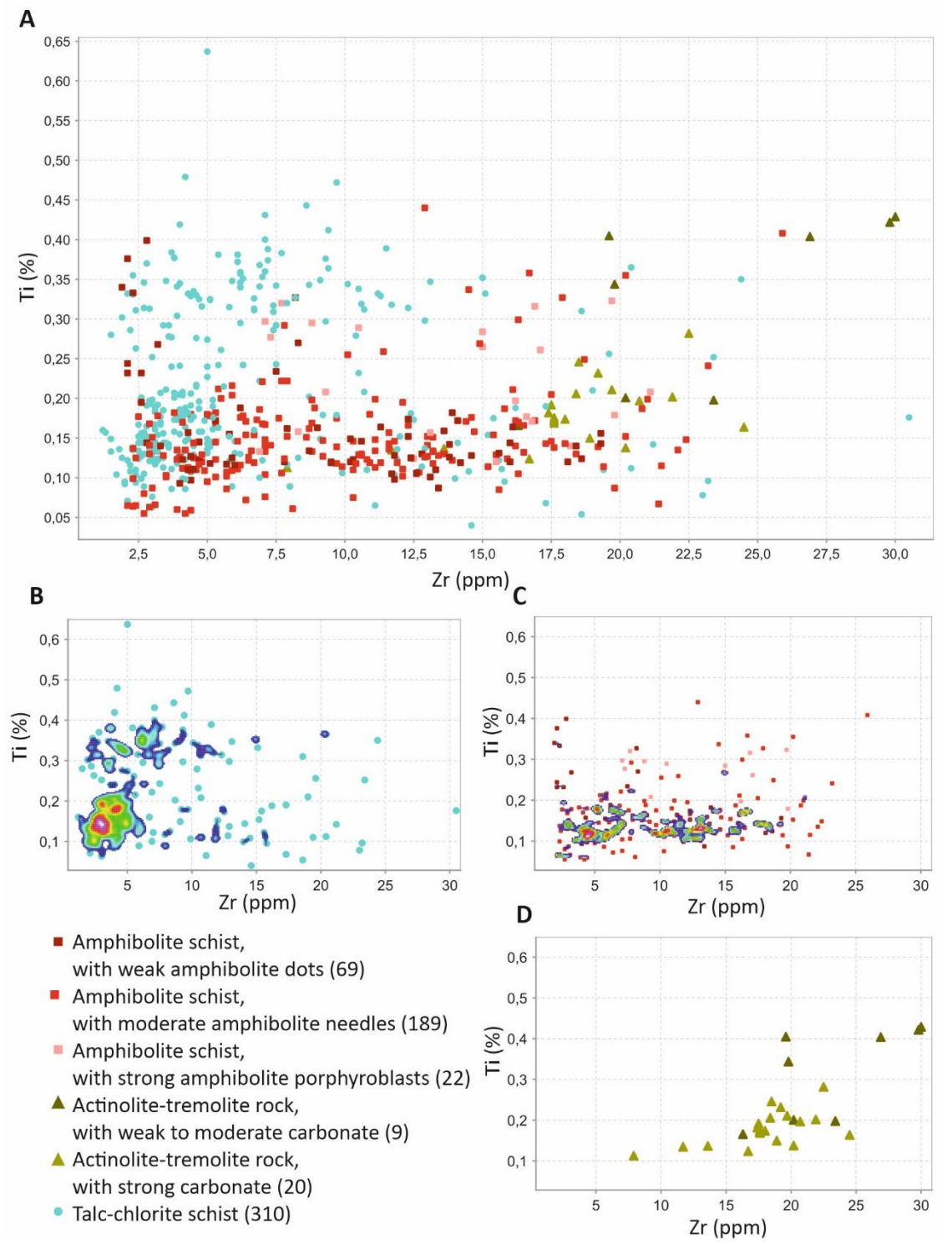

Figure 21. The distribution of different lithological units of Pahtavaara in the Zr vs Ti binary diagram. A) All units B) talc-chlorite schists, C) amphibolite schist and D) actinolite-tremolite rocks.

7.3 Hydrothermal alteration

7.3.1 Style of alteration

All the Pahtavaara and Sattasvaara (Saverikko, 1985; Hanski et al., 2001) samples are located between plagioclase and clay minerals (i.e. chlorite and epidote) ends in the K/Al vs. Na/Al molar ratio plot (Figure 22). When viewing closely the distribution of the rocks, it seems that the different lithological units are slightly differently distributed: the actinolite-tremolite rocks and amphibolite schists with moderate amphibolite needles are closer to the plagioclase end than the others. Assuming the Pahtavaara and Sattasvaara rocks have (ultra-)mafic protolith, the AI-CCPI alteration box plot (Figure 23) shows trends of alteration towards to chloritisation and carbonatisation. Again, seems that the alteration trend of actinolite-tremolite rocks differs from the others as located closer the carbonates. Even though the rocks in the Pahtavaara alteration zone are considered as more altered than the surrounding rock, the samples from Sattasvaara appeared to be fitting in the same alteration trends.

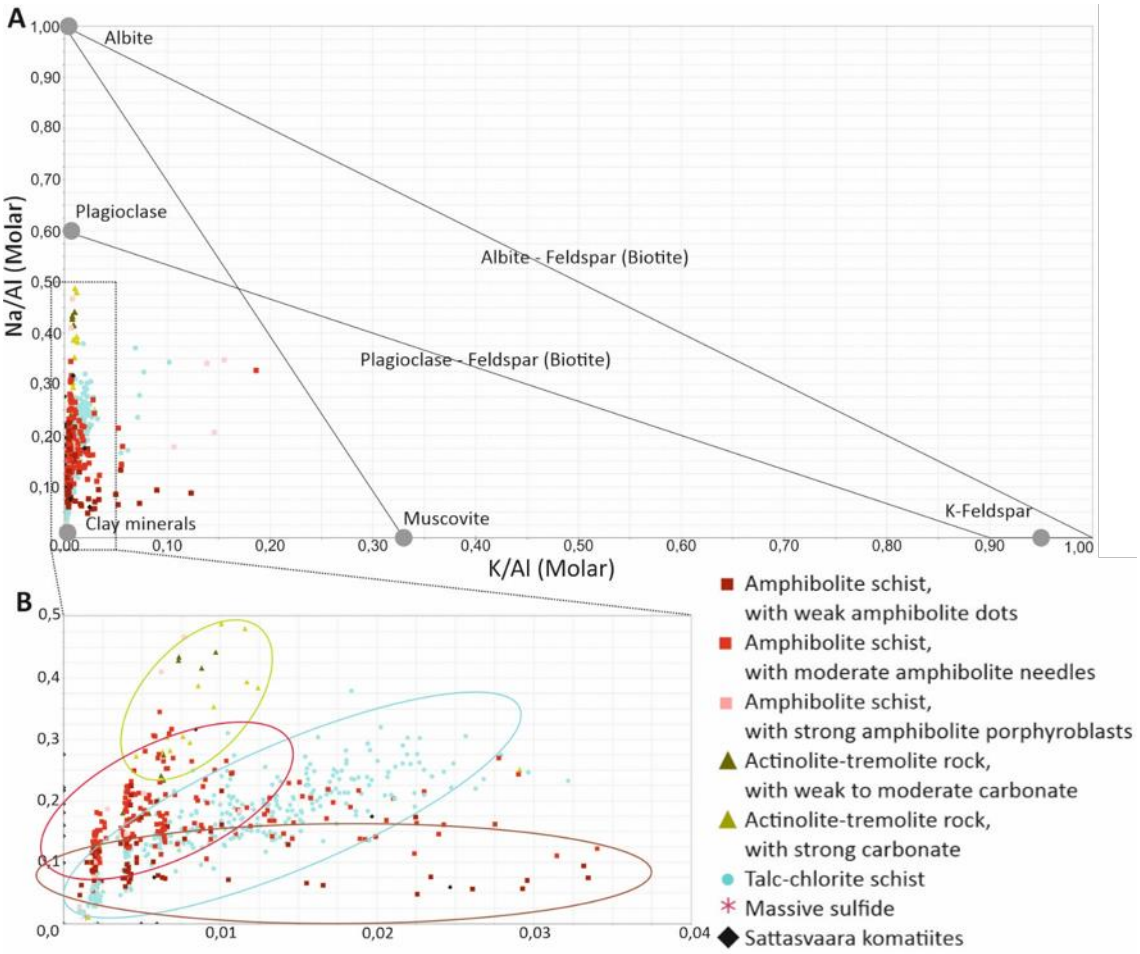

Figure 22. A) K/Al vs Na/Al molar ratio plot (Davies and Whitehead, 2006) and B) close up view of the K/Al vs Na/Al molar ratio plot of Pahtavaara and Sattasvaara komatiites.

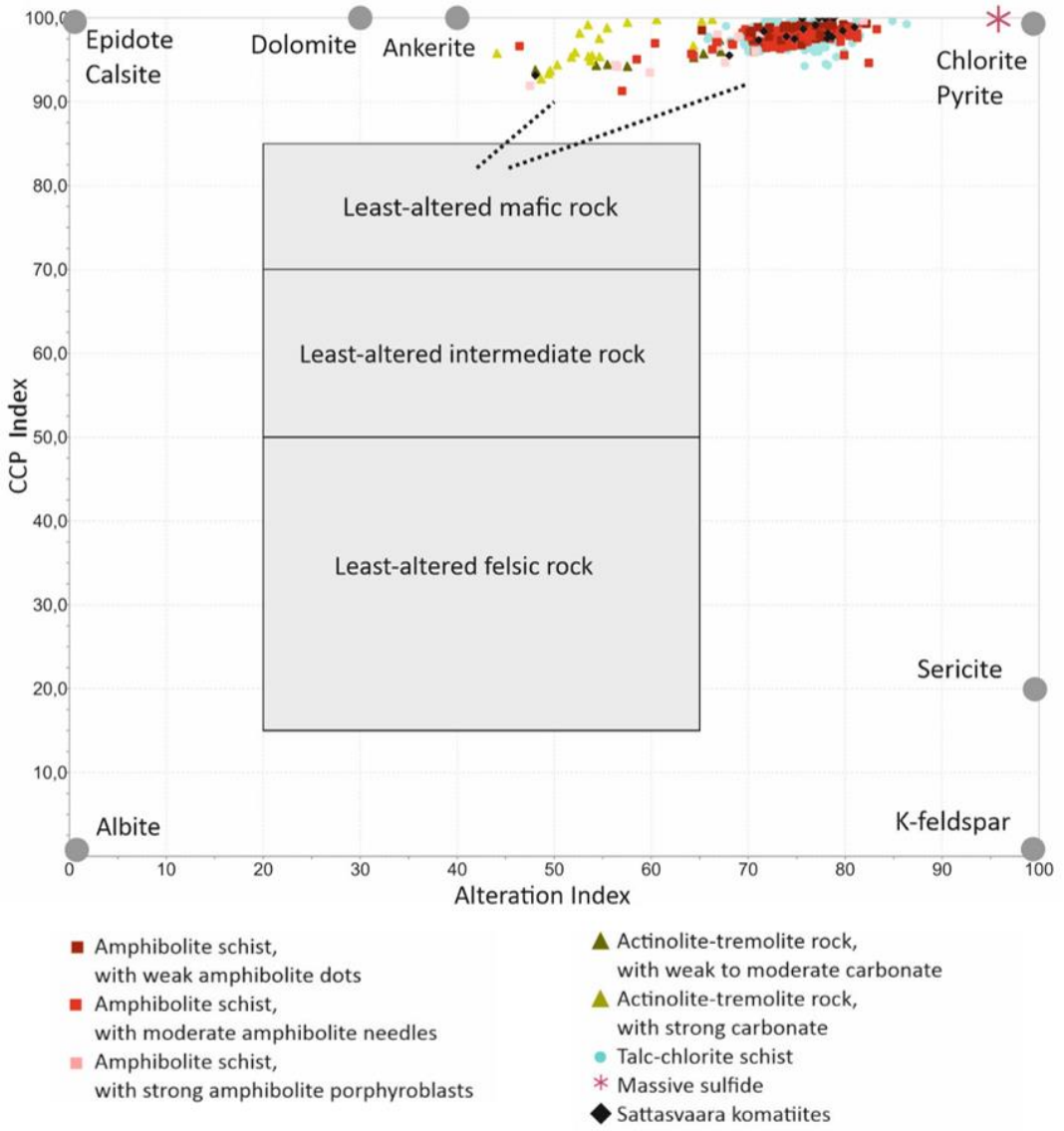

Figure 23. AI-CCPI alteration box plot (Large et al., 2001) of Pahtavaara and Sattasvaara komatiites. Fields of the least altered volcanic rocks after Gifkins et al. (2005).

7.3.2 Mass balance changes

The mass balance calculations were conducted for each the three different lithological units in the study area: talc-chlorite schist, amphibolite schist and actinolite-tremolite rock. For each lithological unit, the average geochemical composition of the laboratory analysed samples was calculated and used as an altered sample. The talc-chlorite schist from the exploration drill hole 11730 was used as the least-altered precursor.

Due to the lack of densities of both the least altered and altered samples, immobile elements were used as a reference for mass balance calculations. In the EASYGRESGRANT Excel spreadsheet, it was possible to choose the immobile elements by clusters of slopes. The slopes of elements close to one another were selected as

immobile elements (López-Moro, 2012). However, based on varying slopes of immobile considered elements, using the same immobile elements for the calculation of different lithological units was not possible.

In the case of talc-chlorite schist, Y, Nb and Al_2O_3 were used as immobile elements. ISOCON diagrams in Figure 24A-C shows, that the talc-chlorite schist in the study area are enriched in Ni, Ba, MgO, CaO, TiO_2 and MnO and, depleted in Cr, Fe_2O_3, Na_2O, Mo, K_2O and P_2O_5. The numerical results of the mass balance calculation for the talc-chlorite schists, based on the averages of the slopes, are presented in Appendix 4. The calculation shows that the overall mass change from the least-altered talc-chlorite schist to the altered talc-chlorite schist is 12.31 %.

Figure 25A-C show the ISOCON diagram for the amphibolite schist. Y, Nb and Al_2O_3 were used as immobile elements. It seems that the enrichments and depletions of the elements and oxides are relatively similar compared to the talc-chlorite schist: enriched in Ni, Ba, MgO, CaO, TiO_2 and MnO and, depleted in Cr, Fe_2O_3, Na_2O, K_2O, Mo and P_2O_5. The numerical results of the mass balance calculation of the amphibolite chlorite schist are presented in Appendix 5. The calculation shows that the overall mass change from the least-altered talc-chlorite schist to the altered amphibolite chlorite schist is 5.22 %.

Whereas the ISOCON diagrams of the talc-chlorite schists and amphibolite schist were similar, the ISOCON diagram of actinolite-tremolite (Figure 26A-C) appeared to show differences at least in the intensity although the enriched and depleted elements and oxides remain rather same. The actinolite-tremolite rock are enriched in Ni, Ba, MgO, CaO, MnO and TiO_2 and depleted in Fe_2O_3, Na_2O and K_2O. The numerical results of the mass balance calculation of the amphibolite chlorite schist are presented in Appendix 6. The calculation shows that the overall mass change from the least-altered talc-chlorite schist to the altered actinolite-tremolite rock is 23.19 % which is greatest of the three lithological units. Compared to the other units, the enrichments of CaO, Ba and Sr in the actinolite-tremolite rock are higher. Y, Zr and Al_2O_3 were used as immobile elements in the case of actinolite-tremolite rock.

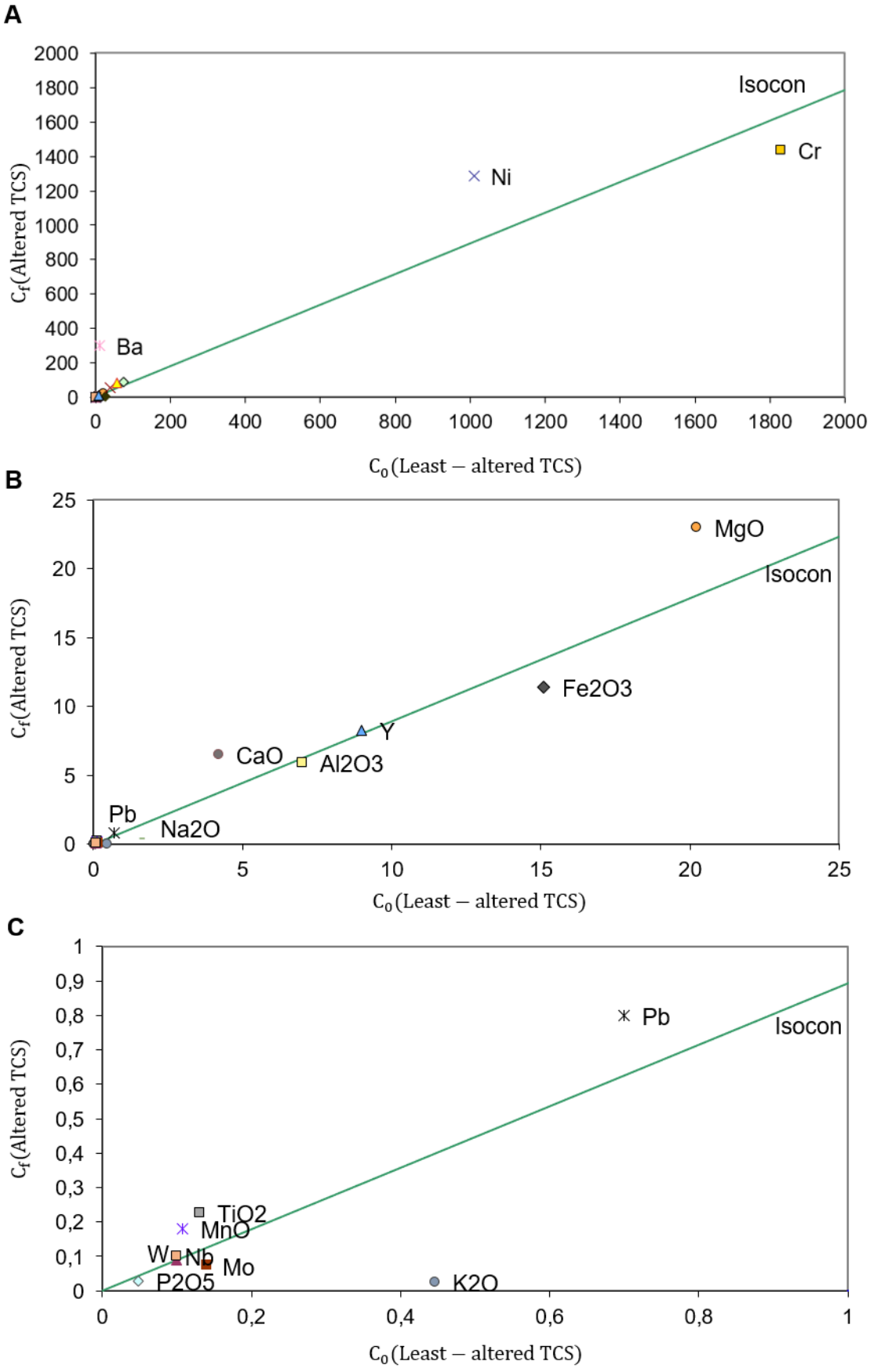

Figure 24. ISOCON diagrams of the talc-chlorite schist with different scales.

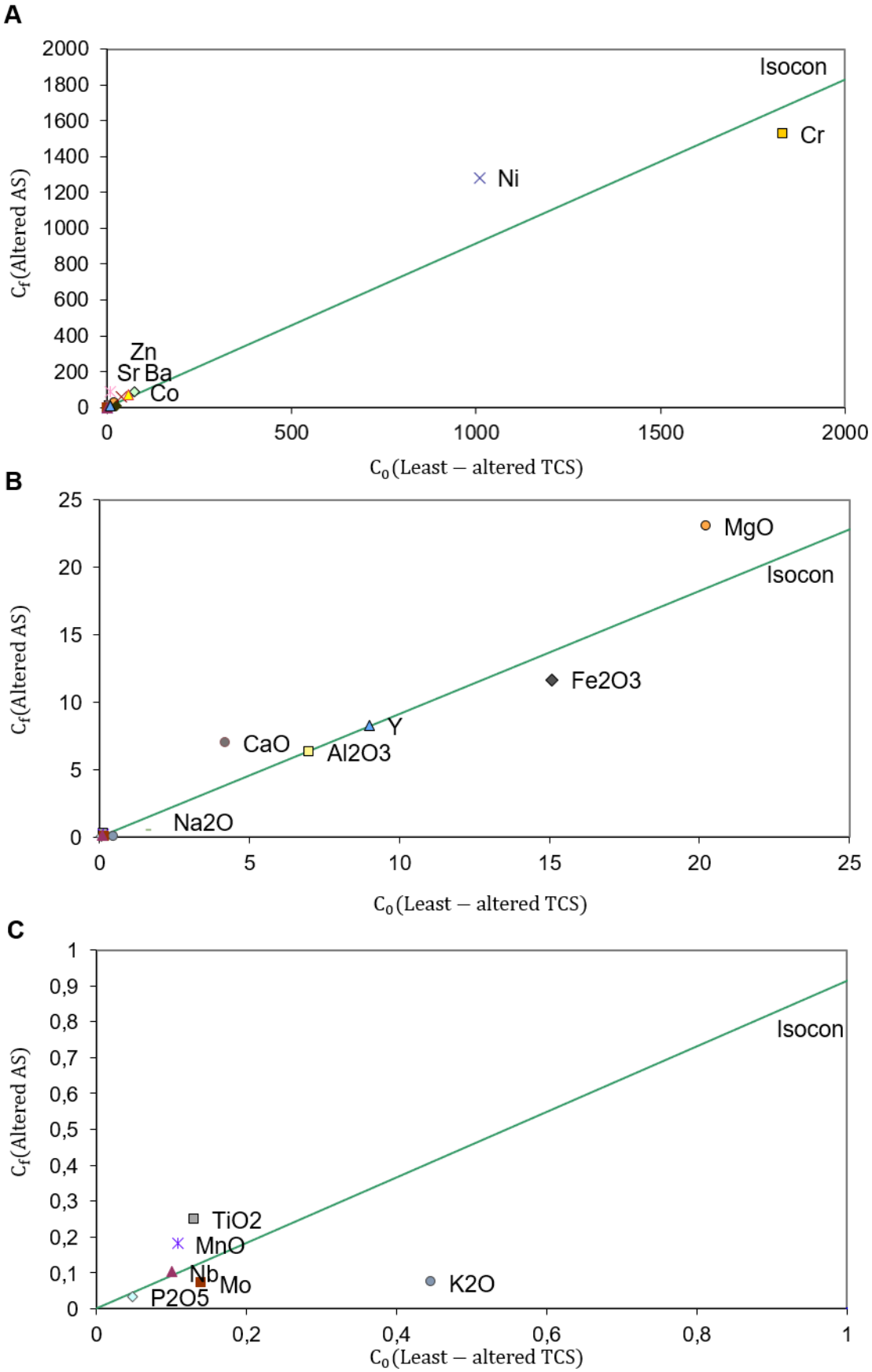

Figure 25. ISOCON diagrams of the amphibolite schist with different scales.

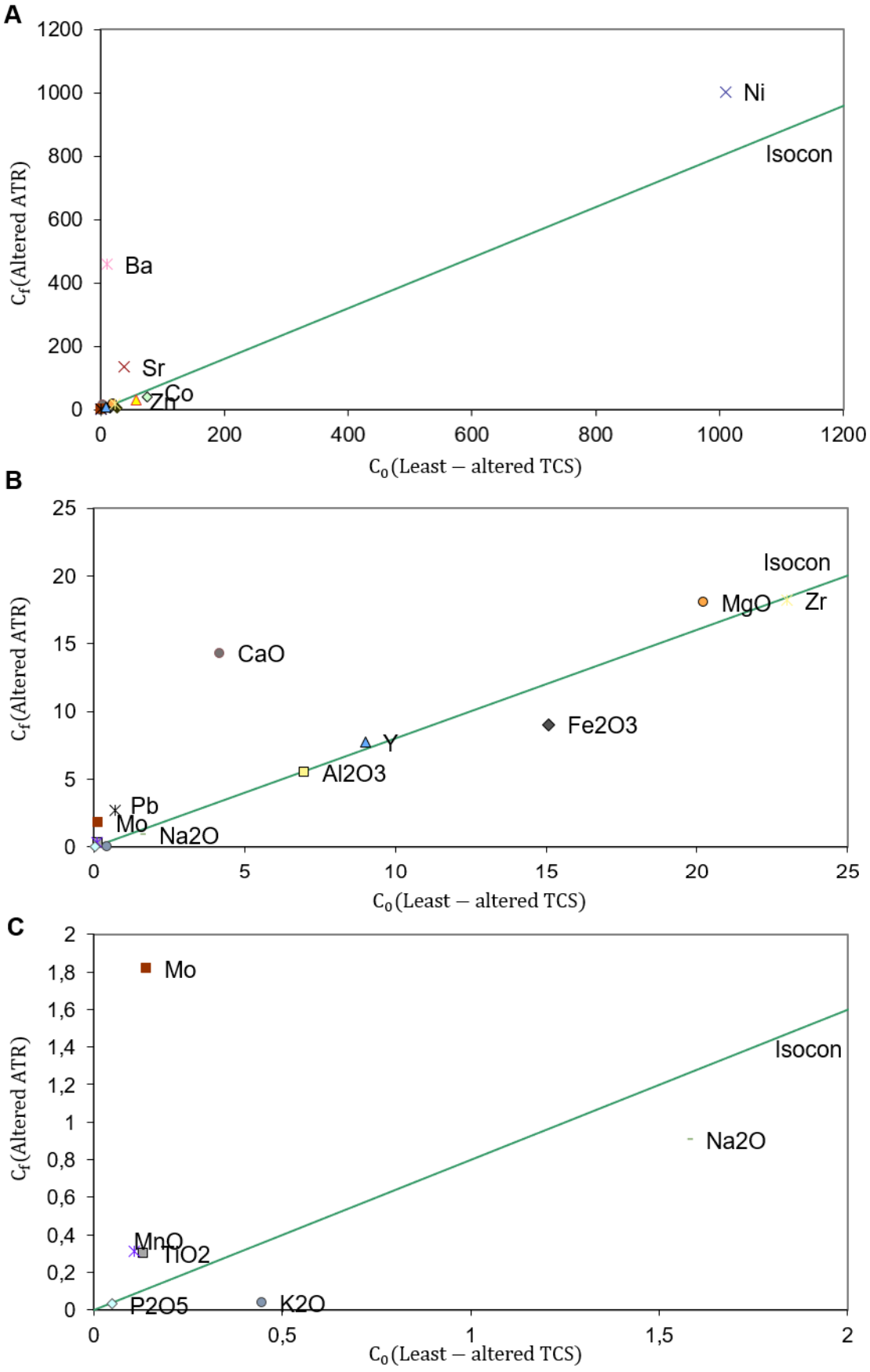

Figure 26. ISOCON diagrams of the actinolite-tremolite rock with different scales.

7.4 Combining the pXRF and laboratory results

Downhole plots of the selected drill holes 116227, 116231, 117310 and 117312 are presented in Figures 27-30. The data used in the downhole plots are a combination of the pXRF and laboratory analyses (Appendices 7-10) and an aim was to cover the parts which did not have pre-existing multi-elemental data from the laboratory. The drill holes in which data were not skewed by the thorium spikes, were selected for presentation. Elements Al, Ca, Cr, Cu, Fe, Mg, Mn, Ni, S, Sr and Zn, in addition of Au, were selected for the plotting due to their accuracy in the pXRF measurements.

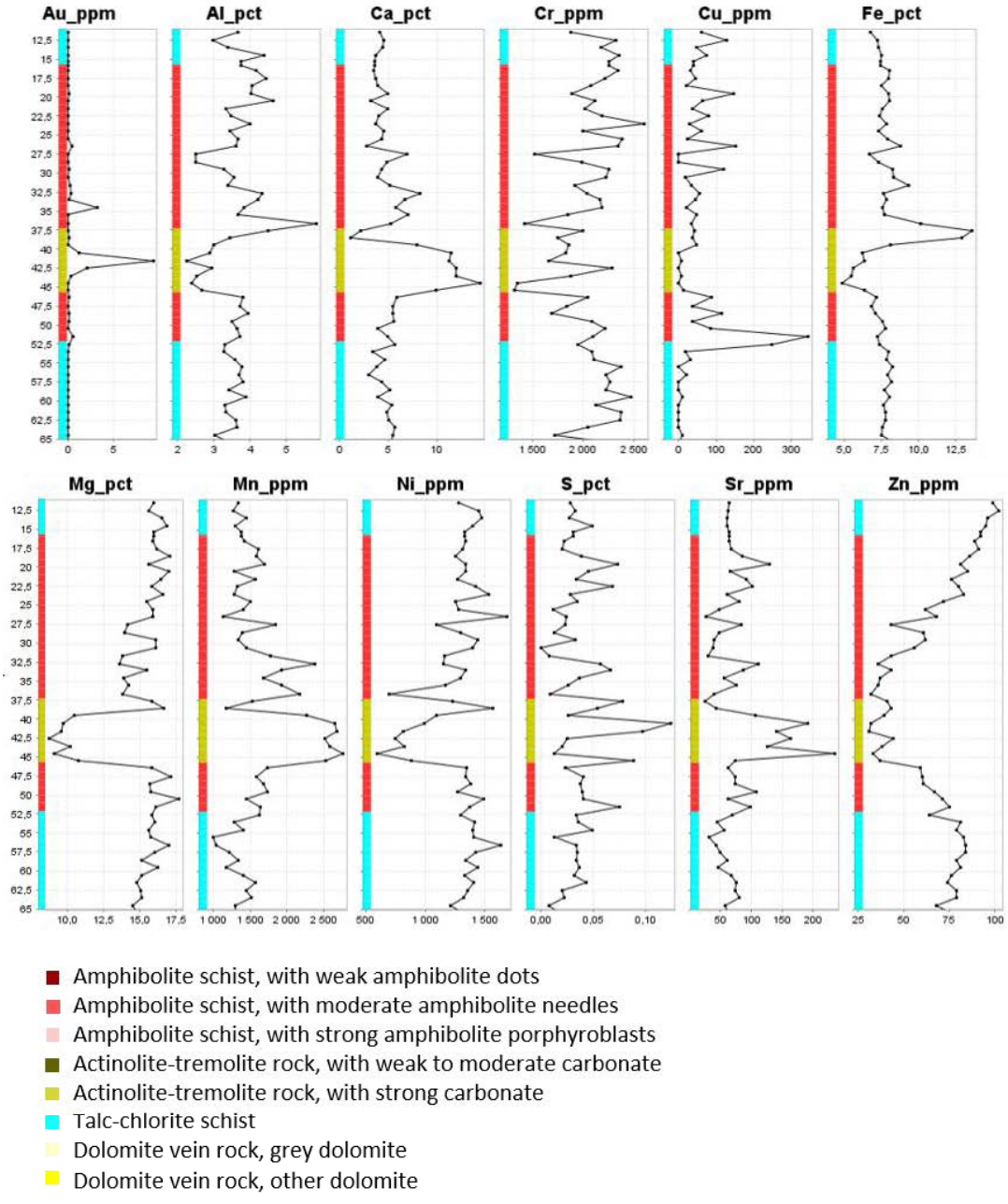

Figure 27. Downhole plot of the drill hole 116227.

Looking at the gold grades of the drill hole 116227 (Figure 27), there are a couple of samples with a higher gold grade. The one with the highest grade 9.36 ppm Au at the depth of 41-42 m is associated with the actinolite-tremolite rock with strong carbonate and shows depletion in Al, Cu, Fe, Mg, Ni, S and Zn and great enrichment in Ca, Mn, and Sr. The sample with a smaller grade, 3.21 ppm Au, at the depth of 34-35m is slightly enriched in Al, Ca, Mg, Mn, Ni and Sr and depleted in Cu, S, and Zn. The zone between those two samples with higher gold grades is characterised by high concentration of Al, Fe, Ni and low Ca, Mn and Sr.

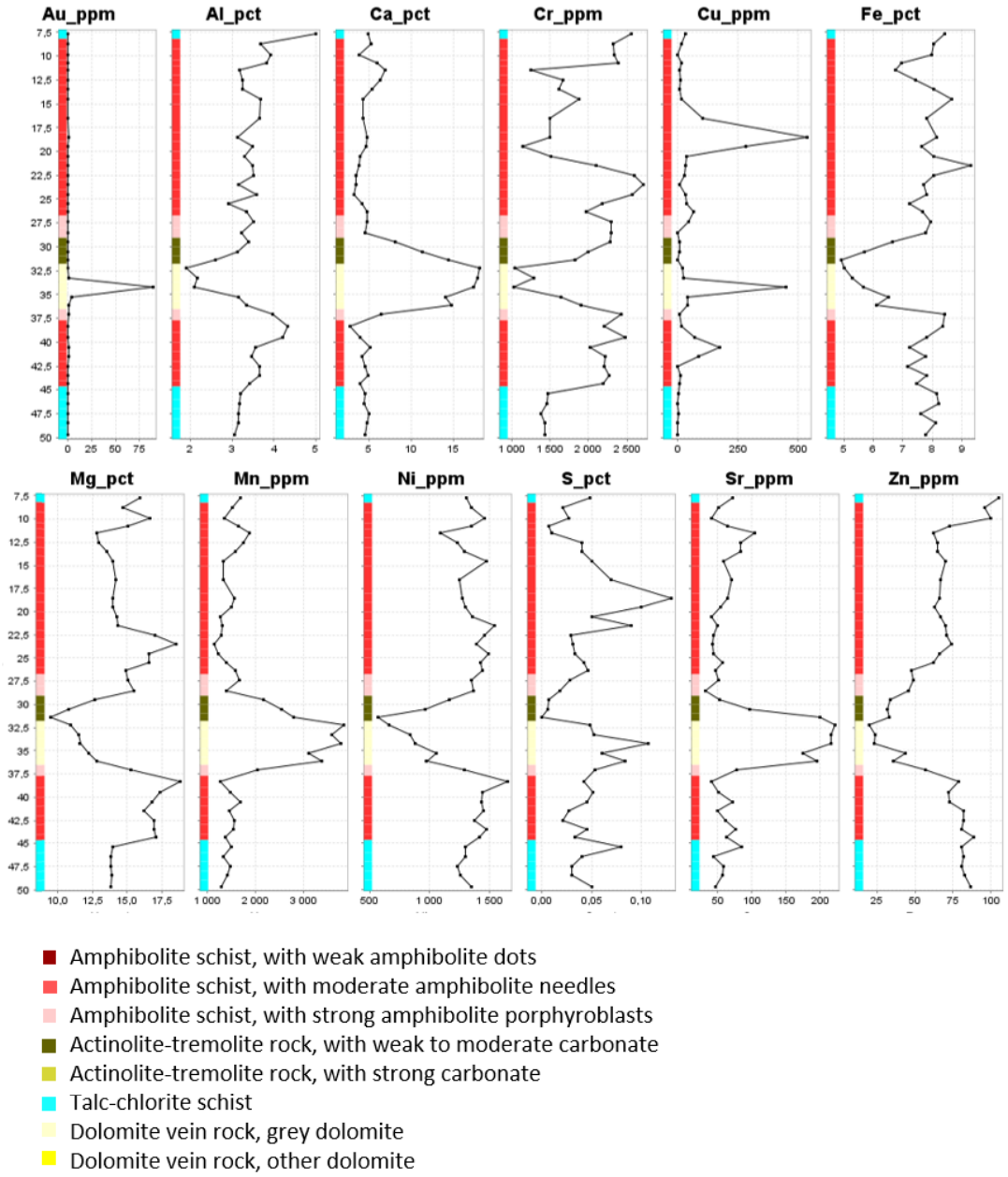

Figure 28. Downhole plot of the drill hole 116231.

The drill hole 116231 (Figure 28) shows a high gold enrichment at the depth of 33.75-34.75 m with a grade of 89.4 ppm Au. It is associated with a dolomite vein, which also

explain the concentration spike of Ca. Also, Mn, Sr, Cu and S appear to show a high enrichment. Al, Cr, Fe, Mg, Ni and Zn in turn, seem to have lower concentrations at the point of high gold grade.

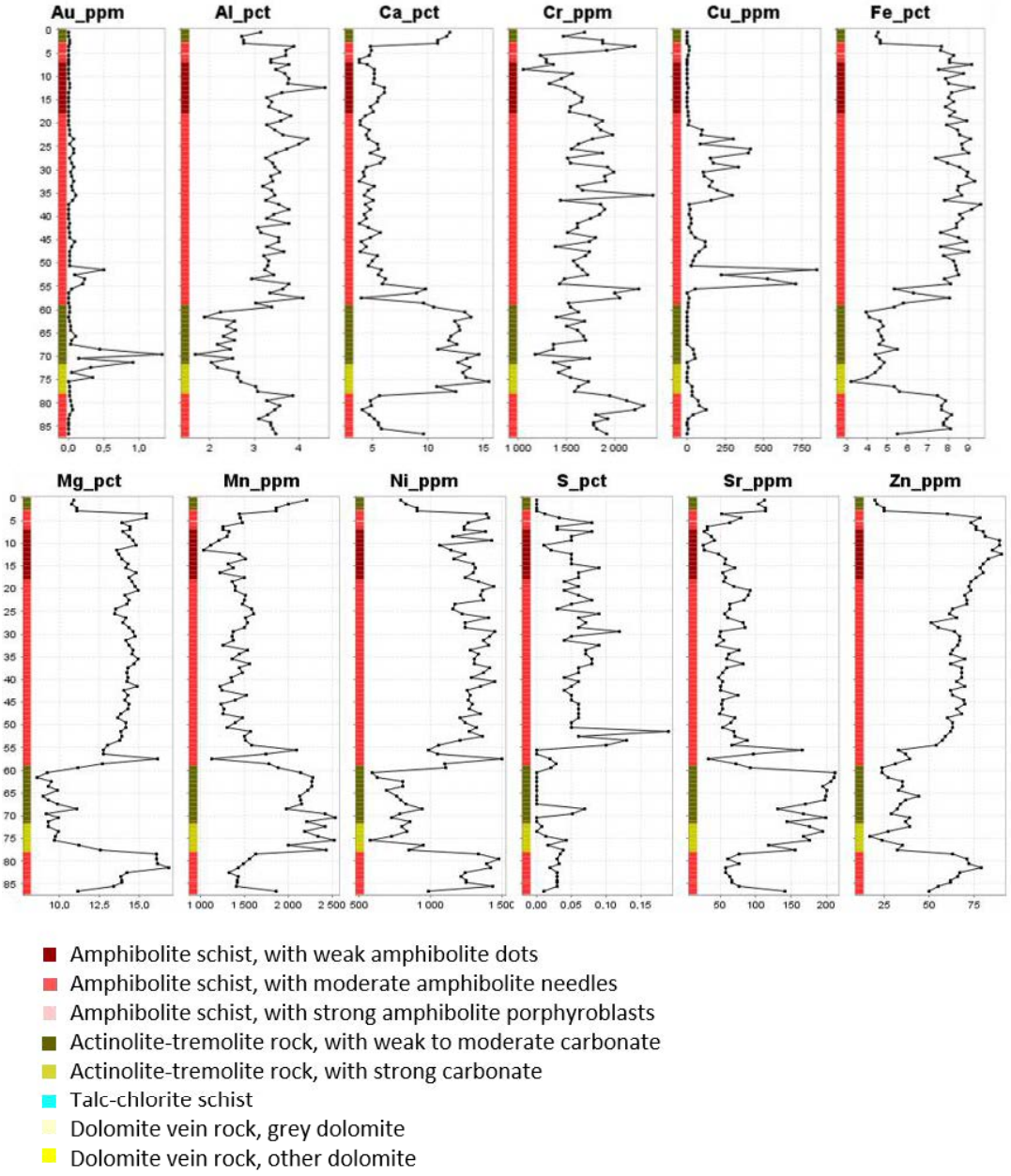

Figure 29. Downhole plot of the drill hole 117310.

The drill hole 117310 (Figure 29) includes two zones of gold enrichment with relatively low gold grades at depths of 51-55m and 68-75m. The first one, associated with amphibolite schist, is characterised by high concentrations of Al, Cu, Fe, Mg, Ni and S, and low Ca, Mn and Sr. The second enrichment, associated with actinolite tremolite rocks, shows enrichment of Ca, Mn, S and Sr whereas it is depleted in Al, Cr, Mg, Ni and Zn.

The drill hole 117312 (Figure 30) shows 7.49 ppm Au at depth of 24.24-25m. It is associated with dolomite veins with higher concentrations of Ca, Fe, Mn, S and Sr, and lower Al, Cr, Cu, Mg, Ni and Zn.

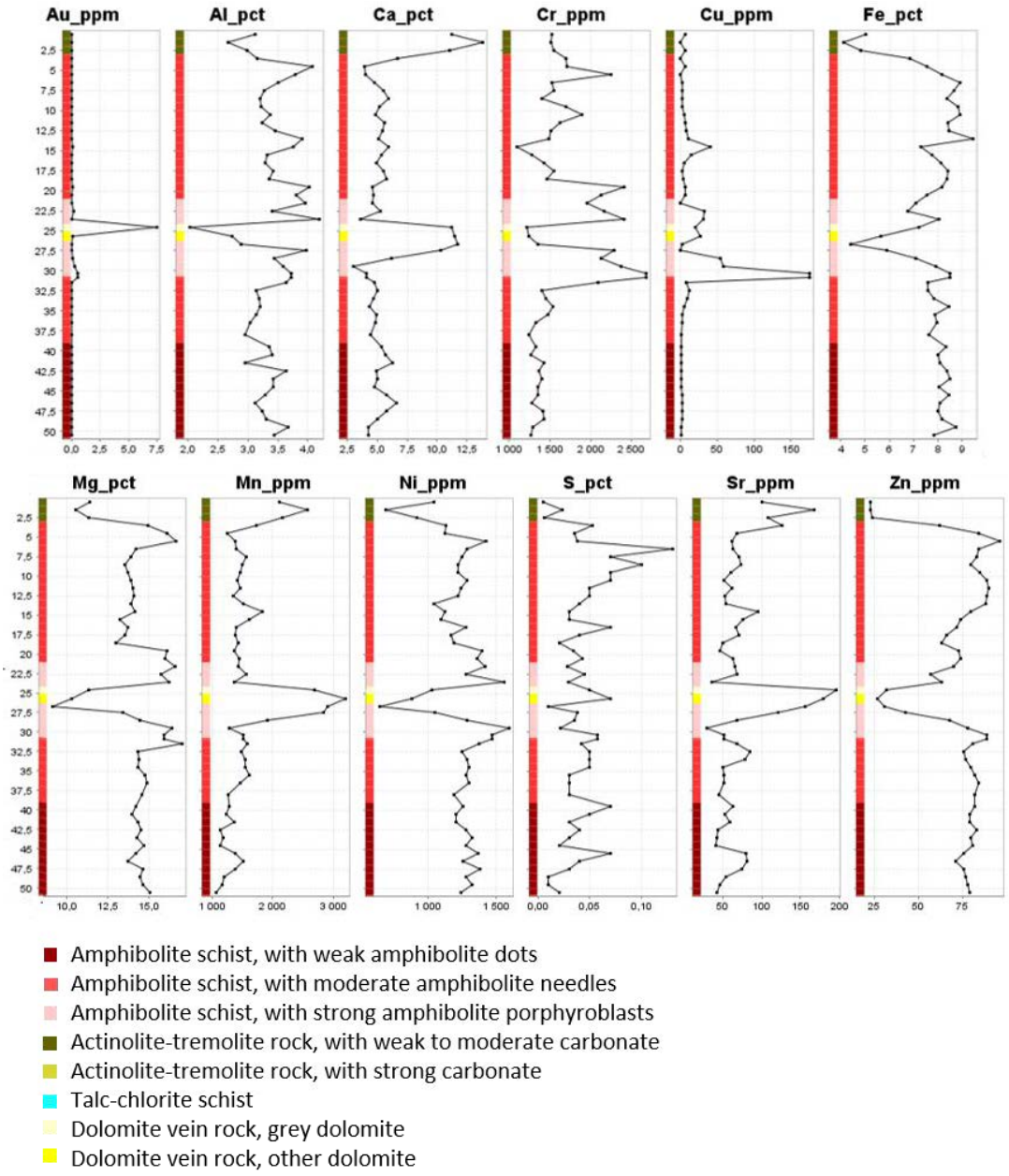

Figure 30. Downhole plot of the drill hole 117312.

8 DISCUSSION

8.1 Sources of error in the pXRF measurements

8.1.1 Sample material and preparation

According to Parsons (2012), the presence of water in the sample material has a negative impact to the pXRF results. Homogeneous sample material in turn, results a better repeatability of the measurements. Due to these facts, the pulp samples which are rather dry and homogeneous based on the fineness of material, should be suitable to use for the pXRF measurements (see Hatakka et al., 2016).

The facilities during the pXRF measurements were not as clinical as they would be in a laboratory. Even though the plastic bags and Prolene® thin films were changed and the table was cleaned after each sample, contamination could have still happened when using the same gloves and equipment. Due to a high number of measurements of the blank sample it should be the most exposed for contamination. However, the results of the blank sample did not show significant variation between the first and the last samples and, therefore, it may be concluded that the contamination level during the project was not remarkable high.

Errors can be involved in the sample preparation. To avoid them, it is needed to repeat every preparation and measurement as same way as possible. Differences in packing the samples can cause unwanted variations in the results. Although the samples were grinded as very fine, variations can be seen in the texture of the pulp samples. Some samples are easy to pack tightly in the cup whereas some samples are looser and more difficult to pack that tightly.

Hatakka et al. (2016) noticed that measurements through a plastic sample bag may be affected by the material and thickness of the bag. In this study the measurements were conducted through the Prolene® thin film which may also have an effect to the results even though it was not separately studied. However, the use of separate thin film for each sample decreases the risk of contamination.

8.1.2 Limits of detection

The manufacturer has given limits of detection to the Olympus Vanta C analyser and Geochem mode. However, the limits are only indicative and are depending on the factors which have been installed on the device (e.g. the rock type which the device is mostly used for) before shipping to the customer. According to that, the devices with the same model and mode may give different results due to the different calibration and, therefore, it is undesirable to focus on only the numbers of the limits of detection (Juha Lyytikäinen, personal communication). In this study for example, the concentration of K lower than 1500 ppm were not detected at all, or the pXRF gives a much lower concentration than it should. However, in greater concentrations the results were relatively accurate.

8.1.3 Effect of uranium

According to Parsons et al. (2012), there may occur an interference of the emission lines of some elements which affects to the detected concentrations. The resolution of the detector may not be able to segregate the emission lines close to each other. They also noted that elements with similar atomic number (Z) may influence concentration of each other: an element with atomic number Z affects to the concentration of Z+1 and Z-1 more likely if the element Z occurs in concentration more than 10% (see Hatakka et al., 2016).

The atomic number of U is 92 and Th is 90. The samples with increased thorium concentrations had uranium only several tens of ppm. Therefore, the effect of similar atomic number cannot be directly assumed as the reason of skewed results. However, it seems quite evident that the increased concentration of uranium, shown as thorium spikes in the results, is somehow affecting to the concentration of the other elements, especially Mn, Sr and S. The reason may be related to the interference of emission lines. In any case, more detailed study is needed to verify this.

8.2 Quality of the pXRF data

Looking at the correlation coefficients of the original dataset with the outliers, all the correlation methods showed a positive correlation > 0.5 for mainly all detected elements: Al, Ca, Cr, Cu, Mg, Ni, Sr, Y and Zn. The pXRF measurements of the elements Ti, V and Zr in turn, seemed not be correlating with their laboratory analyses. The statement of

Reimann and Filzmoser (1999) of why the use of parametric, no-robust methods for the geochemical data are not recommended is also seen in here in the case of Mn and S. The Pearson correlation coefficient is very sensitive to the outliers and according to that, it does not indicate of correlation in Mn and S analyses, whose distributions were highly affected by the outliers. However, the Spearman and Kendall-tau, more outlier robust methods, showed a great correlation between the elements and their laboratory analyses even with the presence of the outliers. When taking into an account the nature of geochemical data, it might not be necessary to clean the dataset from the outliers but be aware of the presence of them and choose the suitable methods for that kind of data.

It is interesting to note that the elements which were assumed to be relatively accurate based on the correlation coefficients, appeared to show varying and, in some cases relatively unacceptable deviations in the R%-charts of the standard and blank samples. That is the case for example with Cr, Cu, Mg, Mn, S and Y. The deviation of Cr in the R%-chart of the standard samples, is a way above the 30 % deviation. Also, the charts of Cu, S and Y showed high variations in the measured values and often greater than 30% deviation. The deviation of Mn in the blank sample were highly varying above and under the ± 30% deviation. However, the measurements of duplicate samples indicate excellent repeatability for Al, Ca, Cr, Cu, Fe, Mn, Ni, Rb, K, S, Si, Sr, Ti, V, and Zn whereas the distribution of Mg, Y and Zr were not as linear as the others.

It is needed to note that many of the examined elements occur in a scale of several tens of ppm and according to that, a variation of couple of ppm may lead to a high deviation between the comparable values. It is possible that the concentration of some element is affecting to the concentration of the others, for example by the interference of emission lines or closeness of the atomic numbers like discussed before, and, therefore, the deviation of an element may differ between the quality control samples.

8.3 Usability of the pXRF data

Although many elements in the conducted statistical analyses showed accuracy and precision, it is in order to ask which purposes the data are suitable for. For the downhole plots, a combined data of the pXRF and laboratory analyses were used, and the elements were chosen for plotting by their reliability, or at least well indicative features based on the statistical analyses. In the downhole plots, similar trends of the elements at the points

of higher gold grade were detected: the concentrations of Al, Fe, Mg, Ni and Zn decrease whereas Ca, Mn and Sr increase. Sometimes the concentrations of Cu and S are increased, possible due to presence of chalcopyrite. Cr showed a high depletion in cases where the gold is associated with dolomite veins. However, due to the number of studied drill holes, the conclusion of which elements are depleted or enriched cannot assumed to be valid in the deposit as a whole, especially when the previous studies (e.g. Korkiakoski, 1992) have shown the occurrence of gold is diverse.

The use of pXRF data for modelling the hydrothermal alteration is troublesome due to the absence of Na measurements and, K measurements which are many times under the limits of detection. However, the pXRF is capable to detect Si, which is not detected by the ICP-MS method. Unfortunately, due to the lack of Si analyses of the Pahtavaara rocks, it was not possibly to study the accuracy of Si results of the pXRF.

Many geochemical studies require trace element analyses but the detection of these elements by the pXRF is commonly characterised by problems with the limits of detection. The studies based on the immobile elements often requires the analyses of trace elements. Major elements Al and Ti and trace elements Y and Zr, which can be assumed rather immobile (see Mathieu, 2018 and references therein), were possible to detect by the pXRF. Nonetheless, of these elements only Al and Y showed that kind of accuracy which may be used in further studies.

8.4 Geochemical modelling

8.4.1 Immobile elements

Immobility of elements were utilised in the modelling of geochemistry, ISOCON diagrams and related mass balance calculations. Making right choices in the selection of the immobile elements is crucial because choosing of relatively mobile element instead of immobile may lead to serious misinterpretations. The elements Al, Nb, Ti, Zr and, rare earth elements such as Sc and Y are some of the commonly used immobile elements (see Mathieu, 2018 and references therein). Eilu (2015) also concluded that, Al, Ti and Zr are immobile in the alteration haloes of orogenic gold deposits. Based on these research results, Zr and Ti, as well as Sc, Y, Zr, were used in the comparison of Pahtavaara and other komatiite deposits, and in the distribution of the lithological units of the study area.

The EASYGRESGRANT Excel spreadsheet provided a way to conduct the mass balance calculations by using the immobile elements which was needed because both unaltered and altered samples did not have density values. In the spreadsheet, it was possible to choose the immobile element by clusters of slopes. The slopes of elements close to one another were selected as immobile elements (López-Moro, 2012). The talc-chlorite and amphibolite schist showed close slopes for Al_2O_3, Zr and Nb. However, the slopes were different for the actinolite-tremolite rock, in which the chosen immobile elements were Al_2O_3, Zr and Y. This led to a suspect that the elements considered as immobile have actually behaved relatively mobile in some lithological units.

8.4.2 Precursors

There were difficulties to find a suitable precursor for the mass balance calculations and modelling the hydrothermal alteration since all the komatiites near by the Pahtavaara deposit show some styles of alteration. As seen in the alteration box plots, the Sattasvaara komatiites also showed the same alteration trends as the rocks in Pahtavaara and, therefore, cannot be considered as a precursor. The talc-chlorite sample from the exploration drill hole 117300 is also at least talc and chlorite altered, but due to the proposal of Korkiakoski (1992) the amphibole-chlorite schist, occurring occasionally as talc-rich varieties with homogeneous and fine-grained texture, being the least-altered rock type in the deposits, the mass balance calculation were conducted with the talc-chlorite unit which may be considered as the closest of rock type to the amphibole-chlorite rock. An advantage for using the sample from the exploration drill hole was that the sample was analysed for the same elements as the altered samples.

The lithological units of the Pahtavaara were differently distributed in the Zr vs Ti diagram. This division of immobile element contents between the lithological units is thought-provoking since it means that the precursor may not be the same for all the units. Taking this into an account, it further complicates the selection of precursors for the Pahtavaara lithological units.

8.4.3 Hydrothermal alteration

The AI-CCPI diagram indicated intensive chloritisation for the talc-chlorite and amphibolite schists. The alteration of actinolite-tremolite rock in turn, was trending more towards carbonatisation. In the K/Al vs. Na/Al molar ratio diagram, the actinolite-tremolite rocks plotted closer the plagioclase end whereas the other two units were located in the corner of clay minerals. Chlorite is also part of the clay mineral group but so are the kaolinite group minerals, and therefore, two scenarios are possible: the talc-chlorite and amphibolite schists are 1) chloritised or 2) rocks show argillic alteration. However, the other clay minerals in addition the chlorite have not been detected in the Pahtavaara deposit (Rupert Resources, unpublished report) and therefore, the trending towards the clay minerals indicates most probably of chloritisation.

Sericite, K-feldspar, biotite and albite alteration, which are common in orogenic gold deposits (Eilu, 2015), were totally absent. However, the data did not include any biotite-rich lithological units, which are common in some parts of the Pahtavaara deposit and due to that, some of the alteration styles were not observed. Carbonatisation is typical alteration style for both orogenic and VMS deposits. Chloritisation in turn, are more common for VMS system.

However, the formation of chlorite can also be related to carbonatisation of komatiites producing talc+chlorite+carbonate alteration assemblages (see Table 2) by a reaction of CO_2 (metamorphic fluid) and tremolite (metavolcanic rock):

$$\text{Tremolite} + 4CO_2 = 2\ \text{dolomite} + H_2Mg_3Si_4O_{12} + 4SiO_2, \text{talc (Pirajno, 2009)}$$

It thus seems possible that the actinolite-tremolite rock may actually be the least-altered unit in Pahtavaara and the talc-chlorite schists are produced by talc-chlorite-carbonate alteration of tremolite-dominated rock. However, the talc-chlorite schist did not show trending towards carbonate in the geochemical alteration diagrams so more detailed study is needed to verify this.

8.4.4 Mass balance calculation

The mass balance calculation showed the same trends in enrichment and depletion for all the lithological units: enrichments in Ni, Ba, MgO, CaO, TiO_2, Sr and MnO, and depletions in Cr, Fe_2O_3, Na_2O, Mo, K_2O and P_2O_5. The results of mass balance calculation of the talc-chlorite schist and amphibolite schist were almost identical. The actinolite-tremolite rocks in turn, showed higher concentrations of Ba, Mn and Sr than the former two.

The results are partially inconsistent with the proposal of Korkiakoski et al. (1987) in which they stated the alteration halo of Pahtavaara is characterised by high K, Ba, Sr contents and relatively low Mg, Co and Zn. The mass balance calculation of this study showed higher concentration of MgO and lower K_2O for all the altered rock types, and higher contents of Co and Zn for the talc-chlorite and amphibolite rocks. However, the depletion of Co and Zn is consistent in the case of altered actinolite-tremolite rock.

The hydrothermal alteration models showed the intensive chloritisation of the talc-chlorite and amphibolite schist units. In that case, the mass balance calculation should show enrichment in Fe, Mg and depletion in Na, Ca, K (Table 2). However, the mass balance calculations showed depletion in Fe and enrichment in Ca which is inconsistent with the expected alteration style. As discussed above, the formation of chlorite in the talc-chlorite and amphibolite schists may be related to carbonatisation of tremolite-dominated rock instead of chloritisation. In that case, the enrichment of Ca in the mass balance calculations is consistent with the style of hydrothermal alteration. The mass balance calculation of the actinolite-tremolite rock also showed a great enrichment of Ca which is consistent with carbonatisation detected in the alteration modelling.

The calculations of the talc-chlorite and amphibolite schist did not seem to have many differences. It may be related to a unsuitable precursor, but it is also possible that the average compositions of the altered samples used in the calculations were affecting to the results and, therefore, results could have been different if only one sample had been selected to representing the altered rock type. However, in that case, an unsuitable selection would have also led to a skewed result. When using the average composition of the rock types, it is also depending of the possible mistakes occurred during the logging process.

9 CONCLUSIONS

Based on the result and discussion above, the following conclusions can be drawn:

1. Based on the statistical analyses of the geochemical data of Pahtavaara rocks gained with Olympus Vanta portable X-ray fluorescence analyser, the results are

- Excellent for Ca, Fe, Ni, Sr and Zn
- Very good for Mn
- Good for Al and Mg
- Satisfactory for Cr, Cu, S and Y
- Bad for Ti, V and Zr
- in need of more detailed study for K, Si, Rb and undetected elements Ag, As, Bi, Cd, Co, Hg, Mo, Nd, P, Pb, Sb, Se, Sn, Th, U, and W.

2. Gold enrichments in the drill holes 116227, 116231, 117310 and 1171312 are depleted in Al, Fe, Mg, Ni and Zn and enriched in Ca, Mn and Sr based on the combined data of pXRF and ICP-MS analyses.

3. Although the portable XRF provides fast and cost efficient method for geochemical analyses with good accuracy and repeatability in some elements, due to the limits of detection and elements completely out of the detection, such as K, Na and certain trace elements, the use of portable XRF is recommended only as an indicative method and it cannot replace the laboratory analyses.

4. There is no correlation between the komatiites of Pahtavaara and Peuramaa. The composition of Lomalampi and Jeesiörova komatiites are closer the ones of Pahtavaara but, however, no significant correlation is detected.

5. There are two possible scenarios related to the precursors of the Pahtavaara rocks: 1) the rocks have different precursors based on the varying contents of immobile element Zr and Ti between the lithological units or, 2) the precursor is same for all the units and either Zr or Ti has been relatively mobile during the hydrothermal processes and the units have characterised by different styles of alteration.

6. Alteration of the talc-chlorite and amphibolite schist were trending towards chloritisation. However, the mass balance calculation suggest that the formation of chlorite is more likely related to carbonatisation of tremolite-dominated rock unit producing the talc-chlorite-carbonate mineral assemblages instead of chloritisation. If so,

the least-altered lithological unit in Pahtavaara is the actinolite-tremolite rock instead of the talc-chlorite schist assumed in the literature. The actinolite-tremolite rock, in turn, was characterised by carbonatisation which is consistent with the mass balance calculations. The absence of K-feldspar and sericitic alteration may be related lack of biotite-rich units in the dataset.

7. Based on the mass balance calculation, all the lithological units of the study area – talc-chlorite and amphibolite schists and, actinolite-tremolite rock, were enriched in MgO, CaO, TiO_2, MnO, Ba and Sr, and depleted in Fe_2O_3, Na_2O, and K_2O. The actinolite-tremolite rock appeared to show greater enrichments of Ba, Sr and Mn compared to the other units. Whereas Co and Zn were enriched in the talc-chlorite schist, they were depleted in the actinolite-tremolite rock. However, it is needed to keep in mind that the precursor used in the calculation, the least-altered talc-chlorite schist, may not be the most suitable one due to the reasons mentioned above.

10 ACKNOWLEDGEMENTS

I wish to thank the following people for their help during the thesis project:

- My supervisor, Jukka-Pekka Ranta for guiding me though the project and sharing his knowledge about the subject.
- Exploration manager of Rupert Resources, Charlotte Seabrook for trusting my abilities by offering me the topic and letting me to develop the subject in my point of view.
- Project geologists of Rupert Resources, Kalle-Pekka Kotiaho, Karoliina Penttinen and Otso Mäkimattila for continuous support and answers for multiple questions. Special thanks also for guiding me on my first steps as becoming a geologist.
- Anssi Mäkisalo, Ukko-Pekka Yliranta and Anni Piispanen for their time for pre-reading the thesis and especially for the comments which gave an important perspective for refining the text to its final form.
- Juha Lyytikäinen and Anna Railo from GWM Engineering for helping with the use of Olympus Vanta pXRF analyser and for the discussions about the capability of the device.
- Hannu and my family for the endless support and encouragement.

REFERENCES

Agnico Eagle Mines Limited, 2019. Annual Information Form for the year ended December 31, 2018 [online document]. Available from https://s21.q4cdn.com/374334112/files/doc_financials/annual/2018/AIF-2018.pdf [Accessed 15 April 2020]

Ahrens, L.H., 1954. The lognormal distribution of the elements (A fundamental law of geochemistry and its subsidiary). Geochim Comochim Acta, 5, 49-74 pp.

ALS, 2020. Schedule of services and fees [online document]. Available from https://www.alsglobal.com/-/media/als/resources/services-and-products/geochemistry/fee-schedules/als-geochemistry-fee-schedule-aud.pdf [Accessed 17 April 2020]

Arndt, N.T. and Nisbet, E.G., 1982. What is komatiite? In: Arndt, N.T. and Nisbet, E.G. (eds.), Komatiites. London: George Allen & Unwin, p. 19 - 27.

Digital map database - Bedrock of Finland 1:5 000 000 [Electronic resource]. Espoo: Geological Survey of Finland [referred 15.04.2020]. Version 2.0.

Digital map database - Bedrock of Finland 1:200 000 [Electronic resource]. Espoo: Geological Survey of Finland [referred 15.04.2020]. Version 2.1.

Digital map database – Mineral Deposits of Finland [Electronic resource]. Espoo: Geological Survey of Finland [referred 15.04.2020]. Version 1.0.

Boyle, R.W., 1979. The geochemistry of gold and its deposits. Geological Survey of Canada, Bulletin 280, p. 584 p.

Brown, P.E., 1998. Fluid inclusion modelling for hydrothermal systems. Reviews in Economic Geology 10, p. 151-171.

Böhlke, J.K., 1982. Orogenic (metamorphic-hosted) gold-quartz veins. U.S. Geological Survey, Open-File Report 82–795, p. 70–76.

Cline, J.S., Hofstra, A.H., Muntean, J.L., Tosdal, R.M. and Hickey, K.A., 2005. Carlin-Type Gold Deposits in Nevada: Critical Geologic Characteristics and Viable Models. Economic Geology 100th Anniversary Volume, p. 451-484.

Davies, J.F. and Whitehead, R.E., 2006. Alkali-Alumina and MgO-Alumina Molar Ratios of Altered and Unaltered Rhyolites. Exploration and Mining Geology 15 (1), p. 75-88.

Eilu, P. (ed.) 1999. FINGOLD – a public database on gold deposits in Finland. Geological Survey of Finland, Report of Investigation 146, 224 p.

Eilu, P., 2015. Gold deposits. In Maier, W., Lahtinen, R. and O'Brien, H. (eds.), Mineral Deposits of Finland. Elsevier, p. 377-410.

Eilu, P., Mathison, C., Groves, D. and Allardyce, W., 1999. Atlas of Alteration Assemblages, Styles and Zoning in Orogenic Lode-Gold Deposits in a Variety of Host Rock and Metamorphic Settings. Geology and Geophysics Department (Centre for Strategic Mineral Deposits) and UWA Extension, The University of Western Australia, Publication 30, 50 p.

Eilu, P., Pankka, H., Keinänen, V., Kortelainen, V., Niiranen, T. and Pulkkinen, E., 2007. Characteristics of gold mineralisation in the greenstone belts of northern Finland. In:

Ojala, J. (ed.), Gold in the Central Lapland Greenstone belt. Geological Survey of Finland, Special Paper 44, p. 57−106.

Eilu, P., Pankka, H., 2009. FINGOLD—A public database on gold deposits in Finland. Version 1.0. Geological Survey of Finland. Digital data product 4. Optical disc (CDROM).

Eilu, P., Niiranen, T., Hulkki, H. and Nykänen, V., 2012. Metallogenic areas in Finland - F043 Kittilä Au, Cu. In Eilu, P. (ed.), Mineral deposits and metallogeny of Fennoscandia. Geological Survey of Finland, Special Paper 53, p. 314-317.

Galley, A.D., Hannington, M.D. and Jonasson, I.R., 2007. Volcanogenic massive sulphide deposits. In: Goodfellow, W.D. (ed.), Mineral Deposits of Canada: A Synthesis of Major Deposit-Types, District Metallogeny, the Evolution of Geological Provinces, and Exploration Methods. Geological Association of Canada, Mineral Deposits Division, Special Publication 5, p. 141-161.

Gifkins, C.C., Herrmann, W. and Large, R.R., 2005. Altered Volcanic Rocks: A Guide to Description and Interpretation. Centre for Ore Deposit Research, University of Tasmania, 275p.

Goldfarb, R.J., Groves, D.I. and Gardoll, S., 2001. Orogenic gold and geologic time: A global synthesis. Ore Geology Reviews 18, p. 1–75.

Goldfarb, R.J., Baker, T., Dube, B., Groves, D.I., Hart, C.J.R. and Gosselin, P., 2005. Distribution, character, and genesis of gold deposits in metamorphic terranes. Economic Geology 100th Anniversary Volume, p. 407–450.

Goldfarb, R.J and Groves, D.I., 2015. Orogenic gold: Common or evolving fluid and metal sources through time. Lithos 233, p. 2-26.

Groves, D.I., Ridley, J.R., Bloem, E.M.J., Gebre-Mariam, M., Hagemann, S., Hronsky, J.M.A., Knight, J.T., McNaughton, N.J., Ojala, J., Vielreicher, R.M., McCuaig, T.C. and Holyland, P., 1995. Lode-gold deposits of the Yilgarn block: Products of Late Archaean crustal-scale overpressured hydrothermal systems. Geological Society, London, Special Publications 95, p. 155-172.

Groves, D.I., Condie, K.C., Goldfarb, R.J., Hronsky, J.M.A. and Vielreicher, R., 2005. Secular changes in global tectonic processes and their influence on the temporal distribution of gold-bearing mineral deposits. Economic Geology 100th Anniversary Volume, p. 203–224.

Groves, D.I., Bierlein, F.P., Meinert, L.D. and Hitzman, M.W., 2010. Iron Oxide Copper-Gold (IOCG) Deposits through Earth History: Implications for Origin, Lithospheric Setting, and Distinction from Other Epigenetic Iron Oxide Deposits. Economic Geology 105, p. 641–654

Groves, D.I., Santosh, M., Goldfarb, R.J and Zhang., L., 2018. Structural geometry of orogenic gold deposits: Implications for exploration of world-class and giant deposits. Geoscience Frontiers 9(4), 16 p.

Hanski, E., 1986. Intrusions of the gabbro-wehrlite association and their stratigraphic implications in Finland. In: V.A. Sokolov and K.I. Heiskanen (eds.), Early Proterozoic of the Baltic Shield. Proceedings of the Finnish Soviet Symposium held in Petrozavodsk 19th–27th August 1985. Karel'skij Filial AN SSSR, Petrozavodsk, p. 123–136.

Hanski, E., 1987. Differentiated albite diabases - gabbro wehrlite association. Geological Survey of Finland, Report of Investigation 76, p. 35-44.

Hanski, E., 1992. Petrology of the Pechenga ferropicrites and cogenetic, Ni-bearing gabbro-wehrlite intrusions, Kola Peninsula, Russia. Geological Survey of Finland, Bulletin 367, 192 p.

Hanski, E., 1997. The Nuttio serpentinite belt, Central Lapland: An example of Paleoproterozoic ophiolitic mantle rocks in Finland. Ofioliti 22, p. 35–46.

Hanski, E., Mänttäri, I., Huhma, H., and Rastas., P. 2000. Post-1.88 Ga deposition of the Kumpu and Lainoa Group molasses-type sediments in northern Finland: evidence from conventional and NORDSIM zircon dating. 24th Geological Winter Meeting, Trondhem, January 6-9, 2000, Abstracts, p. 75.

Hanski, E., Huhma, H., Rastas, P. and Kamenetsky, V.S., 2001. The Palaeoproterozoic Komatiite-Picrite Associates of Finnish Lapland. Journal of Petrology, Volume 45, Issue 5, p. 855-876.

Hanski, E. and Huhma, H., 2005. Central Lapland greenstone belt. In: Lehtinen, M., Nurmi, P.A. and Rämö, O.T. (eds.), Precambrian Geology of Finland – Key to the Evolution of the Fennoscandian Shield. Amsterdam: Elsevier, p. 139–194.

Hart, C.J.R. and Goldfarb, R.J., 2005. Distinguishing intrusion-related from orogenic gold systems. Proceedings of the 2005 New Zealand Minerals Conference, Auckland, November 13–16, p. 125–133.

Hart, C.J.R., 2007. Reduced intrusion-related gold systems. In: Goodfellow, W.D. (ed.), Mineral deposits of Canada: A Synthesis of Major Deposit Types, District Metallogeny, the Evolution of Geological Provinces, and Exploration Methods. Geological Association of Canada, Mineral Deposits Division, Special Publication 5, p. 95-112.

Hartwig, F., and Dearling, B.E., 1979. Exploratory Data Analysis. Beverly Hills, California: Sage University Paper Series on Quantitative Research Methods 16, 83 p.

Hatakka, T., Nuottimäki, K., Sarala, P., Taivalkoski, A. and Tarvainen., T., 2016. Kenttä-XRF analysaattion soveltuvuus geokemiallisiin taustapitoisuus tutkimuksiin. Geological Survey of Finland, Archive report 97/2015, 112 p.

Hofstra, A. H. and Cline, J.S., 2000. Characteristics and models for Carlin type gold deposits. Reviews in Economic Geology 13, p. 163-220.

Hokka, J. and Soukka, T., 2016. Kannettavalle XRF-analysaattorille suunnatun näytteenottolaitteen menetelmäkehitys ja sen soveltaminen litogeokemialliseen malminetsintään. Geological Survey of Finland, Research report 85/2016, 19 p.

Hulkki, H., 1990. Sodankylän Sattasvaaran komatiittikompleksin Au-kriittinen muuttumisvyöhyke. MSc thesis. Department of Geology, University of Helsinki, 190 p.

Huhma, H., 1986. Sm-Nd, U-Pb and Pb-Pb isotopic evidence for the origin of the Early Proterozoic Svecokarelian crust in Finland. Geological Survey of Finland, Bulletin 337, 48 p.

Härkönen, I., 1992. Tutkimustyöselostus Kittilän kunnassa valtausalueella Suurikuusikko 1, kaiv.rek. n:o 4283/1 suoritetuista malmitutkimuksista. Geological Survey of Finland, Report M06/2743/-92/1/10, 5 p.

Härkönen, I., 1997. Tutkimustyöselostus Kittilän kunnassa valtausalueilla Suurikuusikko 2 ja Rouravaara 1–10 (kaivosrekisterinumerot 5965/1, 6160/1, 6288/1–6288/9) suoritetuista kultatutkimuksista vuosina 1987–1997. Geological Survey of Finland, Report M 06/2743/97/1, 47 p.

Hölttä, P., Väisänen, M., Väänänen, J. and Manninen, T., 2007. Paleoproterotzoic metamorphism and deformation in Central Lapland, Finland. In: Ojala, J. (ed.) Gold in the Central Lapland Greenstone belt. Geological Survey of Finland, Special Paper 44, p. 7-56.

Hölttä, P., Heilimo, E., Huhma, H., et al., 2012. The Archaean of the Karelia Province in Finland. Geological Survey of Finland, Special Paper 54, p. 21–73.

Kojonen, K. and Johanson, B., 1989. Pahtavaaran Au-malmiaiheen malmimineraaleista. Geologian tutkimuskeskus, Raportti M 40/3714/-88/1/41.2, 2 p.

Korkiakoski, E., 1992. Geology and geochemistry of the metakomatiite hosted Pahtavaara gold deposit in Sodankylä, northern Finland, with emphasis on hydrothermal alteration. Geological Survey of Finland, Bulletin 360, 96 p.

Korkiakoski, E.A., Pulkkinen, E., Hulkki, H. and Manner, R., 1987. Mineralogical and geochemical alteration associated with the gold prospect in the early Proterozoic Sattasvaara Komatiite Complex, Northern Finland. IGCP 217. Abstracts. Proterozoic geochemistry. Lund, June 3- 6, 52 p.

Korkiakoski, E.A., Karvinen, A. and Pulkkinen, E., 1989. Geochemistry and hydrothermal alteration of the Pahtavaara gold mineralization, Finnish Lapland. Geological Survey of Finland, Special Paper 10, p. 83 – 89.

Korvuo, E., 1997. The Saattopora gold ore and the Pahtavuoma Cu-Zn-U occurrences in the Kittilä region, northern Finland. Geological Survey of Finland, Guide 43, p. 21-25

Korkiakoski, E. A. and Kilpelä, M., 1997. The komatiite-hosted Pahtavaara gold mine near Sodankylä, northern Finland. Geological Survey of Finland, Guide 43, p. 27-29.

Köykkä, J. and Luukas, J., 2019. Keski-Lapin temaattinen kallioperätutkimus ja kartoitus 2019. Geological Survey of Finland, Report 99/2019, 30 p.

Lahtinen, R., Korja, A. and Nironen, M., 2003. Paleoproterozoic orogenic evolution of the Fennoscandian Shield at 1.92–1.77 Ga with notes on the metallogeny of FeOx-Cu-Au, VMS, and orogenic gold deposits. In: D.G. Eliopoulos (ed.) Mineral Exploration and Sustainable Development. Proceedings of the Seventh Biennial SGA Meeting, Athens, Greece, August 24-28. Rotterdam: Millpress, p. 1057–1060.

Lang, J.R. and Baker, T., 2001, Intrusion-related gold systems: the present level of understanding. Mineralium Deposita 36, p. 477-489.

Large, R.R., Gemmell, J.B., Paulick, H. and Huston, D.L., 2001. The alteration box plot: A simple approach to understanding the relationship between alteration mineralogy and lithogeochemistry associated with volcanic-hosted massive sulfide deposits. Economic Geology 96, p. 957–971.

Lehtonen, M. and Rastas, P., 1988. Aluetutkimukset - Keski-Lappi. In: Manninen, T., Hanski, E., and Kesola, R. (eds.), Lapin vulkaniittiprojektin vuosikertomus 1987. Geological Survey of Finland, Report K/1988/1, p. 4-15.

Lehtonen, M., Airo, M.-L., Eilu, P., Hanski, E., Kortelainen, V., Lanne, E., Manninen, T., Rastas, P., Räsänen, J. and Virransalo, P., 1998. Kittilän vihreäkivialueen geologia.

Lapin vulkaniittiprojektin raportti. Geological Survey of Finland, Report of Investigation 140, 144 p.

López Moro, F.J., 2012. EASYGRESGRANT—A Microsoft Excel spreadsheet to quantify volume changes and to perform mass-balance modeling in metasomatic systems. Computers and Geosiences 39 (2012), p. 191-196.

Luukas, J., Kousa, J., Nironen, M., and Vuollo, J., 2017. Major stratigraphic units in the bedrock of Finland, and an approach to tectonostratigraphic division. Geological Survey of Finland, Special Paper 60, p. 9-40.

Mathieu, L., 2018. Quantifying Hydrothermal Alteration: A Review of Methods. Geosciences, 8(7), 27 p.

McDonough, W.F. and Sun, S., 1995. The composition of the Earth. Chemical Geology 120, Issues 3-4, p. 223–253.

Molnár, F., 2019. Cobalt in orogenic gold mineral systems of northern Fennoscandia. NEXT – 3rd Progress meeting 7-10th October 2019, 3 p.

Mutanen, T. and Huhma, H., 2001. U-Pb geochronology of the Koitelainen, Akanvaara and Keivitsa mafic layered intrusions and related rocks. In: Vaasjoki, M. (ed.), Radiometric age determinations from Finnish Lapland and their bearing on the timing of Precambrian volcano-sedimentary sequences. Geological Survey of Finland, Special Paper 33, p. 229–246.

Mänttäri I., 1995. Lead isotope characteristics of epigenetic gold mineralisation in the Palaeoproterozoic Lapland greenstone belt, northern Finland. Geological Survey of Finland, Bulletin 381, 70 p.

Nesbitt, R.W., Sun, S.-S. and Purvis, A.C., 1979. Komatiites: geochemistry and genesis. Canadian Mineralogists 17, p. 165 -186.

Nurmi, P., Lestinen, P. and Niskavaara, H., 1991. Geochemical characteristics of mesothermal gold deposits in the Fennoscandian Shield, and a comparison with selected Canadian and Australian deposits. Geological Survey of Finland, Bulletin 351, 101 p.

Parsons, C., Margui Grabulosa, E., Pili, E., Floor, G.H., Roman-Ross, G. and Charlet, L. 2012. Quantification of trace arsenic in soils by field-portable X-ray fluorescence spectrometry: Considerations for sample preparation and measurement conditions. Journal of Hazardous Materials 2012, p. 10.

Patison, N.J., 2007. Structural controls on gold mineralization in the Central Lapland Greenstone Belt. In: Ojala, J. (ed.), Gold in the Central Lapland Greenstone belt. Geological Survey of Finland, Special Paper 44, p. 107-124.

Pearson, R.G., 1963. Hard and soft acids and bases. Journal of the American Chemical Society 85, p. 3533–3539.

Peltonen, P.T., Manninen, T. and Pihlaja, P., 1988. The late Archaean volcaniclastic Rookkiaapa Formation in Peurasuvanto, northern Finland. In: Laajoki, K. and Paakkola, J. (eds.), Sedimentology of the Precambrian formations in eastern and northern Finland. Geological Survey of Finland, Special Paper 5, p. 165–176.

Perttunen, V. and Vaasjoki, M, 2001. U-Pb geochronology of the Peräpohja Schist Belt, northwestern Finland. Geological Survey of Finland, Special Paper 33, p. 45-84.

Phillips, G.N. and Powell, R., 2010. Formation of gold deposits: A metamorphic devolatilization model. Journal of Metamorphic Geology 28, p. 689–718.

Piispanen, R., 1972. On the spilitic rocks of the Karelidic belt in western Kuusamo, north eastern Finland. Acta Universitatis Ouluensis, Ser A, Geologica 2, p. 1–73.

Pirajno., F., 2009. Hydrothermal Processes and Mineral Systems. Geological Survey of Western Australia, Springer, 1250 p.

Poulsen, H., and Hannington, M., 1995. Auriferous Volcanogenic Sulfide Deposits. In: Eckstrand, O.R., Sinclair, W.D. and Thorpe, R.I. (eds.), Geology of Canadian Mineral Deposit Types, Geology of Canada, 8, Decade of North American Geology. Geological Society of America 1, p. 183-196.

Puchtel, I.S., Haase, K.M., Hofmann, A.W., Chauvel, C., Kulikov, V.S., Garbe-Schoenberg, C.D. and Nemchin, A.A., 1997. Petrology and geochemistry of crustally contaminated komatiitic basalts from the Vetreny Belt, southeastern Baltic Shield; evidence for an early Proterozoic mantle plume beneath rifted Archean continental lithosphere. Geochimica et Cosmochimica Acta 61, 6, p. 1205–1222.

Ranta, J.-P., 2018. Geological evolution and gold mineralization in the northern part of the Peräpohja belt, Finland: Evidence from whole-rock and mineral chemistry, and radiogenic and stable isotopes. Res Terrae, Ser. A, No. 38, Oulu, 52 p.

Rasilainen, K., 1996. Geochemical alteration of gold occurrences in the late Archean Hattu schist belt, Ilomantsi, eastern Finland. Geological Survey of Finland, Bulletin 388, 80 p.

Rastas, P., Huhma, H., Hanski, E., Lehtonen, M.I., Paakkola, J., Mänttäri, I. and Härkönen, I., 2001. U-Pb isotopic studies on the Kittilä greenstone area, Central Lapland, Finland. In: Vaasjoki, M., (ed.), Radiometric Age determinations from Finnish Lapland and their bearing on the timing of Precambrian volcano-sedimentary sequences. Geological Survey of Finland, Special Paper 33, p. 95–141.

Reed, M.H., 1997. Hydrothermal alteration and its relationship to ore fluid composition. In: Barnes, H.L. (ed.), Geochemistry of Hydrothermal Ore Deposits. Canada: John Wiley & Sons, pp. 303-366.

Reimann, C. and Filzmoser, P., 1999. Normal and lognormal data distribution in geochemistry: death of a myth. Consequences for the statistical treatment of geochemical and environmental data. Environmental Geology 39, p. 1001–1014.

Reimann, C., Filzmoser, P., Hron, K., Kynčlová, P. and Garrett, R.G., 2017. A new method for correlation analysis of compositional (environmental) data – a worked example. The Science of the total environment 607-608, p. 965-971.

Ridley, W.I., 2012. Geochemical Characteristics. In: Shanks, P.W.C. III and Thurston, R. (eds.), Volcanogenic massive sulfide occurrence model. U.S. Geological Survey Scientific Investigations Report 2010–5070–C, p. 207-222.

Ridley J.R. and Diamond L.W., 2000. Fluid chemistry of lode-gold deposits and implications for genetic models. In: Hagemann S.G. and Brown P. (eds.), Gold in 2000. Reviews in Economic Geology 13, p. 141-162.

Robb, L. 2005. Introduction to Ore-Forming Processes. United Kingdom: Blackwell, 373 p.

Rupert Resources, 2018. NI 43-101 Technical Report: Pahtavaara Project, Finland [online document]. Available from https://rupertresources.com/wp-

content/uploads/2018/05/300518_NI43-101_SEDAR_Technical_Report_RUP_PahtavaaraProjectFinland.pdf [Accessed 15 April 2020]

Rupert Resources, 2020. Pahtavaara – geology & exploration [online document]. Available from: https://rupertresources.com/pahtavaara-geology-exploration/ [Accessed 25 May 2020]

Räsänen, J., Hanski, E. and Lehtonen, M., 1989. Komatiites, low-Ti basalts and andesites in the Möykkelma area, Central Finnish Lapland. Geological Survey of Finland, Report of Investigation 88, 41 p.

Räsänen, J., 1999. On the Sattasvaara komatiite formation. In: Papunen, H. and Eilu, P. (eds.), Geodynamic evolution and metallogeny of the Central Lapland, Kuhmo and Suomussalmi greenstone belts, Finland: joint field excursion and workshop of the GEODE subprojects: Archaean Greenstone Belts and Ore Deposits: Palaeoproterozoic Greenstone Belts and Ore Deposits, 11–16 September 1999. Abstracts. Turun yliopiston geologian ja mineralogian osaston julkaisuja 42, p. 10–11.

Räsänen, J. and Huhma, H., 2001. U-Pb datings in the Sodankylä schist area, the central Finnish Lapland. In: Vaasjoki, M. (ed.), Radio-metric age determinations from Finnish Lapland and their bearing on the timing of Precambrian volcano-sedimentary sequences. Geological Survey of Finland, Special Paper 33, p. 153–188.

Sarala, P., Taivalkoski, A. and Valkama, J. 2014. Kannettavan XRF-analysaattorin käyttö moreenigeokemiallisessa tutkimuksessa. Geological Survey of Finland, Archive report 120/2014, 9 p.

Saverikko, M., 1985. The pyroc1astic komatiite complex at Sattasvaara in northern Finland. Geological Survey of Finland, Bulletin 57, p. 55 - 87.

Seward, T.M., Williams-Jones, A.E. and Migdisov, A.A., 2014. The Chemistry of Metal Transport and Deposition by Ore-Forming Hydrothermal Fluids. In: Holland, H., and Turekian, K. (eds.), Treatise on Geochemistry, Chapter: Volume 13: Geochemistry of Mineral Deposits. Elsevier, p. 29-57.

Shanks, P.W.C. III, 2012. Hydrothermal Alteration; Theory of Deposit Formation. In: Shanks, P.W.C. III and Thurston, R. (eds.), Volcanogenic massive sulfide occurrence model: U.S. Geological Survey Scientific Investigations Report 2010–5070–C, p. 169-178, 293-298.

Sibson R., Moore, J. and Rankin, A., 1975. Seismic pumping – a hydrothermal fluid transport mechanism. Journal of the Geological Society London 131, p. 653–659.

Sillitoe, R.H., 1991. Intrusion-related gold deposits. In: Foster, R.P. (ed.), Gold metallogeny and exploration. Glasgow: Blackie and Son, p. 165–209.

Sillitoe, R.H., 2010. Porphyry Copper Systems. Economic Geology 105, p. 3–41.

Skinner, B.J., 1997. Hydrothermal Mineral Deposits: What We Do and Don't Know. In: Barnes, H.L. (ed.), Geochemistry of Hydrothermal Ore Deposits. Canada: John Wiley & Sons, pp. 3-26.

Sorjonen-Ward, P., 1993. An overview of structural evolution and lithic units within and intruding the late Archaean Hattu schist belt, Ilomantsi, eastern Finland. Geological Survey of Finland, Special Paper 17, p. 9–102.

Sorjonen-Ward, P., Nurmi, P.A., Härkönen, I. and Pankka, H.S., 1992. Epigenetic gold mineralisation and tectonic evolution of a Lower Proterozoic Greenstone Terrane in the northern Fennoscandian (Baltic) Shield. In: Sarkar, S.C. (ed.), Metallogeny related to tectonics of the Proterozoic mobile belts. New Delhi: Oxford and IBH Publishing, p. 375–452.

Sorjonen-Ward, P., Nironen, M. and Luukkonen, E. 1997. Greenstone associations in Finland. In: de Wit, M.J. and Ashwal, L.D. (eds.), Greenstone Belts. Oxford: Clarendon Press, p. 677–698.

Sorjonen-Ward, P., Ojala, V.J. and Airo, M.-L., 2003. Structural modelling and magmatic expression of hydrothermal alteration in the Paleoproterozoic lapland greenstone belt, northern Fennoscandian Shield. In: Eliopoulos, D.G. (eds.), Mineral Exploration and Sustainable Development. Proceedings of the Seventh Biennial SGA Meeting, Athens, Greece, August 24–28. Rotterdam: Millpress, p. 1107–1110.

Stefansson, A. and Seward, T.M., 2003b. The hydrolysis of gold(I) in aqueous solutions to 600°C and 1500 bar. Geochimica et Cosmochimica Acta 67, p. 1677–1688.

Taylor, B.E., 2007. Epithermal gold deposits. In Goodfellow, W.D. (ed.) Mineral Deposits of Canada: A Synthesis of Major Deposit-Types, District Metallogeny, the Evolution of Geological Provinces, and Exploration Methods. Geological Association of Canada, Mineral Deposits Division, Special Publication 5, p. 113-139.

Törmänen, T., Konnunaho, J.P., Hanski, E., Moilanen, M. and Heikura, P., 2016. The Paleoproterozoic komatiite-hosted PGE mineralization at Lomalampi, Central Lapland Greenstone Belt, northern Finland. Mineral Deposita 51, p 411-430.

Vasilopoulos, M., Molnár, F., O´Brien, H., Lahaye, Y. and Ranta, J.-P., 2019. Discrimination of gold and cobalt mineralising events at the Juomasuo Au-Co deposit, Kuusamo belt, northeastern Finland. NEXT – 3rd Progress meeting 7-10th October 2019, 2 p.

Ward, P., Härkönen, 1., Nurmi, P. and Pankka, H., 1989. Structural studies in the Lapland greens tone belt, northern Finland and their application to gold mineralization. Geological Survey of Finland, Special Paper 10, p. 71 - 77.

Wesolowski, D.J., Ziemniak, S.E., Anovitz, L.M., Machesky, M.L., Bénézeth, P. and Palmer, D.A., 2004. Solubility and surface adsorption characteristics of metal oxides. In: Palmer, D.A., Fernandez-Prini, R. and Harvey, A.H. (eds.), Aqueous Systems at Elevated Temperatures and Pressures: Physical Chemistry in Water, Steam and Hydrothermal Solutions. Amsterdam: Elsevier, p. 493–595.

Williams, P. J., Barton, M. D., Johnson, D. A., Fontboté, L., De Haller, A., Mark, G., Oliver, N.H.S. and Marschik, R., 2005. Iron Oxide Copper-Gold Deposits: Geology, Space-Time Distribution, and Possible Modes of Origin. Economic Geology 100th Anniversary Volume, p. 371-405.

Wood, S.A. and Samson, I.M., 1998. Solubility of ore minerals and complexation of ore minerals in hydrothermal solutions. Reviews in Economic Geology, 10, p. 33-80.

Yardley, B.W.D. and Graham, J.T., 2002. The origins of salinity in metamorphic fluids. Geofluids 2, p. 249–256.

APPENDICES

Appendix 1. The drill holes and number of samples included in the project.

Location	**Hole ID**	**Portable XRF analyses** (comparable laboratory analyses)	**Laboratory analyses**
Pahtavaara	116071	109	-
	116218	52	-
	116225	27	-
	116227	55	-
	116228	51	-
	116231	40 (13)	14
	116234	44 (11)	45
	117041	90 (12)	12
	117042	106 (12)	12
	117310	32	57
	117311	45 (3)	25
	117312	19 (3)	34
	117313	22 (4)	46
	117300	-	372
	Total	**692 (58)**	**617**
Lomalampi	(Törmänen et al., 2016)		10
Peuramaa	(Hanski et al., 2001)		11
Jeesiörova	(Hanski et al., 2001)		15
Sattasvaara	(Saverikko, 1985)		15
Sattasvaara	(Hanski, 1992)		2
	Total		**53**

Appendix 2. Geochemistry of the outliers.

Hole ID		117311		117311	
Sample ID		990013144		990013150	
		Olympus Vanta	Laboratory	Olympus Vanta	Laboratory
Au	ppm		16,85		10,65
Ag	ppm	0	0,01	0	0,005
Al	%	1,8539	0,94	1,1392	0,08
As	ppm	9	0,1	16	0,4
Bi	ppm	0	0,04	0	0,15
Ca	%	3,1991	2,13	2,178	1,28
Cd	ppm	0	0,01	0	0,01
Co	ppm	0	34,6	0	5,6
Cr	ppm	0	551	0	54
Cu	ppm	57	19,7	86	9,1
Fe	%	10,696	10,1	1,1141	0,89
K	ppm	3367	2100	257	50
Mg	%	11,4753	6,03	7,2201	1,1
Mn	ppm	7948	2610	14001	430
Mo	ppm	24	0,2	60	0,09
Ni	ppm	965	776	327	128,5
P	ppm	0	40	0	10
Pb	ppm	29	13,4	58	8,6
Rb	ppm	0	6,6	0	0,2
S	%	5,4946	0,45	13,4121	0,2
Sb	ppm	0	0,06	0	0,025
Se	ppm	0	1	9	0,5
Sn	ppm	0	0,2	0	0,1
Sr	ppm	5294	2680	11792	2600
Th	ppm	129	0,005	315	0,005
Ti	%	9,6037	0,082	25,671	0,007
U	ppm	0	34,7	0	40,9
V	ppm	18079	80	49341	9
W	ppm	71	4,6	131	1,5
Y	ppm	0	2,8	0	0,9
Zn	ppm	20	6	36	2
Zr	ppm	118	5,1	255	0,5

Appendix 3(1). Scatter plots and line diagrams for the determination of distribution and comparison of accuracy of the regularly detected elements from 58 samples which have both laboratory ME-MS61 and pXRF analyses. A) pXRF vs laboratory measurements showing the distribution with the outliers, B) line diagram of pXRF and laboratory measurements showing the accuracy with the outliers, C) distribution without the outliers and D) accuracy without the outliers.

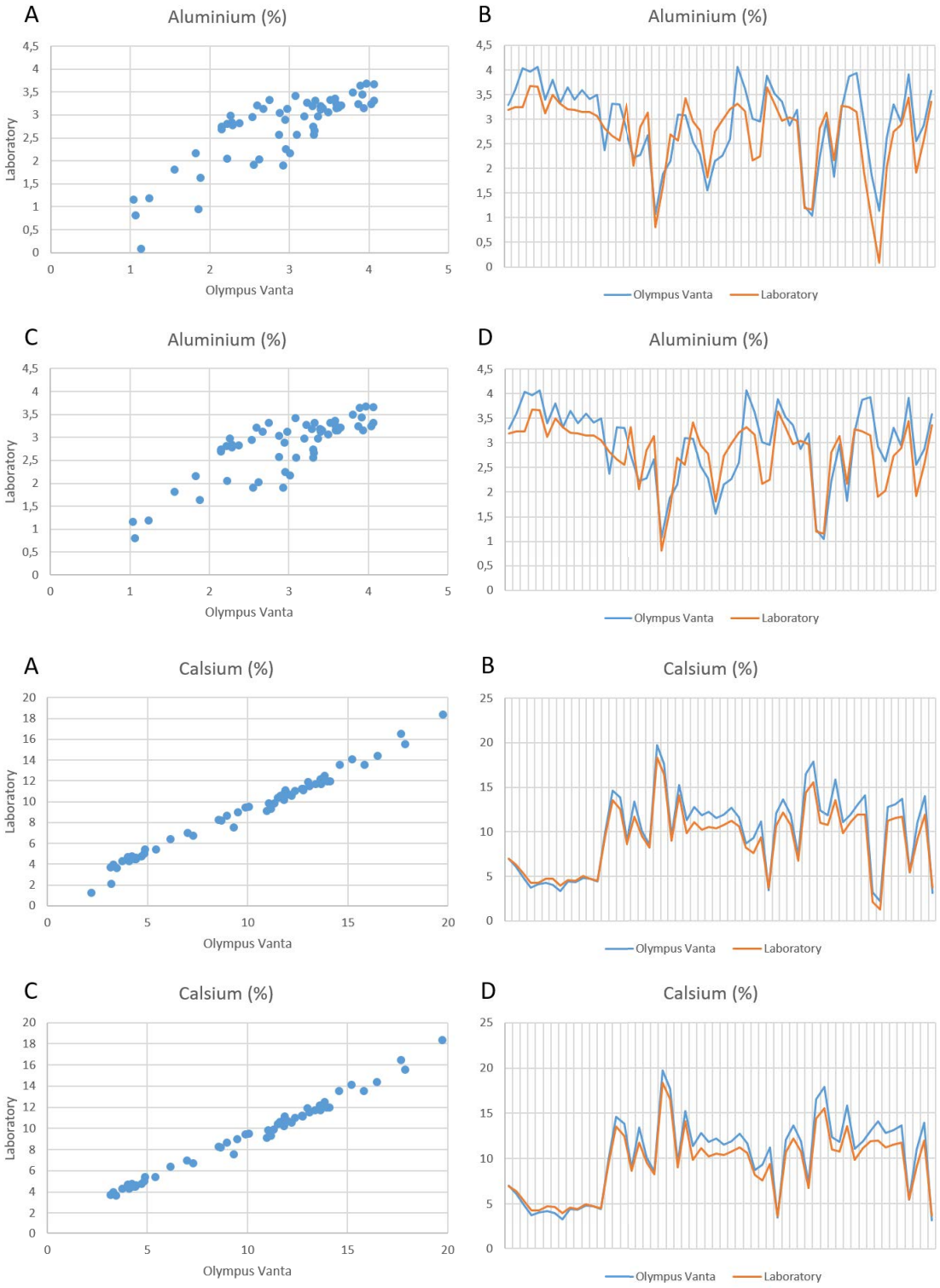

Appendix 3(2).


A
Chromium (ppm)
Laboratory
Olympus Vanta
B
Chromium (ppm)
Olympus Vanta
Laboratory
C
Chromium (ppm)
Laboratory
Olympus Vanta
D
Chromium (ppm)
Olympus Vanta
Laboratory
A
Copper (ppm)
Laboratory
Olympus Vanta
B
Copper (ppm)
Olympus Vanta
Laboratory
C
Copper (ppm)
Laboratory
Olympus Vanta
D
Copper (ppm)
Olympus Vanta
Laboratory

Appendix 3(3).

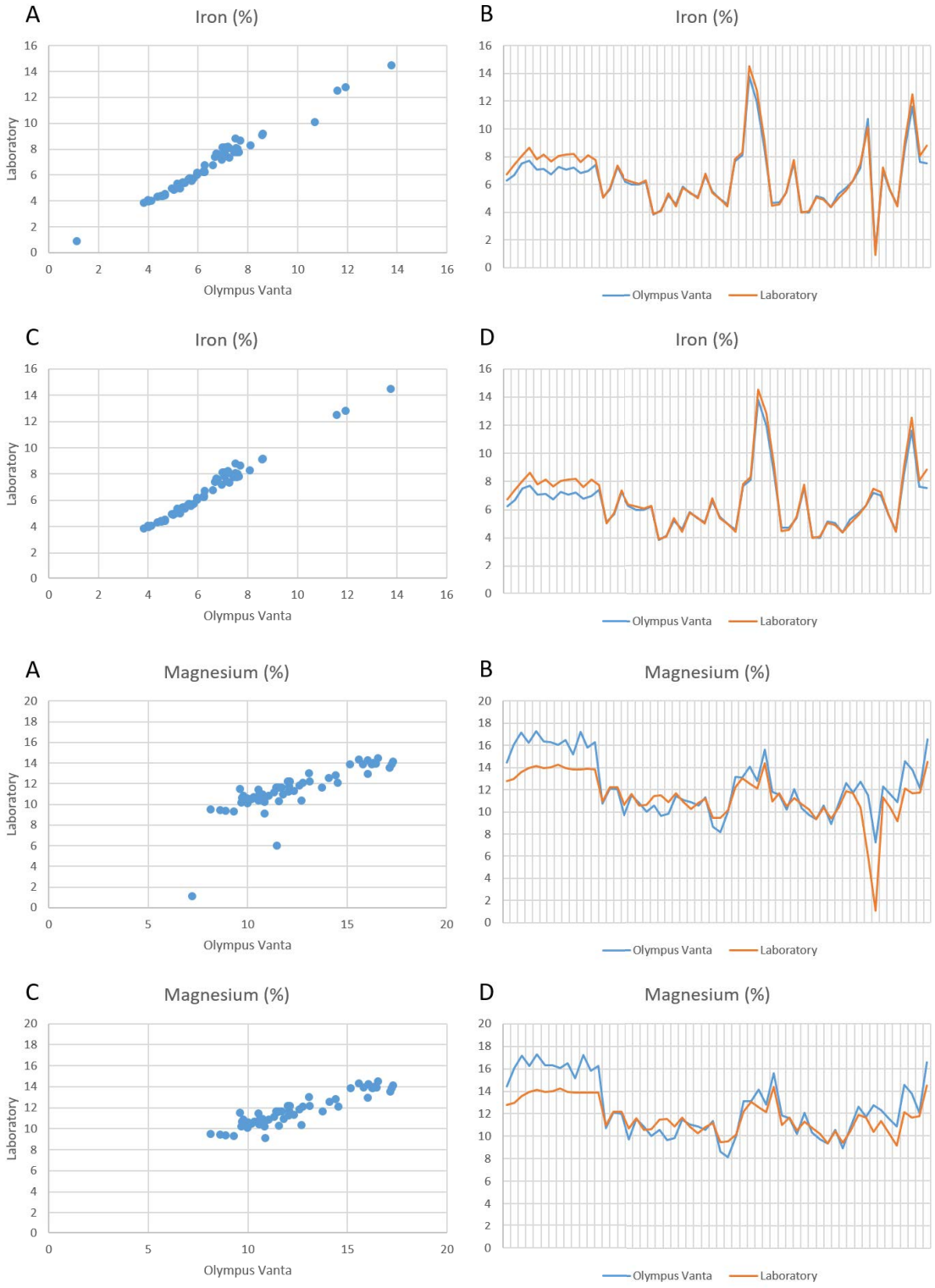
A
Iron (%)
Laboratory
Olympus Vanta
B
Iron (%)
Olympus Vanta
Laboratory
C
Iron (%)
Laboratory
Olympus Vanta
D
Iron (%)
Olympus Vanta
Laboratory
A
Magnesium (%)
Laboratory
Olympus Vanta
B
Magnesium (%)
Olympus Vanta
Laboratory
C
Magnesium (%)
Laboratory
Olympus Vanta
D
Magnesium (%)
Olympus Vanta
Laboratory

Appendix 3(4).

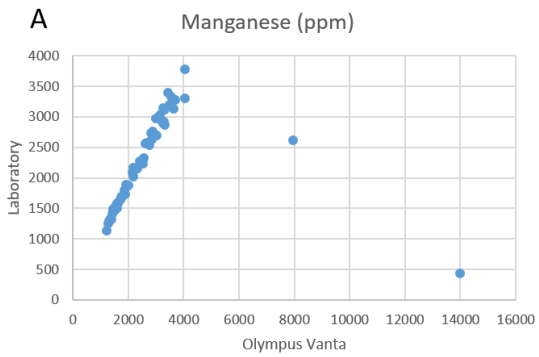
A
Manganese (ppm)
Laboratory
Olympus Vanta
0
500
1000
1500
2000
2500
3000
3500
4000
0
2000
4000
6000
8000
10000
12000
14000
16000

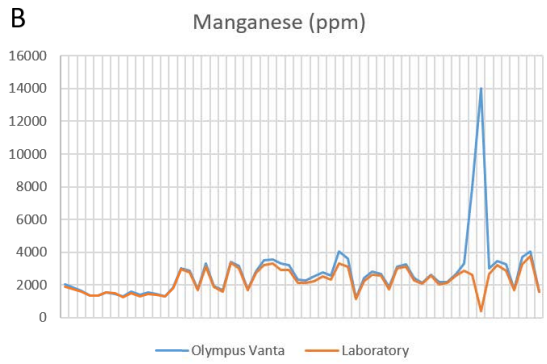
B
Manganese (ppm)
0
2000
4000
6000
8000
10000
12000
14000
16000
Olympus Vanta
Laboratory

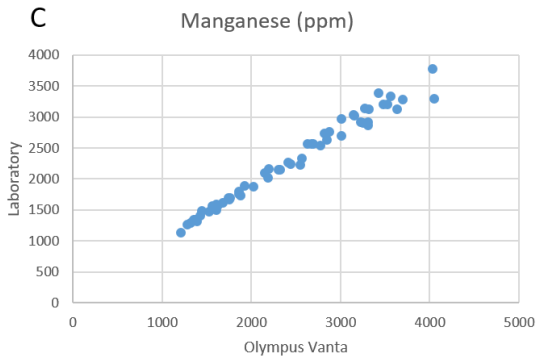
C
Manganese (ppm)
Laboratory
Olympus Vanta
0
500
1000
1500
2000
2500
3000
3500
4000
0
1000
2000
3000
4000
5000

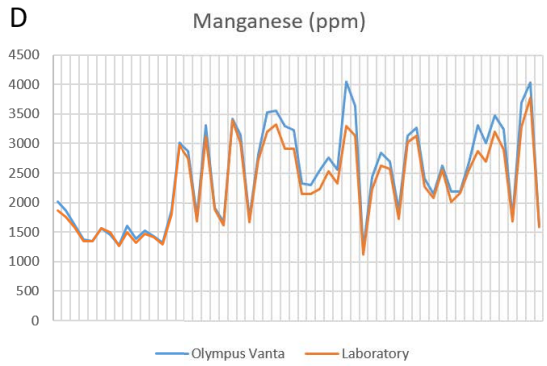
D
Manganese (ppm)
0
500
1000
1500
2000
2500
3000
3500
4000
4500
Olympus Vanta
Laboratory

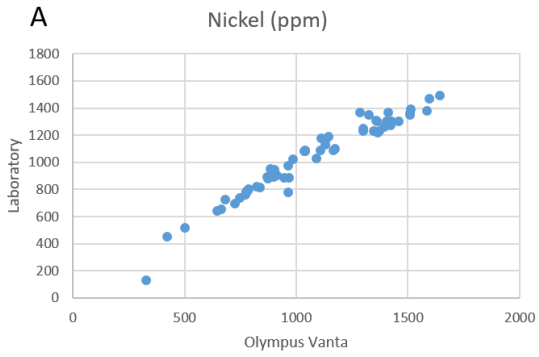
A
Nickel (ppm)
Laboratory
Olympus Vanta
0
200
400
600
800
1000
1200
1400
1600
1800
0
500
1000
1500
2000

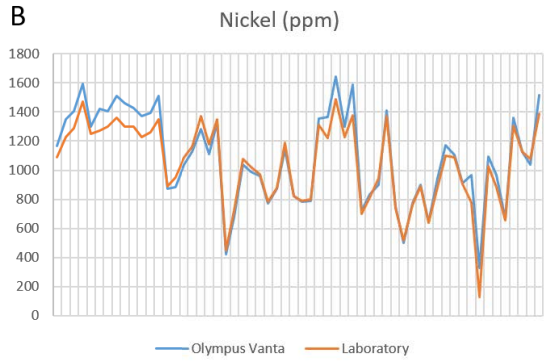
B
Nickel (ppm)
0
200
400
600
800
1000
1200
1400
1600
1800
Olympus Vanta
Laboratory

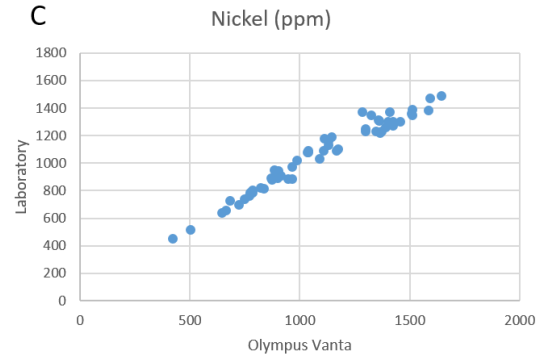
C
Nickel (ppm)
Laboratory
Olympus Vanta
0
200
400
600
800
1000
1200
1400
1600
1800
0
500
1000
1500
2000

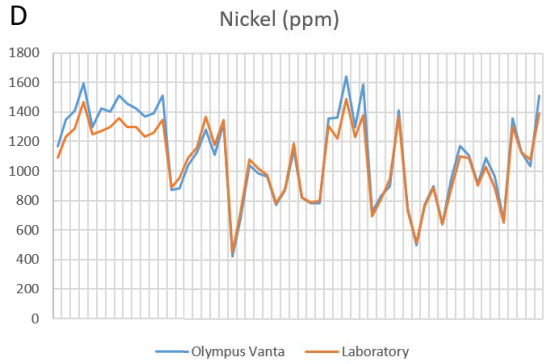
D
Nickel (ppm)
0
200
400
600
800
1000
1200
1400
1600
1800
Olympus Vanta
Laboratory

Appendix 3(5).

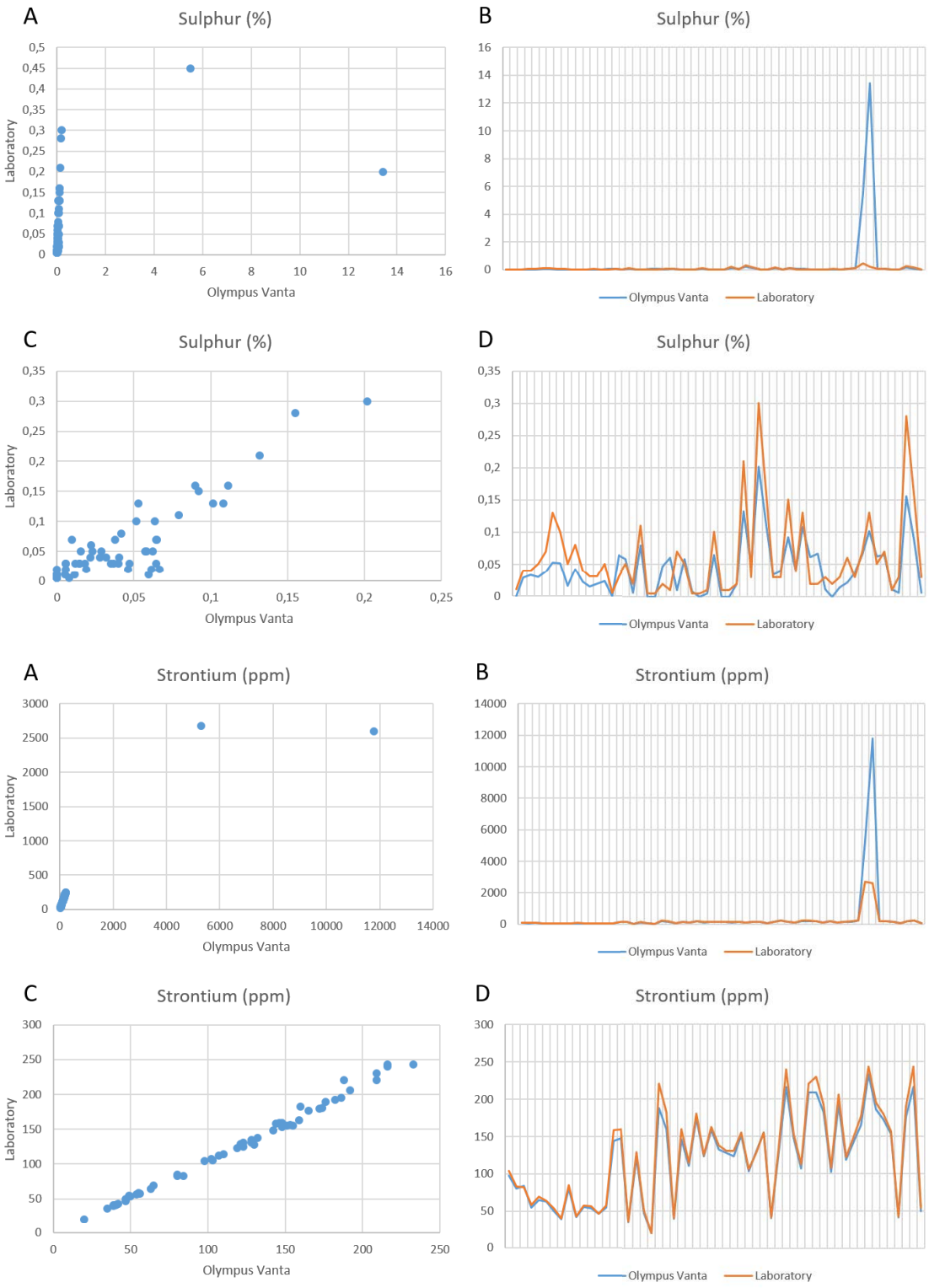
A
Sulphur (%)
Laboratory
Olympus Vanta
B
Sulphur (%)
Olympus Vanta
Laboratory
C
Sulphur (%)
Laboratory
Olympus Vanta
D
Sulphur (%)
Olympus Vanta
Laboratory
A
Strontium (ppm)
Laboratory
Olympus Vanta
B
Strontium (ppm)
Olympus Vanta
Laboratory
C
Strontium (ppm)
Laboratory
Olympus Vanta
D
Strontium (ppm)
Olympus Vanta
Laboratory

Appendix 3(6).


A
Titanium (%)
Laboratory
Olympus Vanta
B
Titanium (%)
Olympus Vanta
Laboratory
C
Titanium (%)
Laboratory
Olympus Vanta
D
Titanium (%)
Olympus Vanta
Laboratory
A
Vanadium (ppm)
Laboratory
Olympus Vanta
B
Vanadium (ppm)
Olympus Vanta
Laboratory
C
Vanadium (ppm)
Laboratory
Olympus Vanta
D
Vanadium (ppm)
Olympus Vanta
Laboratory

Appendix 3(7).


A
Zinc (ppm)
Laboratory
Olympus Vanta
B
Zinc (ppm)
Olympus Vanta
Laboratory
C
Zinc (ppm)
Laboratory
Olympus Vanta
D
Zinc (ppm)
Olympus Vanta
Laboratory
A
Yttrium (ppm)
Laboratory
Olympus Vanta
B
Yttrium (ppm)
Olympus Vanta
Laboratory
C
Yttrium (ppm)
Laboratory
Olympus Vanta
D
Yttrium (ppm)
Olympus Vanta
Laboratory

Appendix 3(8).

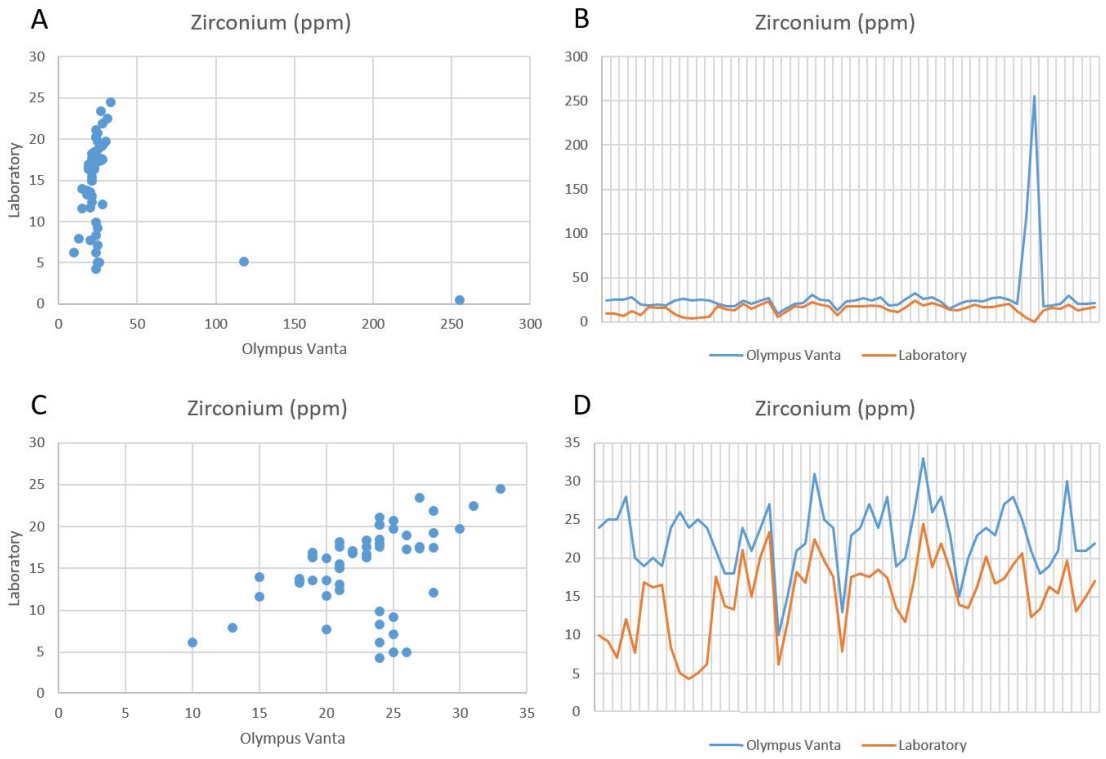
A
Zirconium (ppm)
Laboratory
Olympus Vanta
B
Zirconium (ppm)
Olympus Vanta
Laboratory
C
Zirconium (ppm)
Laboratory
Olympus Vanta
D
Zirconium (ppm)
Olympus Vanta
Laboratory

Appendix 4. Numerical results of the mass balance calculation of the talc-chlorite schist.

	Overall mass change (%)	12.37	Slope	0.89
	Least-altered TCS	Altered TCS	ΔC_i Gain/Loss	
TiO_2	0.13	0.23	0.13	%
Al_2O_3	6.99	5.95	-0.30	%
Fe_2O_3	15.09	11.39	-2.29	%
MnO	0.11	0.18	0.09	%
MgO	20.23	23.01	5.63	%
CaO	4.18	6.52	3.15	%
Na_2O	1.58	0.34	-1.20	%
K_2O	0.45	0.03	-0.42	%
P_2O_5	0.05	0.03	-0.02	%
Ag	0.05	0.01	-0.04	ppm
As	0.30	0.16	-0.12	ppm
Au	0.01	0.01	0.00	ppm
Ba	10.00	303.00	330.49	ppm
Be	0.31	0.21	-0.08	ppm
Bi	0.01	0.02	0.02	ppm
Cd	0.04	0.03	-0.01	ppm
Ce	2.37	1.28	-0.94	ppm
Co	75.50	89.94	25.57	ppm
Cr	1830.00	1438.00	-214.07	ppm
Cs	1.98	0.08	-1.89	ppm
Cu	124.00	1.50	-122.31	ppm
Ga	11.40	9.04	-1.24	ppm
Ge	0.23	0.03	-0.20	ppm
Hf	0.70	0.22	-0.45	ppm
In	0.09	0.04	-0.05	ppm
La	0.50	0.25	-0.22	ppm
Li	25.90	6.50	-18.60	ppm
Mo	0.14	0.07	-0.06	ppm
Nb	0.10	0.09	0.00	ppm
Ni	1010.00	1288.00	437.37	ppm
Pb	0.70	0.80	0.20	ppm
Rb	15.90	1.00	-14.78	ppm
Re	0.00	0.00	0.00	ppm
S	0.41	0.05	-0.36	%
Sb	0.12	0.13	0.02	ppm
Sc	30.60	21.90	-5.99	ppm
Se	1.00	0.50	-0.44	ppm
Sn	0.50	0.30	-0.16	ppm
Sr	37.70	57.84	27.30	ppm
Ta	0.03	0.03	0.00	ppm
Te	0.03	0.03	0.00	ppm
Th	0.06	0.01	-0.05	ppm
Tl	0.18	0.01	-0.17	ppm
U	0.10	0.08	-0.01	ppm
V	249.00	165.00	-63.58	ppm
W	0.10	0.10	0.01	ppm
Y	9.00	8.26	0.28	ppm
Zn	57.00	82.80	36.05	ppm
Zr	23.00	5.76	-16.53	ppm

Appendix 5. Numerical results of the mass balance calculation of the amphibolite schist.

	Overall mass change (%)	5.22	Slope	0.95
	Least-altered TCS	Altered AS	ΔC_i Gain/Loss	
TiO_2	0.13	0.25	0.13	%
Al_2O_3	6.99	6.31	-0.35	%
Fe_2O_3	15.09	11.68	-2.80	%
MnO	0.11	0.18	0.08	%
MgO	20.23	23.10	4.08	%
CaO	4.18	7.00	3.18	%
Na_2O	1.58	0.54	-1.00	%
K_2O	0.45	0.07	-0.37	%
P_2O_5	0.05	0.03	-0.01	%
Ag	0.05	0.04	0.00	ppm
As	0.30	0.26	-0.02	ppm
Au	0.01	0.04	0.03	ppm
Ba	10.00	88.58	83.20	ppm
Be	0.31	0.19	-0.11	ppm
Bi	0.01	0.03	0.03	ppm
Cd	0.04	0.03	-0.01	ppm
Ce	2.37	1.75	-0.53	ppm
Co	75.50	89.82	19.01	ppm
Cr	1830.00	1527.89	-222.41	ppm
Cs	1.98	0.14	-1.83	ppm
Cu	124.00	91.08	-28.16	ppm
Ga	11.40	10.26	-0.61	ppm
Ge	0.23	0.04	-0.19	ppm
Hf	0.70	0.39	-0.29	ppm
In	0.09	0.04	-0.04	ppm
La	0.50	0.40	-0.08	ppm
Li	25.90	8.26	-17.21	ppm
Mo	0.14	0.07	-0.06	ppm
Nb	0.10	0.10	0.01	ppm
Ni	1010.00	1281.34	338.19	ppm
Pb	0.70	0.79	0.14	ppm
Rb	15.90	2.42	-13.35	ppm
Re	0.00	0.00	0.00	ppm
S	0.41	0.05	-0.35	%
Sb	0.12	0.14	0.03	ppm
Sc	30.60	22.90	-6.51	ppm
Se	1.00	0.66	-0.30	ppm
Sn	0.50	0.31	-0.17	ppm
Sr	37.70	61.58	27.09	ppm
Ta	0.03	0.03	0.00	ppm
Te	0.03	0.03	0.01	ppm
Th	0.06	0.02	-0.04	ppm
Tl	0.18	0.02	-0.16	ppm
U	0.10	0.08	-0.02	ppm
V	249.00	174.99	-64.88	ppm
W	0.10	0.87	0.81	ppm
Y	9.00	8.29	-0.28	ppm
Zn	57.00	72.32	19.09	ppm
Zr	23.00	9.77	-12.72	ppm

Appendix 6. Numerical results of the mass balance calculation of the actinolite-tremolite rock.

	Overall mass change (%)	23.19	Slope	0.81
	Least-altered TCS	Altered ATR	ΔC_i Gain/Loss	
TiO_2	0.13	0.30	0.24	%
Al_2O_3	6.99	5.48	-0.24	%
Fe_2O_3	15.09	9.03	-3.96	%
MnO	0.11	0.31	0.28	%
MgO	20.23	18.06	2.02	%
CaO	4.18	14.31	13.44	%
Na_2O	1.58	0.91	-0.46	%
K_2O	0.45	0.04	-0.40	%
P_2O_5	0.05	0.03	-0.01	%
Ag	0.05	0.03	-0.01	ppm
As	0.30	0.55	0.38	ppm
Au	0.01	1.84	2.26	ppm
Ba	10.00	459.17	555.66	ppm
Be	0.31	0.33	0.09	ppm
Bi	0.01	0.02	0.02	ppm
Cd	0.04	0.04	0.01	ppm
Ce	2.37	3.25	1.64	ppm
Co	75.50	39.50	-26.84	ppm
Cr	1830.00	1260.75	-276.85	ppm
Cs	1.98	0.07	-1.89	ppm
Cu	124.00	130.90	37.26	ppm
Ga	11.40	10.21	1.17	ppm
Ge	0.23	0.10	-0.11	ppm
Hf	0.70	0.58	0.01	ppm
In	0.09	0.11	0.05	ppm
La	0.50	1.36	1.18	ppm
Li	25.90	4.94	-19.81	ppm
Mo	0.14	1.82	2.10	ppm
Nb	0.10	0.13	0.05	ppm
Ni	1010.00	1004.13	227.01	ppm
Pb	0.70	2.66	2.58	ppm
Rb	15.90	0.50	-15.28	ppm
Re	0.00	0.00	0.00	ppm
S	0.41	0.06	-0.33	%
Sb	0.12	0.11	0.02	ppm
Sc	30.60	20.81	-4.97	ppm
Se	1.00	0.92	0.13	ppm
Sn	0.50	0.31	-0.12	ppm
Sr	37.70	135.28	128.96	ppm
Ta	0.03	0.03	0.01	ppm
Te	0.03	0.07	0.06	ppm
Th	0.06	0.06	0.02	ppm
Tl	0.18	0.01	-0.17	ppm
U	0.10	1.01	1.15	ppm
V	249.00	166.13	-44.35	ppm
W	0.10	2.07	2.45	ppm
Y	9.00	7.73	0.52	ppm
Zn	57.00	29.33	-20.86	ppm
Zr	23.00	18.23	-0.54	ppm

Appendix 7(1). Combined data for the downhole plot of drill hole 116227.

Hole ID 116227																
Method	Sample ID	from	to	Rock	Ore mineral	Au ppm	Al pct	Ca pct	Cr ppm	Cu ppm	Fe pct	Mg pct	Mn ppm	Ni ppm	S pct	Sr ppm	Zn ppm
pXRF	990029373	11	12	TCS	PY	0.01	3.66	4.16	1875	61	6.76	15.99	1334	1278	0.03	64	99
pXRF	990029374	12	13	TCS	PY	0.03	2.96	4.57	2318	129	7.19	15.68	1278	1449	0.03	62	102
pXRF	990029375	13	14	TCS	PY	0.01	3.36	4.41	2175	47	7.26	16.54	1450	1471	0.03	61	96
pXRF	990029376	14	15	TCS	PY	0.02	4.37	3.74	2354	74	7.47	16.89	1299	1391	0.05	61	95
pXRF	990029377	15	15.64	TCS	PY	0.005	3.74	3.64	2249	39	7.43	15.98	1387	1324	0.03	64	92
pXRF	990029377	15.64	16	AS2		0.005	3.74	3.64	2249	39	7.43	15.98	1387	1324	0.03	64	92
pXRF	990029378	16	17	AS2		0.01	4.15	3.53	2339	32	8.06	15.95	1419	1338	0.02	64	89
pXRF	990029379	17	18	AS2		0.01	4.42	3.74	2213	45	7.98	16.20	1618	1314	0.02	67	91
pXRF	990029380	18	19	AS2		0.01	4.03	3.95	2075	20	7.46	17.09	1586	1250	0.04	86	86
pXRF	990029381	19	20	AS2		0.05	4.01	4.91	1893	147	7.98	15.65	1692	1340	0.07	130	81
pXRF	990029382	20	21	AS2		0.02	4.63	3.19	2113	64	8.06	17.03	1292	1334	0.04	65	85
pXRF	990029383	21	22	AS2		0.01	3.32	4.90	2014	36	7.54	16.46	1574	1269	0.03	92	76
pXRF	990029384	22	23	AS2		0.02	3.46	3.98	2186	81	7.39	15.83	1324	1418	0.07	102	80
pXRF	990029385	23	24	AS2		0.005	3.97	3.67	2595	30	7.84	16.63	1281	1527	0.03	61	83
pXRF	990029386	24	25	AS2		0.02	3.44	4.50	1999	61	7.32	15.50	1506	1248	0.03	80	72
pXRF	990029387	25	26	AS2		0.005	3.66	4.33	2386	24	7.87	15.95	1403	1276	0.01	47	62
pXRF	990029388	26	27	AS2		0.44	3.61	2.73	2347	151	8.74	15.93	1130	1678	0.02	27	68
pXRF	990029389	27	28	AS2		0.005	2.50	6.88	1522	0	6.70	14.20	1841	1094	0.02	84	43
pXRF	990029390	28	29	AS2		0.005	2.49	4.82	1986	0	7.31	13.95	1401	1296	0.01	48	61
pXRF	990029392	29	30	AS2		0.07	3.25	4.29	2254	120	8.25	16.13	1339	1434	0.03	39	62
pXRF	990029393	30	31	AS2		0.005	3.55	3.89	2228	17	8.27	16.17	1446	1397	0.00	38	56
pXRF	990029394	31	32.23	AS2		0.23	3.39	5.15	1922	34	9.31	13.83	1782	1157	0.01	30	43
pXRF	990029395	32.23	33	AS2	PY	0.31	4.32	8.31	2037	57	7.64	13.64	2380	1147	0.06	111	36

Appendix 7(2). Combined data for the downhole plot of drill hole 116227.

Method	Sample ID	from	to	Rock	Ore mineral	Au ppm	Al pct	Ca pct	Cr ppm	Cu ppm	Fe pct	Mg pct	Mn ppm	Ni ppm	S pct	Sr ppm	Zn ppm
pXRF	990029396	33	34	AS2	PY	0.07	4.20	6.74	2163	45	7.80	15.54	1929	1334	0.07	87	43
pXRF	990029397	34	35	AS2	PY	3.21	3.82	5.74	2185	21	7.58	13.94	1684	1294	0.04	55	37
pXRF	990029398	35	36	AS2	PY	0.03	3.67	7.04	1845	49	7.71	14.28	1923	1168	0.03	76	36
pXRF	990029399	36	37.26	AS2	PY	0.02	5.81	5.29	1428	34	10.10	13.84	2176	694	0.01	39	32
pXRF	990029400	37.26	38	AT2	PY	0.005	4.48	2.17	1998	42	13.53	15.87	1528	1227	0.08	25	41
pXRF	990017501	38	39	AT2	PY	0.07	3.44	1.12	1750	36	12.88	16.67	1172	1566	0.05	42	43
pXRF	990017502	39	40	AT2	PY	0.02	3.00	7.96	1862	48	8.12	10.49	2263	1094	0.03	107	39
pXRF	990017503	40	41	AT2	PY	1.23	2.86	11.44	1826	0	6.23	9.74	2645	993	0.12	192	32
pXRF	990017504	41	42	AT2	PY	9.36	2.24	11.28	1664	7	6.35	9.64	2680	817	0.10	140	31
pXRF	990017505	42	43	AT2	PY	2.09	2.94	12.03	2287	0	5.63	8.79	2515	743	0.03	164	44
pXRF	990017506	43	44	AT2	PY	0.35	2.51	12.02	1878	7	5.49	10.25	2580	821	0.02	126	38
pXRF	990017507	44	45	AT2	PY	0.01	2.39	14.46	1354	0	4.87	9.10	2753	597	0.01	235	33
pXRF	990017508	45	45.73	AT2	PY	0.01	2.65	9.92	1328	14	6.37	10.82	2531	881	0.09	74	37
pXRF	990017509	45.73	47	AS2	PY	0.06	3.80	5.89	2047	89	7.16	15.83	1737	1342	0.02	62	59
pXRF	990017510	47	48	AS2	PY	0.01	3.72	5.49	1839	37	6.85	17.19	1589	1332	0.04	74	60
pXRF	990017512	48	49	AS2	PY	0.06	3.93	5.50	1688	115	7.10	15.74	1686	1380	0.04	73	61
pXRF	990017513	49	50	AS2	PY	0.04	3.48	5.57	2087	37	7.56	15.81	1734	1268	0.04	108	67
pXRF	990017514	50	51	AS2	PY	0.02	3.62	3.86	2214	85	7.78	17.71	1451	1487	0.04	62	71
pXRF	990017515	51	52.14	AS2	PY	0.49	3.70	4.99	2096	344	7.20	16.11	1638	1370	0.07	99	75
pXRF	990017516	52.14	53	TCS		0.11	3.29	5.63	1944	249	7.38	15.89	1625	1295	0.03	69	64
pXRF	990017517	53	54	TCS		0.005	3.28	3.34	2086	18	7.99	16.04	1291	1414	0.04	44	81
pXRF	990017518	54	55	TCS		0.005	3.57	4.66	2110	33	7.80	15.67	1414	1398	0.05	55	79
pXRF	990017519	55	56	TCS		0.005	3.76	3.84	2376	0	8.25	15.77	1002	1403	0.01	32	83
pXRF	990017520	56	57	TCS		0.005	3.68	2.99	2228	22	7.90	17.05	1047	1633	0.03	42	84
pXRF	990017521	57	58	TCS		0.005	3.78	4.29	2260	0	8.13	16.07	1224	1417	0.03	49	84

Appendix 7(3). Combined data for the downhole plot of drill hole 116227.

Method	Sample ID	from	to	Rock	Ore mineral	Au ppm	Al pct	Ca pct	Cr ppm	Cu ppm	Fe pct	Mg pct	Mn ppm	Ni ppm	S pct	Sr ppm	Zn ppm
pXRF	990017522	58	59	TCS		0.005	3.40	5.18	2223	0	7.68	15.16	1337	1334	0.03	60	79
pXRF	990017523	59	60	TCS		0.005	3.88	3.92	2473	10	8.06	16.24	1179	1436	0.04	46	81
pXRF	990017524	60	61	TCS		0.005	3.31	5.33	2122	0	7.65	15.19	1409	1330	0.03	68	76
pXRF	990017525	61	62	TCS		0.005	3.32	4.89	2373	0	7.79	14.84	1576	1402	0.04	76	74
pXRF	990017526	62	63	TCS		0.005	3.59	5.03	2359	0	7.76	15.12	1446	1353	0.02	73	79
pXRF	990017527	63	64	TCS		0.01	3.63	5.69	2051	0	7.58	15.17	1516	1315	0.02	80	79
pXRF	990017528	64	65	TCS		0.01	3.00	5.45	1723	9	7.51	14.55	1296	1207	0.01	58	68
pXRF	990017529	65	66	TCS		0.01	3.47	5.24	2342	0	8.42	14.87	1304	1329	0.02	63	77

Appendix 8(1). Combined data for the downhole plot of drill hole 116231.

Hole ID 116231

Method	Sample ID	from	to	Rock	Ore mineral	Au ppm	Al pct	Ca pct	Cr ppm	Cu ppm	Fe pct	Mg pct	Mn ppm	Ni ppm	S pct	Sr ppm	Zn ppm
pXRF	990029210	7.15	8.15	TCS		0.005	4.99	4.94	2554	32	8.43	15.89	1695	1305	0.05	72	105
pXRF	990029211	8.15	9.3	AS2	PY	0.005	3.69	5.22	2320	17	8.03	14.72	1523	1348	0.02	51	96
pXRF	990029212	9.3	10.45	AS2	PY	0.005	3.92	3.87	2339	0	7.98	16.65	1354	1455	0.03	41	100
pXRF	990029213	10.45	11	AS2	PY	0.01	3.82	5.97	2384	17	6.96	15.03	1647	1346	0.01	64	73
LAB	990087608	11	12	AS2	PY	0.005	3.19	6.97	1250	6.7	6.74	12.80	1870	1090	0.01	104	62
LAB	990087609	12	13	AS2	PY	0.01	3.24	6.39	1670	10.3	7.42	12.95	1760	1230	0.04	82.7	65
LAB	990087611	13	14	AS2	PY	0.005	3.24	5.39	1610	6	8.06	13.55	1580	1290	0.04	82.5	65
LAB	990087612	14	15	AS2	PY	0.01	3.68	4.28	1880	15.6	8.64	13.95	1340	1470	0.05	58.2	70
LAB	990087613	15	18	AS2	PY	0.09	3.66	4.31	1500	105.5	7.79	14.15	1340	1250	0.07	69.6	67
LAB	990087614	18	19	AS2	PY	0.46	3.12	4.77	1500	536	8.14	13.95	1560	1270	0.13	64.2	66
LAB	990087615	19	20	AS2	PY	0.25	3.49	4.70	1150	283	7.65	14.00	1490	1300	0.10	53.8	63
LAB	990087616	20	21	AS2	PY	0.03	3.31	3.97	1510	37.2	8.06	14.25	1260	1360	0.05	40.6	67
LAB	990087617	21	22	AS2	PY	0.02	3.50	3.82	2100	34.4	9.29	14.30	1310	1540	0.09	49	70
pXRF	990029214	22	23	AS2	PY	0.005	3.52	3.45	2590	27	8.03	17.04	1280	1457	0.03	44	71
pXRF	990029215	23	24	AS2	PY	0.005	3.15	3.46	2706	9	7.71	18.55	1145	1391	0.03	42	74
pXRF	990029216	24	25	AS2	PY	0.02	3.59	3.26	2562	31	7.79	16.58	1217	1489	0.03	43	66
pXRF	990029217	25	26	AS2	PY	0.04	2.93	4.24	2182	38	7.22	16.57	1386	1425	0.04	57	62
pXRF	990029218	26	26.7	AS2	PY	0.05	3.34	4.77	1974	65	7.66	14.88	1573	1438	0.05	47	48
pXRF	990029219	26.7	28	AS3	PY	0.06	3.52	4.80	2293	45	7.92	15.09	1659	1347	0.03	51	49
pXRF	990029220	28	29.05	AS3	PY	0.02	3.23	4.52	2291	0	7.76	15.51	1388	1368	0.02	32	46
pXRF	990029221	29.05	30	AT1	PY	0.01	3.40	8.12	2283	8	6.63	12.68	2171	1160	0.01	53	34
pXRF	990029222	30	31	AT1	PY	0.02	3.14	11.30	1998	7	5.71	10.79	2545	960	0.01	96	32
pXRF	990029223	31	31.8	AT1	PY	0.01	2.61	14.51	1819	0	4.92	9.49	2797	572	0.00	199	33

Appendix 8(2). Combined data for the downhole plot of drill hole 116231.

Method	Sample ID	from	to	Rock	Ore mineral	Au ppm	Al pct	Ca pct	Cr ppm	Cu ppm	Fe pct	Mg pct	Mn ppm	Ni ppm	S pct	Sr ppm	Zn ppm
pXRF	990029224	31.8	32.75	ZD1	CP	0.12	1.91	18.11	1048	22	5.02	10.89	3840	665	0.05	221	20
pXRF	990029225	32.75	33.75	ZD1	CP	0.74	2.18	17.93	1288	26	5.29	11.51	3604	836	0.05	215	24
pXRF	990029226	33.75	34.75	ZD1	CP	89.4	2.09	17.39	1032	451	5.68	11.61	3785	877	0.11	216	23
pXRF	990029227	34.75	35.75	ZD1	CP	3.93	3.15	14.13	1645	40	6.51	12.20	3121	1059	0.06	175	44
pXRF	990029229	35.75	36.5	ZD1	CP	1.3	3.34	14.77	1901	42	6.10	12.78	3390	976	0.08	195	36
pXRF	990029230	36.5	37.75	AS3	PY	0.41	3.98	6.48	2430	7	8.40	15.27	2047	1287	0.05	77	57
pXRF	990029231	37.75	39	AS2	PY	0.04	4.32	2.78	2207	18	8.36	18.80	1276	1646	0.04	40	79
pXRF	990029232	39	40	AS2	PY	0.1	4.22	3.95	2474	72	7.80	17.35	1469	1444	0.05	51	72
pXRF	990029233	40	41	AS2	PY	0.36	3.56	5.12	2015	175	7.24	16.78	1680	1433	0.05	71	73
pXRF	990029234	41	42	AS2	PY	0.43	3.47	4.19	2220	87	7.76	16.24	1450	1448	0.03	49	82
pXRF	990029235	42	43	AS2	PY	0.01	3.65	4.58	2203	0	7.17	16.95	1552	1370	0.02	61	82
pXRF	990029236	43	44	AS2	PY	0.01	3.66	4.94	2263	13	7.80	16.91	1535	1472	0.05	76	81
pXRF	990029237	44	44.7	AS2	PY	0.01	3.43	3.89	2183	8	7.47	17.10	1379	1419	0.03	62	89
LAB	990087618	44.7	46	TCS	PY	0.005	3.21	4.60	1470	2.4	8.13	13.95	1500	1300	0.08	84.8	81
LAB	990087621	46	47	TCS	PY	0.005	3.19	4.48	1460	1.3	8.21	13.85	1320	1300	0.04	42.9	82
LAB	990087622	47	48	TCS	PY	0.005	3.15	5.01	1380	1.6	7.61	13.85	1470	1230	0.03	57.7	81
LAB	990087623	48	49	TCS	PY	0.005	3.15	4.73	1440	1	8.12	13.90	1410	1260	0.03	56.7	83
LAB	990087624	49	50.4	TCS	PY	0.005	3.06	4.49	1440	1.2	7.76	13.85	1290	1350	0.05	47.1	87

Appendix 9(1). Combined data for the downhole plot of drill hole 117310.

Hole ID 117310

Method	Sample ID	from	to	Rock	Ore mineral	Au ppm	Al pct	Ca pct	Cr ppm	Cu ppm	Fe pct	Mg pct	Mn ppm	Ni ppm	S pct	Sr ppm	Zn ppm
pXRF	990013101	0	1	AT1		0.005	3.15	12.01	1693	0	4.55	10.87	2208	793	0.00	112	20
pXRF	990013102	1	2	AT1		0.005	2.73	11.72	1464	0	4.46	10.72	2003	826	0.00	104	21
pXRF	990013103	2	2.65	AT1		0.01	2.76	10.88	1881	0	4.66	11.04	1869	908	0.00	114	25
pXRF	990013103	2.65	3	AS2	PY	0.01	2.76	10.88	1881	0	4.66	11.04	1869	908	0.00	114	25
pXRF	990013104	3	4	AS2	PY	0.005	3.88	4.83	2213	9	7.67	15.40	1449	1393	0.01	52	60
pXRF	990013105	4	5	AS2	PY	0.005	3.70	4.88	1923	11	7.60	15.41	1454	1410	0.03	79	78
LAB	990085568	5.2	6	AS2	PY	0.005	3.70	4.68	1230	2.5	8.24	13.90	1480	1265	0.08	63.3	73
LAB	990085569	6	6.9	AS2	PY	0.005	3.37	3.82	1290	1.1	8.05	14.40	1260	1240	0.03	31.1	76
LAB	990085569	6.9	7	AS1		0.005	3.37	3.82	1290	1.1	8.05	14.40	1260	1240	0.03	31.1	76
LAB	990085570	7	8	AS1		0.005	3.78	4.49	1360	1.1	9.16	13.95	1330	1390	0.08	27.3	80
LAB	990085571	8	9	AS1		0.005	3.49	5.20	1050	1	7.53	14.30	1300	1155	0.05	37.3	81
LAB	990085573	9	10	AS1		0.005	3.68	5.13	1560	1.8	8.75	14.60	1210	1430	0.05	41.7	89
LAB	990085574	10	11	AS1		0.005	3.78	5.15	1450	0.6	7.84	14.80	1120	1065	0.01	26.3	89
LAB	990085575	11	12	AS1		0.01	3.76	5.07	1320	1.6	8.03	13.55	1040	1145	0.02	28	85
LAB	990085576	12	13	AS1		0.02	4.58	6.04	1490	3	9.27	13.70	1440	1245	0.05	48.3	90
LAB	990085577	13	14	AS1		0.005	3.61	6.08	1580	1	8.15	13.90	1510	1165	0.05	57.3	83
LAB	990085578	14	15	AS1		0.005	3.27	5.50	1670	0.9	8.03	14.25	1320	1300	0.05	56.7	80
LAB	990085579	15	16	AS1		0.005	3.40	5.48	1660	1.4	8.27	14.15	1380	1315	0.09	70.7	78
LAB	990085580	16	17	AS1		0.005	3.33	4.80	1540	1.8	7.87	14.80	1220	1300	0.06	52.9	80
LAB	990085583	17	18	AS1		0.005	3.57	5.11	1530	3.6	8.32	14.30	1500	1245	0.06	57.5	76
LAB	990085584	18	19	AS2	PY	0.005	3.81	4.33	1740	5.1	8.08	14.50	1360	1340	0.04	54.9	73
LAB	990085585	19	20	AS2	PY	0.005	3.59	3.90	1880	12.8	8.92	14.70	1400	1445	0.06	68.6	72
LAB	990085586	20	21	AS2	PY	0.005	3.29	3.94	1800	4	7.89	14.90	1400	1365	0.04	92.4	73

Appendix 9(2). Combined data for the downhole plot of drill hole 117310.

Method	Sample ID	from	to	Rock	Ore mineral	Au ppm	Al pct	Ca pct	Cr ppm	Cu ppm	Fe pct	Mg pct	Mn ppm	Ni ppm	S pct	Sr ppm	Zn ppm
LAB	990085587	21	22	AS2	PY	0.02	3.47	4.74	1860	95.6	8.45	14.10	1520	1355	0.06	88.9	70
LAB	990085588	22	23	AS2	PY	0.02	3.63	4.47	1980	88.8	8.54	14.30	1500	1375	0.08	83.7	71
LAB	990085589	23	24	AS2	PY	0.07	4.21	4.64	1770	303	9.12	14.20	1480	1170	0.05	63	71
LAB	990085590	24	25	AS2	PY	0.01	4.00	5.48	1630	82.6	8.68	13.50	1580	1155	0.03	63.1	63
LAB	990085591	25	26	AS2	PY	0.08	3.73	5.52	1550	414	8.69	13.45	1610	1225	0.09	55.8	61
LAB	990085593	26	27	AS2	PY	0.08	3.48	4.83	1880	400	9.02	14.15	1520	1410	0.06	60.7	65
LAB	990085594	27	28	AS2	PY	0.02	3.26	6.09	1510	151.5	7.37	13.95	1540	1245	0.07	82.6	51
LAB	990085595	28	29	AS2	PY	0.04	3.42	5.67	1540	172.5	7.94	14.30	1500	1245	0.06	84.4	55
LAB	990085596	29	30	AS2	PY	0.08	3.47	4.47	1930	335	8.54	14.60	1380	1455	0.12	49.8	64
LAB	990085597	30	31	AS2	PY	0.03	3.58	4.17	1990	101	8.95	14.70	1360	1415	0.05	49.4	67
LAB	990085598	31	32	AS2	PY	0.04	3.36	4.23	1900	109.5	8.88	14.15	1370	1370	0.04	54.2	67
LAB	990085599	32	33	AS2	PY	0.07	3.42	3.84	1910	166	9.31	14.35	1260	1410	0.09	45.4	66
LAB	990085600	33	34	AS2	PY	0.04	3.20	5.20	1620	141.5	8.49	14.60	1540	1280	0.07	76.8	63
LAB	990085603	34	35	AS2	PY	0.06	3.39	4.63	1670	195.5	8.48	14.50	1440	1335	0.07	62.5	62
LAB	990085604	35	36	AS2	PY	0.11	3.45	4.29	2400	293	8.64	14.90	1360	1310	0.08	59.4	70
LAB	990085605	36	37	AS2	PY	0.06	3.26	5.05	1440	154	7.79	14.65	1560	1310	0.08	81.9	62
LAB	990085606	37	38	AS2	PY	0.005	3.54	4.37	1860	14.7	9.58	14.25	1450	1415	0.06	58.4	68
LAB	990085607	38	39	AS2	PY	0.005	3.77	4.78	1900	20	9.14	14.20	1480	1375	0.06	53.6	68
LAB	990085608	39	40	AS2	PY	0.005	3.44	4.26	1850	9.4	8.54	14.25	1350	1290	0.04	48.3	68
LAB	990085609	40	41	AS2	PY	0.005	3.28	4.43	1750	22.5	8.73	14.20	1360	1450	0.06	53.4	65
LAB	990085610	41	42	AS2	PY	0.01	3.78	3.84	1620	23.7	8.39	14.85	1220	1355	0.05	50.5	70
LAB	990085611	42	43	AS2	PY	0.005	3.08	4.62	1620	12	8.40	14.00	1250	1260	0.04	50.6	62
LAB	990085613	43	44	AS2	PY	0.01	3.15	5.71	1510	27.7	7.60	14.25	1530	1280	0.05	74.9	63
LAB	990085614	44	45	AS2	PY	0.02	3.54	4.81	1800	51.3	8.53	14.05	1400	1265	0.05	52.9	69
LAB	990085615	45	46	AS2	PY	0.09	3.56	3.95	1740	116.5	8.90	14.30	1240	1295	0.06	51.6	70

Appendix 9(3). Combined data for the downhole plot of drill hole 117310.

Method	Sample ID	from	to	Rock	Ore mineral	Au ppm	Al pct	Ca pct	Cr ppm	Cu ppm	Fe pct	Mg pct	Mn ppm	Ni ppm	S pct	Sr ppm	Zn ppm
LAB	990085616	46	47	AS2	PY	0.04	3.29	4.46	1380	120.5	7.60	14.25	1270	1275	0.06	53.1	65
LAB	990085617	47	48	AS2	PY	0.02	3.67	3.92	1740	78.9	8.98	13.80	1260	1350	0.06	49.5	68
LAB	990085618	48	49	AS2	PY	0.02	3.21	5.48	1700	52.6	7.76	13.65	1480	1205	0.06	71.1	60
LAB	990085619	49	50	AS2	PY	0.02	3.32	4.97	1570	41.1	8.24	14.15	1400	1245	0.05	65.5	63
LAB	990085620	50	51	AS2	PY	0.01	3.30	4.62	1620	23.5	8.38	14.15	1310	1325	0.05	53.8	63
LAB	990085623	51	52	AS2	PY	0.5	3.23	5.82	1670	845	8.41	13.80	1570	1270	0.19	69.7	62
LAB	990085624	52	53	AS2	PY	0.09	3.43	5.50	1720	221	8.53	13.90	1500	1365	0.06	71	59
LAB	990085625	53	54	AS2	PY	0.23	2.94	6.19	1480	522	7.79	13.75	1520	1205	0.13	87.8	57
LAB	990085626	54	55	AS2	PY	0.2	3.77	5.89	1430	709	8.11	13.00	1580	1055	0.10	66.5	54
pXRF	990013106	55	56	AS2	PY	0.05	3.65	9.77	2256	52	5.34	12.70	2099	984	0.00	165	33
pXRF	990013107	56	57	AS2	PY	0.005	3.36	8.96	2007	0	6.29	12.74	1753	1049	0.00	97	37
pXRF	990013108	57	58	AS2	PY	0.005	4.08	4.02	2058	9	8.07	16.09	1127	1500	0.02	33	39
pXRF	990013109	58	59	AS2	PY	0.005	3.03	9.61	1524	8	5.79	12.69	1777	1102	0.03	72	31
pXRF	990013111	59	60	AT1		0.01	3.39	10.51	1543	8	5.34	11.13	1887	1110	0.02	92	24
pXRF	990013112	60	61	AT1		0.02	2.25	13.31	1631	0	3.94	9.22	2140	590	0.00	211	24
pXRF	990013113	61	62	AT1		0.005	1.87	13.93	1391	0	4.11	8.58	2281	626	0.00	210	27
pXRF	990013114	62	63	AT1		0.01	2.56	12.47	1694	0	4.63	9.44	2268	803	0.00	206	35
pXRF	990013115	63	64	AT1		0.03	2.38	12.83	1497	0	4.78	9.30	2275	805	0.00	194	35
pXRF	990013116	64	65	AT1		0.03	2.58	12.88	1615	0	4.55	9.84	2229	693	0.00	200	33
pXRF	990013117	65	66.2	AT1		0.1	2.30	12.11	1683	0	4.72	8.92	2132	760	0.00	198	44
pXRF	990013168	66.2	67	AT1		0.04	2.55	11.90	1697	0	4.81	9.30	2147	791	0.00	197	37
pXRF	990013169	67	68	AT1		0.03	2.18	12.63	1368	0	4.58	9.87	2157	831	0.00	170	34
pXRF	990013171	68	69	AT1		0.44	2.46	10.87	1367	39	5.47	11.04	1984	943	0.07	131	32
pXRF	990013172	69	70	AT1		1.33	1.68	14.62	1174	47	4.39	9.16	2419	784	0.05	167	29
pXRF	990013173	70	71	AT1		0.15	2.51	13.56	1739	50	4.59	9.89	2535	729	0.00	199	39

Appendix 9(4). Combined data for the downhole plot of drill hole 117310.

Method	Sample ID	from	to	Rock	Ore mineral	Au ppm	Al pct	Ca pct	Cr ppm	Cu ppm	Fe pct	Mg pct	Mn ppm	Ni ppm	S pct	Sr ppm	Zn ppm
pXRF	990013174	71	71.72	AT1		0.92	2.03	12.70	1362	0	4.83	9.28	2216	854	0.00	144	37
pXRF	990013175	71.72	73	AT2	CP	0.32	2.17	13.78	1529	6	4.64	9.30	2422	799	0.01	176	39
pXRF	990013176	73	74	AT2	CP	0.05	2.65	13.17	1421	0	4.40	9.92	2195	832	0.00	194	27
pXRF	990013177	74	75	AT2	CP	0.34	2.62	13.45	1540	0	4.01	9.70	2346	731	0.01	167	17
pXRF	990013178	75	76	AT2	CP	0.005	2.69	15.50	1730	0	3.22	9.67	2528	578	0.04	175	24
pXRF	990013179	76	77	AT2	CP	0.01	3.04	10.83	1630	30	5.32	11.22	2006	950	0.02	118	35
pXRF	990013181	77	78	AT2	CP	0.01	3.08	12.55	1582	34	5.59	12.54	2434	851	0.04	155	32
pXRF	990013182	78	79	AS2		0.02	3.86	5.67	1955	35	7.46	16.05	1634	1335	0.03	77	63
pXRF	990013183	79	80	AS2		0.03	3.28	4.81	2131	69	7.85	16.07	1556	1479	0.03	61	71
pXRF	990013184	80	81	AS2		0.04	3.58	4.86	2313	81	7.67	16.14	1490	1392	0.03	77	72
pXRF	990013185	81	82	AS2		0.06	3.47	4.11	2219	122	7.66	16.80	1433	1422	0.02	58	79
LAB	990085627	82	83	AS2		0.01	3.31	4.68	1800	37.2	8.15	14.20	1330	1245	0.03	58.2	67
LAB	990085628	83	84	AS2		0.005	3.11	5.17	1930	3.2	7.93	13.80	1430	1215	0.03	63.2	66
LAB	990085629	84	84.57	AS2		0.005	3.36	5.50	1780	1.5	7.74	13.85	1420	1250	0.03	66.6	62
LAB	990085629	84.57	85	AS2		0.005	3.36	5.50	1780	1.5	7.74	13.85	1420	1250	0.03	66.6	62
LAB	990085630	85	86	AS2		0.005	3.42	5.78	1820	2.9	8.11	13.35	1410	1435	0.03	76.7	55
LAB	990085631	86	87.2	AS2		0.005	3.48	9.65	1920	1.1	5.51	11.15	1860	987	0.01	141	50

Appendix 10(1). Combined data for the downhole plot of drill hole 117312.

Hole ID 117312																
Method	Sample ID	from	to	Rock	Ore mineral	Au ppm	Al pct	Ca pct	Cr ppm	Cu ppm	Fe pct	Mg pct	Mn ppm	Ni ppm	S pct	Sr ppm	Zn ppm
pXRF	990013201	0	1	AT1		0.005	3.12	11.27	1523	7	5.01	11.36	2107	1050	0.01	100	23
pXRF	990013202	1	2	AT1		0.005	2.67	13.81	1512	0	4.12	10.50	2569	697	0.02	168	23
pXRF	990013203	2	3	AT1		0.005	2.98	11.05	1546	7	4.83	11.32	2160	925	0.01	108	24
pXRF	990013204	3	4	AS2	PY	0.02	3.16	6.66	1698	0	6.85	14.95	1730	1132	0.05	126	62
pXRF	990013205	4	5	AS2	PY	0.005	4.09	3.95	1711	7	7.55	16.08	1247	1125	0.04	68	84
pXRF	990013206	5	6	AS2	PY	0.005	3.79	4.02	2252	0	8.16	16.62	1374	1423	0.04	62	96
LAB	990085634	6	7	AS2	PY	0.005	3.50	4.72	1530	2.5	8.92	14.20	1400	1290	0.13	63.4	84
LAB	990085635	7	8	AS2	PY	0.005	3.27	5.48	1550	3.1	8.65	13.90	1560	1250	0.07	70.6	83
LAB	990085636	8	9	AS2	PY	0.005	3.20	5.97	1410	2.9	8.37	13.50	1500	1220	0.10	73.3	80
LAB	990085637	9	10	AS2	PY	0.005	3.22	5.20	1700	3.1	8.82	13.70	1460	1220	0.07	61.3	85
LAB	990085638	10	11	AS2	PY	0.005	3.37	4.87	1890	5	8.89	13.90	1420	1290	0.07	51.4	89
LAB	990085639	11	12	AS2	PY	0.005	3.24	5.63	1620	6.9	8.41	14.00	1460	1240	0.05	62.4	90
LAB	990085640	12	13	AS2	PY	0.005	3.45	5.45	1520	8.1	8.46	14.10	1350	1220	0.05	52.7	89
LAB	990085641	13	14	AS2	PY	0.005	3.91	5.11	1490	11	9.43	13.90	1520	1050	0.04	54.5	88
LAB	990085643	14	15	AS2	PY	0.05	3.76	5.96	1100	40.3	7.28	14.15	1830	1130	0.03	95	80
LAB	990085644	15	16	AS2	PY	0.005	3.32	5.38	1280	14.2	7.73	13.20	1610	1100	0.03	75.7	74
LAB	990085645	16	17	AS2	PY	0.005	3.28	4.95	1430	4.8	8.14	13.70	1400	1280	0.07	67.1	72
LAB	990085646	17	18	AS2	PY	0.005	3.42	5.48	1550	2.7	8.43	13.55	1380	1170	0.04	70.9	66
LAB	990085647	18	19	AS2	PY	0.005	3.35	5.75	1470	3.5	8.36	13.00	1440	1190	0.02	51	63
pXRF	990013207	19	20	AS2	PY	0.03	4.02	4.54	2415	7	8.18	16.09	1358	1395	0.03	47	73
pXRF	990013208	20	21	AS2	PY	0.005	3.80	4.71	2131	7	7.56	15.98	1442	1361	0.04	63	74
pXRF	990013209	21	22	AS3		0.005	3.97	4.57	1962	0	7.10	16.62	1434	1421	0.03	66	70
pXRF	990013211	22	23	AS3		0.13	3.40	5.29	2168	32	6.75	15.75	1565	1276	0.05	69	57

Appendix 10(2). Combined data for the downhole plot of drill hole 117312.

Method	Sample ID	from	to	Rock	Ore mineral	Au ppm	Al pct	Ca pct	Cr ppm	Cu ppm	Fe pct	Mg pct	Mn ppm	Ni ppm	S pct	Sr ppm	Zn ppm
pXRF	990013212	23	24.24	AS3		0.02	4.19	3.55	2405	31	8.04	16.24	1363	1558	0.03	36	63
LAB	990013213	24.24	25	ZD1		7.49	2.03	11.20	1220	20.2	7.21	11.30	2700	1030	0.05	195.5	32
LAB	990013214	25	26.3	ZD2		0.1	2.74	11.50	1240	27.1	5.64	10.30	3200	886	0.07	179.5	27
LAB	990013215	26.3	27	AS3		0.02	2.89	11.70	1350	1.9	4.41	9.13	2900	655	0.01	156.5	31
pXRF	990013216	27	28	AS3		0.01	3.97	10.28	2288	0	5.91	13.40	2843	1051	0.04	121	43
pXRF	990013217	28	29	AS3		0.05	3.44	6.16	2133	54	7.09	14.42	1910	1288	0.04	68	68
pXRF	990013218	29	30	AS3		0.22	3.59	3.00	2371	59	7.93	16.39	1275	1590	0.02	30	78
pXRF	990013219	30	30.65	AS3		0.48	3.72	4.07	2675	175	8.48	15.94	1512	1466	0.06	52	89
pXRF	990013219	30.65	31	AS2	PY	0.48	3.72	4.07	2675	175	8.48	15.94	1512	1466	0.06	52	89
pXRF	990013221	31	32	AS2	PY	0.01	3.63	4.73	2086	8	7.57	17.00	1576	1374	0.04	68	81
LAB	990085648	32	33	AS2	PY	0.005	3.14	5.04	1400	11.6	7.60	14.35	1480	1250	0.05	84.6	76
LAB	990085649	33	34	AS2	PY	0.005	3.19	4.66	1450	8.7	7.83	14.40	1540	1290	0.05	78.9	77
LAB	990085650	34	35	AS2	PY	0.005	3.20	4.35	1540	5	8.44	14.30	1540	1300	0.05	50.5	80
LAB	990085653	35	36	AS2	PY	0.005	3.13	4.95	1480	2.7	7.89	14.75	1620	1280	0.03	51.3	82
LAB	990085654	36	37	AS2	PY	0.005	3.03	4.82	1330	2.4	7.94	14.90	1460	1300	0.03	52.1	84
LAB	990085655	37	39	AS2	PY	0.005	2.96	4.44	1240	1.4	7.64	14.55	1260	1190	0.03	45.3	82
LAB	990085656	39	40	AS1	PY	0.005	3.36	5.38	1330	1.2	8.31	14.20	1280	1260	0.07	62.9	82
LAB	990085657	40	41	AS1	PY	0.005	3.40	5.65	1270	1.1	8.01	13.95	1240	1210	0.05	52.6	79
LAB	990085658	41	42	AS1	PY	0.005	2.95	6.28	1430	1.2	8.07	14.35	1360	1210	0.03	59.4	79
LAB	990085659	42	43	AS1	PY	0.005	3.64	4.91	1370	1.2	8.37	14.50	1140	1280	0.04	44.2	83
LAB	990085660	43	44	AS1	PY	0.005	3.42	5.04	1410	1.7	8.49	14.25	1180	1320	0.03	43.3	80
LAB	990085661	44	45	AS1	PY	0.005	3.43	4.76	1350	1.2	8.03	14.70	1140	1280	0.02	41.3	81
LAB	990085663	45	46	AS1	PY	0.005	3.28	5.75	1360	2.7	8.47	14.20	1380	1370	0.07	79.9	76
LAB	990085664	46	47	AS1	PY	0.005	3.12	6.62	1280	2.3	8.09	13.70	1510	1260	0.04	81.2	71
LAB	990085665	47	48	AS1	PY	0.005	3.24	5.79	1420	2.5	8.01	14.60	1380	1380	0.03	74.5	76

Appendix 10(3). Combined data for the downhole plot of drill hole 117312.

Method	Sample ID	from	to	Rock	Ore mineral	Au ppm	Al pct	Ca pct	Cr ppm	Cu ppm	Fe pct	Mg pct	Mn ppm	Ni ppm	S pct	Sr ppm	Zn ppm
LAB	990085666	48	49	AS1	PY	0.005	3.30	5.00	1430	2.8	8.15	14.45	1200	1280	0.01	54.8	77
LAB	990085667	49	50	AS1	PY	0.005	3.67	4.25	1300	1.2	8.76	14.65	1170	1320	0.01	46.9	78
LAB	990085668	50	50.9	AS1	PY	0.005	3.44	4.29	1270	1	7.85	15.05	1070	1240	0.02	42.7	79